Arts & Sciences Electronic Theses and Dissertations

Arts & Sciences

Summer 8-15-2017

Studies of Magic-size II-VI Nanoclusters and Surface Exchange on Flat Colloidal Nanocrystals

Yang Zhou
Washington University in St. Louis

WASHINGTON UNIVERSITY IN ST. LOUIS

Department of Chemistry

Dissertation Examination Committee:

William E. Buhro, Chair

John Bleeke

Richard A. Loomis

Bryce Sadtler

Elijah Thimsen

Studies of Magic-size II-VI Nanoclusters and Surface Exchange on Flat Colloidal Nanocrystals

by Yang Zhou

A dissertation presented to

The Graduate School

of Washington University in

partial fulfillment of the

requirements for the degree

of Doctor of Philosophy

August 2017

St. Louis, Missouri

Table of Contents

List of Figures

**Chapter 2   Isolation of Amine Derivatives of $(ZnSe)_{34}$ and $(CdTe)_{34}$.
Spectroscopic Comparisons of the $(II\text{-}VI)_{13}$ and $(II\text{-}VI)_{34}$ Magic-Size
Nanoclusters**

Chapter 3 Large Exciton-Energy Shifts by Reversible Surface Exchange in 2D II-VI Nanocrystals

Chapter 4   Reversible Exchange of L-type and Bound-Ion-Pair X-type Ligation on Cadmium Selenide Quantum Belts

List of Tables

List of Abbreviations

TEM	transmission electron microscope
HRTEM	high-resolution transmission electron microscope
IR	infrared
XRD	X-ray diffraction
PL	photoluminescence
2D	two-dimensional
ML	monolayer
QB	quantum belt
QP	quantum platelet

Acknowledgement

I would like to thank many people for their kind help and encouragement during my graduate research.

First of all, I would like to thank my advisor, Prof. William E. Buhro. It is him who taught me how to think, talk and write during my Ph.D. study. Without his everlasting support and encouragement, as well as the instruction he gave me, I could never find how interesting research is. It is my honor to work in his group.

I appreciate my committee members, Prof. Richard Loomis and Prof. John Bleeke. They shared their valuable time on my annual committee meetings and my dissertation, and generously provided me with valuable suggestions which help me to become a qualified Ph.D. I would also like to thank Prof. Bryce Sadtler and Prof. Elijah Thimsen for spending time in my dissertation.

I would like to thank Professor Patrick C. Gibbons and Dr. Huafang Li for training me in low-resolution TEM and Dr. Tyrone Daulton for SEM. Without you, I could never finish my projects.

I should thank my former and present labmates in Buhro group and Loomis group. I especially thank Dr. Fudong Wang for his generous help and valuable suggestions during my Ph.D. study. And many thanks to Dr. Yuanyuan Wang, Dr. Linjia Mu, Callyn Morrison, William Sanderson, Yuewei Yao and Haochen Sun. I would remember the happy time discussing research and life with you. Thank all the other members for all your time and help during my graduate study in Buhro and Loomis lab.

Dedicated to my family and friends.

ABSTRACT OF THE DISSERTATION

Studies of Magic-size II-VI Nanoclusters and Surface Exchange on Flat Colloidal

Nanocrystals

By

Yang Zhou

Doctor of Philosophy in Chemistry

Washington University in St. Louis, 2017

Professor William E. Buhro, Chair

This dissertation presents the isolation, characterization and reactivity of two magic size

clusters, $(ZnSe)_{34}$ and $(CdTe)_{34}$,   as well as the L-, Z- and X-type ligand exchange on the CdSe

QBs or CdS QP surface.

The dissertation first reports the spectroscopically observed magic-size nanoclusters

$(ZnSe)_{34}$ and $(CdTe)_{34}$ are isolable as amine derivatives.   The nanoclusters $[(ZnSe)_{34}(n\text{-}$

octylamine$)_{29\pm6}$(di-n-octylamine$)_{5\pm4}]$ and $[(CdTe)_{34}(n\text{-octylamine})_{4\pm3}$(di-$n$-pentylamine$)_{13\pm3}]$

are fully characterized by UV-visible spectroscopy, IR spectroscopy, elemental analysis, and

mass spectrometry.   Amine derivatives of both $(ZnSe)_{34}$ and $(CdTe)_{34}$ are observed to

convert to the corresponding $(ZnSe)_{13}$ and $(CdTe)_{13}$ derivatives, indicating that the former are

kinetic products and the latter thermodynamic products, under the conditions employed.

This conversion process is significantly inhibited in the presence of secondary amines.   The

isolation of the two new nanocluster derivatives adds to a total of nine of twelve possible

isolated derivatives in the $(II\text{-}VI)_{13}$ and $(II\text{-}VI)_{34}$ families (II = Zn, Cd; VI = S, Se, Te),

allowing comparisons of their properties.   The members of these two families exhibit

extensive spectroscopic homologies.   In both the $(\text{II-VI})_{13}$ and $(\text{II-VI})_{34}$ families, linear relationships are established between the lowest-energy nanocluster electronic transition and the band gap of the corresponding bulk semiconductor phase.

Then, the research interest expanded from the magic-size clusters to the flat colloidal nanocrystals. The dissertation demonstrates that reaction of *n*-octylamine-passivated $\{CdSe[n\text{-octylamine}]_{0.53}\}$ QBs with anhydrous metal carboxylates $M(\text{oleate})_2$ (M = Cd, Zn) results in a rapid exchange of the L-type amine passivation to Z-type $M(\text{oleate})_2$ passivation. The cadmium-carboxylate derivative is determined to have the composition $\{CdSe[Cd(\text{oleate})_2]_{0.19\pm0.02}\}$.   The morphologies and crystal structures of the quantum belts are largely unaffected by the exchange processes.   Addition of *n*-octylamine or oleylamine to the $M(\text{oleate})_2$-passivated quantum belts removes $M(\text{oleate})_2$, and restores the L-type amine passivation.   Analogously, reversible surface exchanges are also demonstrated for CdS QPs.   The absorption and emission spectra of the QBs and QPs are reversibly shifted to lower energy by $M(\text{oleate})_2$ passivation vs. amine passivation.   The largest shift of 140 meV is observed for the $Cd(\text{oleate})_2$-passivated CdSe quantum belts. We establish that changes in strain states, which can be calculated from high-angle XRD patterns, and confinement dimensions contribute roughly equally to the spectral shifts in the $Cd(\text{oleate})_2$-passivated nanocrystals. Notably, addition of $Cd(\text{oleate})_2$, which electronically couples to the nanocrystal lattices, increases the effective thickness of the belts and platelets by approximately a half of a momolayer, thus increasing the confinement dimension. However, these shifts are attributed entirely to changes in the strain states in the $Zn(\text{oleate})_2$-passivated nanocrystals.

Last, the dissertation describes facile interchange of neutral-donor amine (L-type) and anionic (X-type) ligation on CdSe QBs. Reaction of *n*-octylamine-passivated QBs with protic acids HX (X = halide, nitrate, or carboxylate) results in displacement, protonation and liberation of the amines. The newly formed *n*-octylammonium ions will balance the surface charge of X$^-$ anions in the form of surface-bound ion pairs. Addition of *n*-octylamine to the bound-ion-pair X-type ligation quantum belts restores the L-type amine passivation. These ligand exchanges are readily monitored spectroscopically. The shifts in the lowest-energy feature ranged from 49 meV to 112 meV, depending on the different X$^-$ anions. We attribute the red spectral shifts in X-type ligation to negative surface charges and associated dipoles, which slightly increase the energy of the valence-band edge, and decrease the energy of the conduction-band edge.

Chapter 1

Introduction

In this dissertation, amine derivatives of $(ZnSe)_{34}$ and $(CdTe)_{34}$, which are the synthons for flat colloidal Nanocrystals were isolated and characterized (Chapter 2). Earlier work had showed that $(CdSe)_{34}$ magic-size clusters prepared in primary-amine, secondary-amine cosolvent mixtures were potent nanocrystals precursor for CdSe QPs synthesis[1], thus here we monitored the generation of $(ZnSe)_{34}$ and $(CdTe)_{34}$ in primary-amine, secondary-amine cosolvent mixtures as well. Precipitation and redispersion in secondary-amine solvent significantly slowed down the interconversion to $(ZnSe)_{13}$ and $(CdTe)_{13}$. The stoichiometries of $[(ZnSe)_{34}(n\text{-octylamine})_{29}(\text{di-}n\text{-octylamine})_5]$ and $[(CdTe)_{34}(n\text{-octylamine})_5(\text{di-}n\text{-pentylamine})_{12}]$ characterized by IR spectroscopy, mass spectrometry and elemental analysis were consistent with other amine-ligated $(II\text{-}VI)_{34}$ derivatives we previously obtained[1,3].

In Chapter 3, we studied the reversible surface exchange of the L-type amine passivation to Z-type $M(\text{oleate})_2$ (M= Cd, Zn) passivation in CdSe QBs[2] and CdS QPs[3]. Exchange in nanocrystal surface passivation generally doesn't induce large energetic shifts in absorption spectra, while a few counterexamples exist. In this chapter, we describe the large exciton energy shifts as large as 140mmeV by reversible L-type and Z-type surface exchange[4] in 2D II-VI nanocrystals, and proposed that the change in both thickness dimension and lattice strain states should be considered to explain the energy shifts.

In Chapter 4, the reversible surface exchange on the CdSe QBs was extended from L-type to Z- type to L-type to bound-ion-pair X-type. Addition of protic acids HX (X = halide, nitrate, or carboxylate) to the n-octylamine passivated CdSe QBs resulted in the surface displacement of the amine ligands by X^- anions and protonation of the liberated amines, forming surface-bound ion pairs,[5,6] with the newly formed n-octylammonium ions and/or

2

TOPH$^+$ balancing the surface charge. The spectral shift, expected IR features, inter-QB spacing measured by low-angle XRD, TEM images and the elemental-analysis data all supported the retention of the original L-type ligands as protonated *n*-octylammonium groups. Finally, the L- for X-type exchanges were fully reversible in three of the cases (X = OBz, OAc, and NO$_3$).

1.1 Magic-Size II-VI Nanoclusters and related Flat Colloidal Nanocrystals

Clusters composed of main-group elements have fascinated inorganic chemists since the structures of the polyhedral boranes were discovered in the 1950s.[7]   Main-group cluster chemistry developed rapidly in that area with the expansion of the carborane,[8] metallaborane,[9] and metallacarborane[8] fields, in which the clusters exhibited analogous deltahedral structures and conformed to the same skeletal-electron-counting principles.[10]

The Zintl-anion clusters composed of Sn, Ge, Pb, Bi, Sb, and their combinations subsequently joined these families of deltahedral clusters.[11]   Corbett provided a major advance in the chemistry of Zintl anions by sequestering their counter-cations within 2,2,2-crypt, stabilizing the clusters against back electron transfer.[12]   The stabilized cluster compounds were isolated in crystalline form, allowing Corbett and coworkers to obtain the first x-ray structural characterizations of Zintl-anion clusters.

Discrete molecular clusters of elemental carbon were first isolated by Kratschmer and Huffman in 1990,[13] resulting in the dramatic growth of the carbon-fullerene field at that time. The C$_{60}$ and C$_{70}$ clusters are the best-known and most-stable fullerenes, although the even-numbered carbon clusters larger than C$_{32}$ are stable.[14]   As is well known, the structures of

these clusters consist of hollow cages constructed by the fusion of five- and six-membered rings.   The field has expanded to include endohedral metallofullerenes having atoms, molecules, or clusters encapsulated within the fullerene cages,[15] and heterofullerenes, having heteroatom substitutions of cage carbon atoms.[16]

A newly emergent family of main-group clusters consists of the so-called magic-size nanoclusters of CdSe, $(CdSe)_x$ where $x = 13, 19, 33, 34$, etc., and their II-VI congeners.[17-24] Magic-size nanoclusters were first detected in the early II-VI nanoparticle research of Henglein and coworkers in the 1980s.[25]   They were suggested to be small, discretely sized clusters by their blue-shifted and comparatively sharp absorption spectra relative to those of the larger nanoparticles.   Magic-size nanocluster spectral features have been observed frequently in the early stages of nanocrystal synthesis since that time.[23,26,27, 28]   In an important study, Manna and coworkers demonstrated that the spectra of magic-size CdSe nanoclusters evolve in discrete rather than continuous shifts as the nanoclusters grow from one discrete, stable size to the next.[17]

The precise stoichiometries and structures of these II-VI nanoclusters remain to be fully resolved.   The crystallographically characterized examples that have been isolated from solution syntheses exhibit *nonstoichiometric* (non 1:1) II-VI compositions and close-packed zinc-blende or wurtzite core structures.[29-34]   These nanoclusters also contain anionic ligands to charge balance the nonstoichiometric II-VI compositions.

In contrast, the seminal work of Kasuya and coworkers in 2004 characterized the *stoichiometric* (1:1) nanoclusters $(CdSe)_{13}$, $(CdSe)_{19}$, $(CdSe)_{33}$, and $(CdSe)_{34}$ by mass-spectrometric analysis of solution-derived synthetic mixtures.[20]   The structures and

stabilities of the *stoichiometric* magic-size nanoclusters have been extensively studied theoretically;[35-37] however, to our knowledge, no x-ray crystal-structure determinations have been reported to date for any member of this stoichiometric family. The lack of structural data is largely due to the lack of syntheses that selectively produce nanoclusters of a single size. Most syntheses afford mixtures of the magic sizes,[16-19] which have not proven easily separable. Theoretical studies predict the stoichiometric, charge-neutral $(II-VI)_x$ nanoclusters to have cage-like structures, somewhat reminiscent of the carbon fullerenes.[35-37]

In 2012, we reported the first isolation of a single-size $(CdSe)_x$ nanocluster as the ligated derivative $[(CdSe)_{13}(n\text{-octylamine})_{13}]$.[21] Additional $[(CdSe)_{13}(RNH_2)_{13}]$ derivatives with R = *n*-propyl, *n*-pentyl, and oleyl were subsequently obtained as slushy or normal solids on the gram scale.[21,24] Shortly thereafter, Sardar and coworkers isolated a derivative of $(CdSe)_{34}$.[22] We later described the synthesis of $[(CdSe)_{34}(n\text{-octylamine})_{16}(di\text{-}n\text{-pentylamine})_2]$.[23]

Mechanistic studies established an unexpected formation pathway in our CdSe nanocluster syntheses (Figure 1.1).[26] The $(CdSe)_{13}$ nanoclusters were shown to grow within spontaneously formed, lamellar, primary-amine-bilayer templates (Figure 1.1, upper left and middle). The nanoclusters were liberated from the templates by a ligand-exchange-driven unbundling process (upper right and bottom right). Alternatively, mild heating (at 70–80 °C) of the template-assembled $(CdSe)_{13}$ nanoclusters resulted in their coalescence and recrystallization to afford wurtzitic CdSe quantum belts (ribbon-shaped nanocrystals, figure 1.1, bottom left). The flat morphology of the quantum belts was imposed by the lamellar structure of the template. We subsequently learned that flat wurtzitic CdSe quantum platelets could be grown similarly from $(CdSe)_{34}$ at room temperature, a remarkably low

growth temperature.[1]   We proposed that low-temperature growth was enabled because

$(CdSe)_{34}$ is near to the critical crystal-nucleus size for CdSe, and thus $[(CdSe)_{34}(n\text{-}$

octylamine$)_{16}$(di-n-pentylamine$)_2]$ constitutes crystal nuclei that may be stored in a bottle.

Thus, other magic-size nanoclusters like $(CdSe)_{13}$ and $(CdSe)_{34}$ are expected to be potent

nanocrystal precursors.
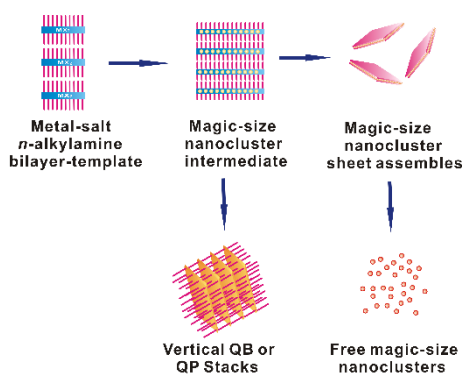
Figure 1.1. Formation pathway in CdSe nanocluster syntheses.

The question addressed in this work is the extent to which the CdSe magic-size-

nanocluster chemistry summarized above may be generalized to other members of the II-VI

family of semiconductors.   We now report spectral data and other characterization of amine-

ligated derivatives of $(CdTe)_{34}$ and $(ZnSe)_{34}$, which appear to be thermodynamically unstable

compared to the corresponding $(II\text{-}VI)_{13}$ clusters.   This is consistent with our observations in

the $(CdSe)_x$-nanocluster system, in which $(CdSe)_{13}$ was shown to be more stable than

$(CdSe)_{34}$.

1.2   L-type and Z-type Surface Exchange on   Colloidal Nanocrystals

Exchange of the surface passivation in semiconductor nanocrystals often profoundly influences photoluminescence efficiencies,[38-40] but generally does not induce significant energetic shifts in their absorption and emission features.   For example, Owen and coworkers recently reported that the surface passivation of CdSe (and other) pseudospherical nanocrystals (quantum dots) may be reversibly exchanged between neutral-acceptor (Z-type) Cd(carboxylate)$_2$ passivation and neutral-donor amine passivation (Figure 1.2).[41]   Although the exchange produces large effects on nanocrystal photoluminescence quantum yields, the lowest-energy absorption feature shifts by only ~4 meV (a ~1 nm shift of a 565-nm absorbance).[41]   Large shifts in the absorption spectra of semiconductor nanocrystals upon changes in surface ligation are not typically observed.
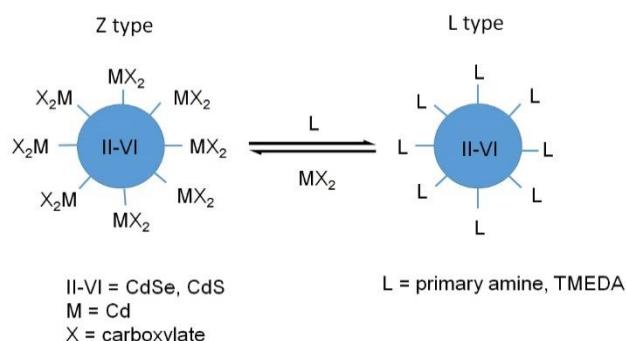
Figure 1.2.   Exchange of Z and L-type surface passivation in II-VI quantum dots.[41]

A few counterexamples to the rule above have been described.   Weiss and coworkers demonstrated that the incorporation of phenyldithiocarbamate (PTC) ligands onto the surfaces of II-VI and IV-VI nanocrystals may result in shifts of the lowest-energy absorption feature of up to 1 eV to lower energy.[42]   In these systems, holes delocalize into the PTC ligand shells, increasing the effective confinement dimension (that is, increasing the box

7

size), and thus decreasing the confinement potential. Thiol, selenol, and tellurol ligation is observed to have a similar effect in II-VI nanocrystals, but of smaller magnitude (energy shifts of 10-40 meV).[43-45] In these latter cases, electronic coupling between the nanocrystal and ligand shell apparently extends the crystal lattice and increases the size of the confinement box.

Lattice strain also modifies the effective band gaps of semiconductor nanocrystals.[46-51] Compressive strain increases effective band gaps, shifting absorption and emission features to higher energies, with tensile strain inducing the opposite effects. The strain states of semiconductor nanocrystals are significantly influenced by surface passivation and the nature of the resulting surface reconstructions.[52-54] In 2D II-VI nanocrystals, compressive and tensile strains as large as 6 and 8%, respectively, have been observed as functions of both passivation and core crystal structure.[3,55]

In this work, we report that surface exchange between amine-passivated (L-type)[41] and metal-carboxylate-passivated (M = Cd, Zn; Z-type[41]) surfaces of CdSe and CdS quantum belts (QBs, nanoribbons) and platelets (QPs) induces exciton-energy shifts as large as 140 meV in the extinction (absorption) and emission spectra. These shifts and the nature of the surface passivation are fully reversible. The reversible electronic perturbations are attributed to changes in the strain states and confinement dimensions of the 2D nanocrystals upon surface exchange. We propose the surface-passivation effects to be magnified in the 2D nanocrystals relative to semiconductor nanocrystals of other morphologies because of their very large surface fractions and thin confinement dimension.

1.3 L-type and Bound-Ion-Pair X-type Surface Exchange on Colloidal Nanocrystals

The surface ligation proposed in Figure 1.3 was previously defined as "bound-ion-pair X-type" ligation by Owens and coworkers.[5,41,56] In this ligation type, anionic X^- groups are bound to a stoichiometric, charge-neutral nanocrystal core. Thus, the negative surface charge acquired by the binding of the X^- ligands must be balanced by associated counter-ions, forming ion pairs. Because these ion pairs are bound to the nanocrystal surface through the X groups, they are bound ion pairs.

We sought to prepare bound-ion-pair X-type ligation to support the Figure 1.3 configuration. Having L-type ligated [(CdSe)(n-octylamine)$_{0.53}$] QBs readily available,[57] we investigated the possibility of L-type to bound-ion-pair X-type surface exchange with these QBs, as previously demonstrated by Owen and coworkers for CdSe quantum dots.[56]
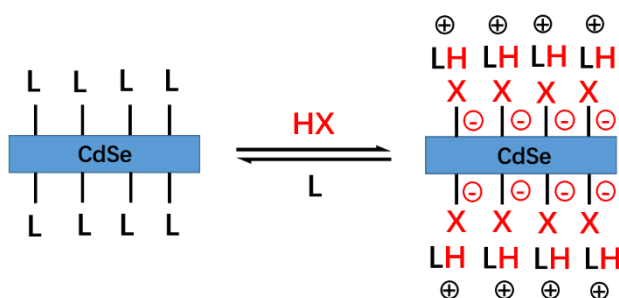
Figure 1.3. L-type to bound-ion-pair X-type surface-exchange pathways in CdSe QBs.

1.4   References

(1) Wang, Y. Y.; Zhang, Y.; Wang, F. D.; Giblin, D. E.; Hoy, J.; Rohrs, H. W.; Loomis, R. A.; Buhro, W. E. *Chem. Mater.* **2014**, *26*, 6318.

(2) Liu, Y. H.; Wang, F. D.; Wang, Y. Y.; Gibbons, P. C.; Buhro, W. E. *J. Am. Chem. Soc.* **2011**, *133*, 17005.

(3) Wang, Y. Y.; Zhou, Y.; Zhang, Y.; Buhro, W. E. *Inorg. Chem.* **2015**, *54*, 1165.

(4) Zhou, Y.; Wang, F.; Buhro, W. E. *J. Am. Chem. Soc.* **2015**, *137*, 15198.

(5) Anderson, N. C.; Owen, J. S. *Chem. Mater.* **2013**, *25*, 69.

(6) Chen, P. E.; Anderson, N. C.; Norman, Z. M.; Owen, J. S. *J. Am. Chem. Soc.* **2017**.

(7) Lipscomb, W. N. *J. Chem. Phys.* **1954**, *22*, 985.

(8) Casanova, J. *The Borane, Carborane, Carbocation Contiuum*; Jon Wiley & Sons, Inc., 1998.

(9) Housecroft, C. E. *Boranes and mettallaboranes*; Ellis Horwood Limited, 1994.

(10) Rudolph, R. W. *Acc. Chem. Res.* **1976**, *9*, 446.

(11) Corbett, J. D. *Chem. Rev.* **1985**, *85*, 383.

(12) Corbett, J. D., Adolphson, D.G., Merryman, D.J., Edwards, P.A., Armatis, F.J. *J. Am. Chem. Soc.* **1975**, *97*, 6267.

(13) Kräetschmer, W., Lamb, L. D., Fostiropoulos, K., Huffman, D. R. *Nature* **1990**, *347*, 354.

(14) Curl, R. F., Smalley, R.E. In *Scientific American* 1991.

(15) Lu, X., Bao, L., Akasaka, T., Nagase, S. *Chem. Comm.* **2014**, ahead of print.

(16) Vostrowsky, O., Hirsch, A. *Chem. Rev.* **2006**, *106*, 5191.

(17) Kudera, S., Zanella, M., Giannini, C., Rizzo, A., Li, Y.Q., Gigli, G., Cingolani, R., Ciccarella, G., Spahl, W., Parak, W. J., Manna, L. *Adv. Mater.* **2007**, *19*, 548.

(18) Dukes, A. D., McBride, J. R., Rosenthal, S. J. *Chem. Mater.* **2010**, *22*, 6402.

(19) Noda, Y., Maekawa, H., Kasuya, A. *Eur. Phys. J. D* **2010**, *57*, 43.

(20) Kasuya, A., Sivamohan, R., Barnakov, Y. A., Dmitruk, I. M., Nirasawa, T., Romanyuk, V. R., Kumar, V., Mamykin, S. V., Tohji, K., Jeyadevan, B., Shinoda, K., Kudo, T., Terasaki, O., Liu, Z., Belosludov, R. V., Sundararajan, V., Kawazoe, Y. *Nat. Mater.* **2004**, *3*, 99.

(21) Wang, Y., Liu, Y.H., Zhang, Y., Wang, F., Kowalski, P. J., Rohrs, H. W., Loomis, R. A., Gross, M. L., Buhro, W. E. *Angew. Chem., Int. Ed.* **2012**, *51*, 6154.

(22) Dolai, S., Nimmala, P. R., Mandal, M., Muhoberac, B. B., Dria, K., Dass, A., Sardar, R. *Chem. Mater.* **2014**, *26*, 1278.

(23) Wang, Y., Zhang, Y., Wang, F., Giblin, D.E., Hoy, J., Rohrs, H. W., Loomis, R.A., Buhro, W. E. *Chem. Mater.* **2014**, *26*, 2233.

(24) Wang, Y., Liu, Y.H., Zhang, Y., Kowalski, P. J., Rohrs, H. W.,Buhro, W. E. *Inorg. Chem* **2013**, *52*, 2933.

(25) Fojtik, A., Weller, H., Koch, U., Henglein, A. *Ber.Bunsenges. Phys. Chem.* **1984**, *88*, 969.

(26) Liu, Y.-H.; Wang, F.; Wang, Y.; Gibbons, P. C.; Buhro, W. E. *J. Am. Chem. Soc.* **2011**, *133*, 17005.

(27) Yu, J. H., Liu, X., Kweon, K.E., Joo, J., Park, J., Ko, K.T., Lee, D.W., Shen, S.P., Tivakornsasithorn, K., Son, J.S., Park, J.H., Kim, Y.W., Hwang, G.S., Dobrowolska, M., Furdyna, J.K., Hyeon, T. *Nat. Mater.* **2009**, *9*, 47.

(28) Peng, Z. A., Peng, X. *J. Am. Chem. Soc.* **2002**, *124*, 3343.

(29) Lee, G. S., Craig. D.C., Ma, I., Scudder, M.L., Bailey, T.D., Dance, I.G. *J. Am. Chem. Soc.* **1988**, *110*, 4863.

(30) Cossairt, M., Owen, J.S. *Chem. Mater.* **2011**, *23*, 3114.

(31) Beecher, A. N., Yang, X., Palmer, J.H., LaGrassa, A.L.,Juhas, P., Billings, S.J.L., Owen, J.S. *J. Am. Chem. Soc.* **2014**, *136*, 10645.

(32) Soloviev, V. N., Eichhofer, A., Fenske,D.,   Banin, U. *J. Am. Chem. Soc.* **2001**, *123*, 2354.

(33) Herron, N., Calabrese, J.C., Farneth, W.E., Wang, Y. *Science* **1993**, *259*, 1426.

(34) Soloviev, V. N., Eichhofer, A., Fenske,D.,   Banin, U. *J. Am. Chem. Soc.* **2000**, *122*, 2673.

(35) Del Ben, M., Havenith, R. W. A., Broer, R., Stener, Mauro *J. Phys. Chem. C* **2011**, *115*, 16782.

(36) Nguyen, K. A., Day, P. N., Pachter, R. *J. Phys. Chem. C* **2010**, *114*, 16197.

(37) Singh, T., Mountziaris, T. J., Maroudas, D. *Appl. Phys. Lett* **2012**, *100*, 053105.

(38) Munro, A. M.; Jen-La Plante, I.; Ng, M. S.; Ginger, D. S. *J. Phys. Chem. C* **2007**, *111*, 6220.

(39) Ji, X. H.; Copenhaver, D.; Sichmeller, C.; Peng, X. G. *J. Am. Chem. Soc.* **2008**, *130*, 5726.

(40) Munro, A. M.; Ginger, D. S. *Nano Lett.* **2008**, *8*, 2585.

(41) Anderson, N. C.; Hendricks, M. P.; Choi, J. J.; Owen, J. S. *J. Am. Chem. Soc.* **2013**, *135*, 18536.

(42) Frederick, M. T.; Amin, V. A.; Weiss, E. A. *J. Phys. Chem. Lett.* **2013**, *4*, 634.

(43) Koole, R.; Liljeroth, P.; Donega, C. D.; Vanmaekelbergh, D.; Meijerink, A. *J. Am. Chem. Soc.* **2006**, *128*, 10436.

(44) Koole, R.; Luigjes, B.; Tachiya, M.; Pool, R.; Vlugt, T. J. H.; Donega, C. D. M.; Meijerink, A.; Vanmaekelbergh, D. *J. Phys. Chem. C* **2007**, *111*, 11208.

(45) Buckley, J. J.; Couderc, E.; Greaney, M. J.; Munteanu, J.; Riche, C. T.; Bradforth, S. E.; Brutchey, R. L. *ACS Nano* **2014**, *8*, 2512.

(46) Haase, M.; Alivisatos, A. P. *J. Phys. Chem-Us* **1992**, *96*, 6756.

(47) Smith, A. M.; Mohs, A. M.; Nie, S. *Nat. Nanotechnol.* **2009**, *4*, 56.

(48) Simmonds, P. J.; Yerino, C. D.; Sun, M.; Liang, B. L.; Huffaker, D. L.; Dorogan, V. G.; Mazur, Y.; Salamo, G.; Lee, M. L. *ACS Nano* **2013**, *7*, 5017.

(49) Sadowski, T.; Ramprasad, R. *J. Phys. Chem. C* **2010**, *114*, 1773.

(50) Choi, C. L.; Koski, K. J.; Sivasankar, S.; Alivisatos, A. P. *Nano. Lett.* **2009**, *9*, 3544.

(51) Kasuya, A.; Sivamohan, R.; Barnakov, Y. A.; Dmitruk, I. M.; Nirasawa, T.; Romanyuk, V. R.; Kumar, V.; Mamykin, S. V.; Tohji, K.; Jeyadevan, B.; Shinoda, K.; Kudo, T.; Terasaki, O.; Liu, Z.; Belosludov, R. V.; Sundararajan, V.; Kawazoe, Y. *Nat. Mater.* **2004**, *3*, 99.

(52) Zhang, J. Y.; Wang, X. Y.; Xiao, M.; Qu, L.; Peng, X. *Appl. Phys. Lett.* **2002**, *81*, 2076.

(53) Wang, Y.; Herron, N. *Phys. Rev. B* **1990**, *42*, 7253.

(54) Meulenberg, R. W.; Jennings, T.; Strouse, G. F. *Phys. Rev. B* **2004**, *70*.

(55) Wang, F.; Wang, Y.; Liu, Y.-H.; Morrison, P. J.; Loomis, R. A.; Buhro, W. E. *Acc. Chem. Res.* **2015**, *48*, 13.

(56) Chen, P. E.; Anderson, N. C.; Norman, Z. M.; Owen, J. S. *J. Am. Chem. Soc.* **2017**, *139*, 3227.

(57) Zhou, Y.; Wang, F. D.; Buhro, W. E. *J. Am. Chem. Soc.* **2015**, *137*, 15198.

Chapter 2

Isolation of Amine Derivatives of (ZnSe)$_{34}$ and (CdTe)$_{34}$. Spectroscopic Comparisons of the (II-VI)$_{13}$ and (II-VI)$_{34}$ Magic-Size Nanoclusters

2.1 Introduction

In this chapter, we report the isolation and characterization of two new members of the family of stoichiometric II-VI magic-size nanoclusters, which are amine derivatives of $(ZnSe)_{34}$ and $(CdTe)_{34}$. Both were previously observed spectroscopically as reaction intermediates.[1] Both are shown here to be thermodynamically unstable with respect to the corresponding $(II-VI)_{13}$ nanoclusters, and to be readily converted to them. With these new derivatives in hand, we now have isolated derivatives of five of the six $(II-VI)_{34}$ nanoclusters, and four of the six $(II-VI)_{13}$ nanoclusters from the series II = Zn, Cd; VI = S, Se, Te. We show that these two series of nanoclusters exhibit remarkable spectroscopic homologies. Periodic trends in their formation and reactivity are also discussed.

Magic-size nancluster intermediates have been observed as reaction intermediates from the earliest semiconductor-nanoparticle syntheses.[2-5] In recent years, several magic-size nanoclusters have been isolated in discrete, single-size purity.[1, 6-11] The isolated examples suggest that these nanoclusters may occur in two types: stoichiometric and nonstoichiometric. In the II-VI semiconductor family, the II:VI ratio in the stoichiometric nanoclusters is strictly 1:1, as in the parent II-VI phases, and the nanoclusters bear only neutral L-type ligation. Examples are $[(CdSe)_{13}(\textit{n}-octylamine)_{13}]$[9] and $[(CdSe)_{34}(\textit{n}-octylamine)_{16}(di-\textit{n}-pentylamine)_2]$,[10] previously reported from our laboratory. The stoichiometric nanoclusters are theoretically predicted to have cage-like core structures,[12-14] but no crystal structures of these magic-size nanoclusters are yet available.

In contrast, the II:VI ratio in the nonstoichiometric magic-size nanoclusters deviate from 1:1, and are often enriched in the group-II ion (II:VI = 1.25-1.75).[7] Consequently these

nanoclusters possess both neutral L-type and anionic X-type ligation, the latter to balance charge. Examples are $[(Cd_{35}Se_{20})(benzoate)_{30}(n\text{-butylamine})_{30}]$[7] and $[(Cd_{35}Se_{28})(benzoate)_{14}(n\text{-dodecylamine})_{14}]$.[6] Several of the nonstoichiometric II-VI nanoclusters have been structurally characterized, and they exhibit close-packed, generally zinc blende, core structures.[7]

We note that the members of both families of magic-size nanoclusters, stoichiometric and nonstoichiometric, are compositionally well characterized. Even so, the two types exhibit puzzling spectroscopic similarities. Thus, the solution-phase absorption spectra of $[(Cd_{35}Se_{20})(benzoate)_{30}(n\text{-butylamine})_{30}]$[7] and $[(CdSe)_{13}(n\text{-octylamine})_{13}]$[9] are essentially indistinguishable, as are the corresponding spectra of $[(Cd_{42}Se_{28})(benzoate)_{28}(n\text{-dodecylamine})_{14}]$[6] and $[(CdSe)_{34}(n\text{-octylamine})_x]$.[11] The origins of this apparently anomalous spectroscopic behavior are not presently understood, and much remains to be learned about the structures and reactivities of magic-size semiconductor nanoclusters.

Our interest in magic-size II-VI nanoclusters began with the observation of $(CdSe)_{13}$ as a persistent reaction intermediate in the growth of CdSe quantum belts or nanoribbons.[15] We subsequently isolated $[(CdSe)_{13}(n\text{-octylamine})_{13}]$ and three other primary-amine derivatives as the first stoichiometric magic-size II-VI nanoclusters to be obtained in purity.[1, 9] We then isolated $[(CdSe)_{34}(n\text{-octylamine})_{16}(di\text{-}n\text{-pentylamine})_2]$ shortly after Sardar obtained $[(CdSe)_{34}(n\text{-octylamine})_x]$,[11] and showed that it was a potent low-temperature precursor to crystalline CdSe quantum platelets (at 25 °C).[10] Our interest then turned to the preparation of other $(II\text{-}VI)_{13}$ and $(II\text{-}VI)_{34}$ nanoclusters, and we reported isolation of amine derivatives of $(ZnSe)_{13}$, $(ZnTe)_{13}$, $(CdTe)_{13}$, $(ZnS)_{34}$, and $(CdS)_{34}$.[1] Several of these proved to be low-

temperature precursors to II-VI nanocrystals, and in the course of these studies we observed spectroscopic features corresponding to new $(ZnSe)_x$ and $(CdTe)_x$ nanoclusters that were closely analogous to those of $(CdSe)_{34}$. Here we describe the isolation, characterization, and reactivities of amine derivatives of $(ZnSe)_{34}$ and $(CdTe)_{34}$.

2.2 Experimental Section

2.2.1 Materials and General Procedures

Cadmium acetate dihydrate ($Cd(OAc)_2 \cdot 2H_2O$, >98%) was obtained from Sigma-Aldrich and Mallinckrodt. Zinc acetate dihydrate ($Zn(OAc)_2 \cdot 2H_2O$, 98%+) was obtained from Strem Chemicals. Selenourea (98%), Tri-n-octylphosphine (TOP, 97%), Super-Hydride (lithium triethylborohydride, 1.0 M solution in THF), *n*-Octylamine (99%), oleylamine (70%), di-*n*-pentylamine (mixture of isomers, 99%), di-*n*-octylamine (97%), toluene (CHROMASOLV ® for HPLC, 99.9%), acetonitrile (CHROMASOLV ® for HPLC, ≥99.9%), methanol (ACS Reagent, ≥ 99.8%), and cyclohexane (anhydrous, 99.5%) were obtained from Sigma-Aldrich. All reagents were used as received. TOPTe solution (1M in TOP) was prepared as previously reported. TEM sample grids (Cu with holey carbon film) were obtained from Ted Pella, Inc. All reaction mixtures were prepared under dry N_2 in a glove box and maintained under a dry-N_2 atmosphere prior to the later stages of purification.

2.2.2 Analyses

UV-visible spectra were obtained from a Varian Cary 100 Bio UV-visible spectrophotometer. XRD patterns were obtained from a Bruker d8 Advance X-ray Diffractometer. Low-resolution TEM images were obtained from a JEOL 2000FX microscope operating at 200 kV. IR spectra were obtained from Nicolette Nexus 470.

Elemental analyses (C, H, and N) were obtained from Galbraith Laboratories, Inc. (Knoxville, TN).

2.2.3 Preparation of a stock solution of tri-*n*-octylphosphine telluride (TOPTe)

The method developed previously in our laboratory was employed.[1]   A stock solution of TOPTe (1 M) was prepared by mixing Te powder (2.56 g, 20.0 mmol) in TOP (16.62 g, 20 mL) at room temperature.   The mixture was heated in a salt bath at 240 °C under N_2 for 2h to obtain a light-yellow solution.   The stock solution remained stable for at least 6 months when stored in a glovebox at room temperature.

2.2.4 Preparation of [(CdTe)$_{34}$(dioctylamine)$_{73}$]

In a typical synthesis, Cd(OAc)$_2$·2H$_2$O (33 mg, 0.12 mmol) was dissolved in di-*n*-octylamine (2.8 g, 18 mmol) in a septum-capped test tube, which was sealed by parafilm and then placed in a benchtop sonicator bath for 30 min to achieve dissolution.   The test tube was transferred to an oil bath and heated at 70 °C (for about 15 min).   A mixture of TOPTe (0.125 g, 1 M) and lithium triethylborohydride (0.05 g, 0.056 mmol, 1 M solution in THF) was prepared in a separate vial to generate a light-purple, milky dispersion, and then *n*-octylamine (0.6 g, 0.0046 mol) was added to form a dark-purple tellurium-precursor solution.

The tellurium-precursor was injected into the cadmium-precursor solution at 70 °C without stirring.   The colorless reaction mixture turned to light yellow immediately, viscous yellow in 5 s, and cloudy and bright yellowish within 3.5 min.   At this time, toluene (1 mL) and methanol (0.5 mL) were injected into the reaction mixture, which contained a dispersion of (CdTe)$_{34}$ nanoclusters, and the resulting bright yellow precipitate was separated by

18

centrifugation (4500 rpm, 5 min). The colorless supernatant was removed by syringe and discarded. The remaining bright yellow slush was redispersed in di-n-octylamine (1.5 mL) by vigorous shaking and set aside overnight.

The bright yellow, slushy [(CdTe)$_{34}$(di-n-octylamine)$_{73}$] was purified as follows. The test tube containing the yellow slush was opened to the atmosphere, toluene (1 mL) was added, the tube was recapped and shaken, and a bright yellow precipitate was again separated by centrifugation (1500 rpm, 3 min). This purification process was conducted three times in total, yielding [(CdTe)$_{34}$(di-n-octylamine)$_{73}$] as a yellowish-slushy solid (32 mg, 0.0012 mmol, 35% yield) after drying in vacuo for 2 h. Anal. Calcd for [(CdTe)$_{34}$(di-n-octylamine)$_{73}$]: C, 54.40; H, 9.99; N, 3.97. Found: C, 54.42; H, 10.05; N, 3.96. All values are given as percentages.

2.2.5 Preparation of [(CdTe)$_{34}$(n-octylamine)$_5$(di-n-pentylamine)$_{12}$]

The di-n-pentylamine derivative of (CdTe)$_{34}$ was synthesized under the same general conditions, except for the reaction solvent. Di-n-pentylamine, instead of di-n-octylamine, was used in all the steps above, to form [(CdTe)$_{34}$(n-octylamine)$_4$(di-n-pentylamine)$_{13}$] as a bright yellow slushy solid. Anal. Calcd for [(CdTe)$_{34}$(n-octylamine)$_4$(di-n-pentylamine)$_{13}$]: C, 18.15; H, 3.52; N, 2.22. Found: C, 19.48; H, 3.46; N, 2.19. All values are given as percentages.

2.2.6 Preparation of [(ZnSe)$_{34}$(n-octylamine)$_{29}$(di-n-octylamine)$_5$]

In a typical synthesis, Zn(OAc)$_2$·2H$_2$O (28 mg, 0.13 mmol) was dissolved in di-n-octylamine (2.8 g, 18 mmol) in a septum-capped test tube, which was sealed by parafilm and then placed in a benchtop sonicator bath for 10-40 min to achieve dissolution. The test tube was transferred to an oil bath and heated at 100 °C (for about 15 min). Selenourea (25 mg, 0.21 mmol) was combined with n-octylamine (0.6 g, 0.0046 mol) in a septum-capped vial and

19

then transferred to a benchtop sonicator (30 min) to achieve dissolution.

The selenium-precursor solution was injected into the cadmium-precursor solution at 100 °C without stirring. The colorless reaction mixture turned to pale orange immediately, and to cloudy and pale orange within 4 min. After a total reaction time of 4 min, the mixture was removed from the oil bath, selenium byproducts were scavenged from the $(ZnSe)_{34}$ dispersion by injection of TOP (0.5 mL), upon which the dispersion turned from pale orange to white. Toluene (1 mL) and methanol (0.5 mL) were injected into the reaction mixture and the resulting white $(ZnSe)_{34}$-containing precipitate was separated by centrifugation (1500 rpm, 5 min). The colorless supernatant was removed by syringe and discarded. The remaining white solid was redispersed in n-dioctylamine (1.5 mL) by vigorous shaking and set aside overnight.

The resulting white $[(ZnSe)_{34}(n\text{-octylamine})_{25}(\text{di-}n\text{-octylamine})_5]$ was purified as follows. The test tube containing the white solid was opened to the atmosphere, toluene (1 mL) was added, the tube was recapped and shaken, and a white precipitate was again separated by centrifugation (1500 rpm, 3 min). This purification process was conducted three times in total, yielding $[(ZnSe)_{34}(n\text{-octylamine})_{29}(\text{di-}n\text{-octylamine})_5]$ as a white solid (35 mg, 0.0037 mmol, 97% yield) after drying in vacuo for 4 h. Anal. Calcd for $[(ZnSe)_{34}(n\text{-octylamine})_{29}(\text{di-}n\text{-octylamine})_5]$: C, 37.99; H, 7.42; N, 4.83. Found: C, 38.21; H, 7.25; N, 4.82. All values are given as percentages.

2.2.7 Preparation of $[(ZnSe)_{34}(n\text{-octylamine})_x(\text{di-}n\text{-pentylamine})_{34-x}]$

The di-n-pentylamine derivative of $(ZnSe)_{34}$ was synthesized under the same general conditions, except for the reaction solvent. Di-n-pentylamine, instead of di-n-octylamine,

was used in all the steps above, to form $(ZnSe)_{34}(n\text{-octylamine})_x(\text{di-}n\text{-octylamine})_{34-x}$ as a white solid.

2.3 Results

2.3.1 Synthesis of (II-VI)$_{34}$ Nanoclusters

We previously prepared the magic-size nanoclusters $(ZnSe)_{13}$ and $(CdTe)_{13}$ at room temperature, and isolated them as $[(ZnSe)_{13}(\text{primary amine})_{13}]$ and $[(CdTe)_{13}(\text{primary amine})_{13}]$ derivatives.[1]   In that study, we also examined conversion of magic-size nanoclusters to crystalline, wurtzite-structured II-VI quantum platelets or quantum belts at the lowest possible temperatures.   Earlier work had established that conversion of CdSe magic-size nanoclusters in primary-amine, secondary-amine cosolvent mixtures reduced the reaction temperatures by about 50-60 °C in comparison to primary-amine solvents, and ultimately traced the temperature reduction to the intermediacy of $(CdSe)_{34}$, an especially potent nanocrystal precursor formed in the cosolvent mixtures.[10]   Thus, in the prior study of ZnSe and CdTe, we explored the generation and conversion of magic-size nanoclusters in primary-amine, secondary-amine cosolvent mixtures.

These experiments led to spectroscopic observations consistent with $(ZnSe)_{34}$ and $(CdTe)_{34}$ intermediates, respectively, in the formation of ZnSe and CdTe nanocrystals.[1]   Thus, monitoring of the generation of ZnSe magic-size nanoclusters in a cosolvent mixture at 100 °C revealed intermediate absorbances at 313, 294, and 280 nm that were consistent in position and intensity pattern with a putative $(ZnSe)_{34}$ intermediate.   These absorbances subsequently disappeared, and were replaced with those of ZnSe quantum platelets.   Similarly, monitoring

21

of the generation of CdTe magic-size nanoclusters in a cosolvent mixture at 70 °C gave intermediate absorbances at 448, 404, and 375 nm consistent with $(CdTe)_{34}$. These absorbances were subsequently replaced by those for CdTe quantum belts. Consequently, a major goal of the present study was to isolate and fully characterize amine derivatives of $(ZnSe)_{34}$ and $(CdTe)_{34}$.

As before, $(ZnSe)_{34}$ was generated by reaction of $Zn(OAc)_2(H_2O)_2$ and selenourea in an *n*-octylamine, di-*n*-octylamine cosolvent at 100 °C. Spectroscopic monitoring after 4 minutes of reaction time identified absorbances (at 315, 304, and 282 nm) near those previously assigned to $(ZnSe)_{34}$ (Figure 2.1a).[1] The high isolated yield achieved at this stage (see below) confirmed that the reaction was complete after 4 minutes. Monitoring was continued at 100 °C for a total of 2 h, during which $(ZnSe)_{34}$ remained the only spectroscopically detectable product (Figure 2.1b, c). (Conversion of $(ZnSe)_{34}$ to crystalline ZnSe quantum platelets required ca. 12 h at 100 °C.[1])
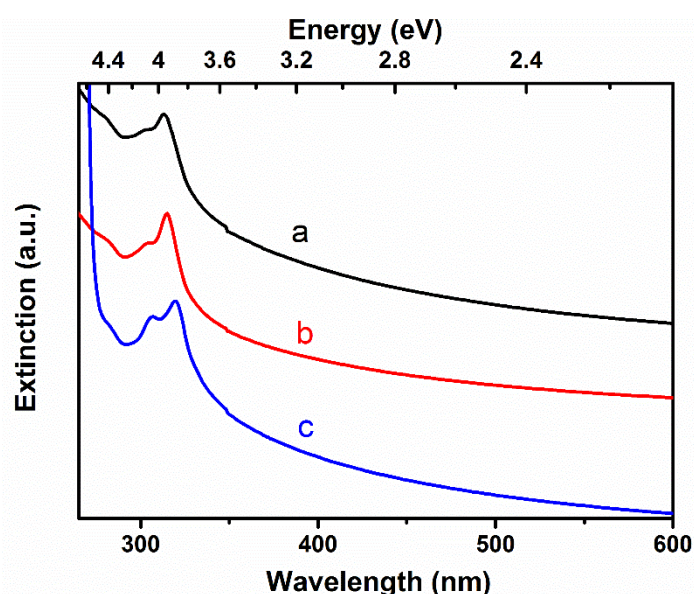
Figure 2.1. UV–visible spectral monitoring (in cyclohexane dispersion) during the synthesis of $(ZnSe)_{34}$ in an *n*-octylamine, di-*n*-octylamine cosolvent after (a) 4 min, (b) 1 h and (c) 2 h of reaction time.

After a reaction mixture (heated at 100 °C for 4 min) was allowed to cool to room temperature and stand overnight, the spectrum of $(ZnSe)_{34}$ persisted (Figure 2.2a). However, after the reaction mixture stood at room temperature for 2 – 7 days, the two prominent absorbances (at 292 and 281 nm) corresponding to $(ZnSe)_{13}$ were observed in the spectrum (Figure 2.2b).[1] This observation indicated that, like the relationship between $(CdSe)_{34}$ and $(CdSe)_{13}$,[10] $(ZnSe)_{34}$ was thermodynamically unstable with respect to $(ZnSe)_{13}$. Complete conversion of $(ZnSe)_{34}$ to $(ZnSe)_{13}$, in the reaction mixture, required 14 – 21 days (Figure 2.2c). However, addition of TOP at the conclusion of the synthesis, to scavenge unreacted selenourea and other selenium-containing byproducts, significantly slowed the conversion of $(ZnSe)_{34}$ to $(ZnSe)_{13}$. After TOP addition, the spectroscopic appearance of $(ZnSe)_{13}$ was delayed to one month.
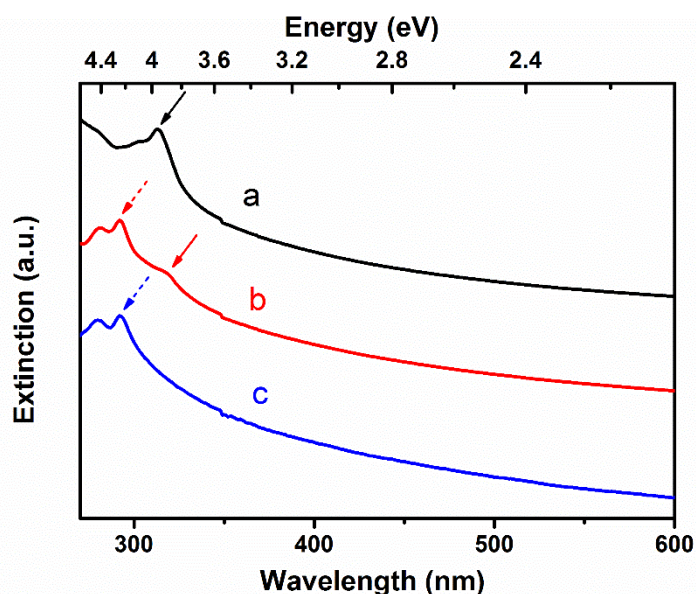
Figure 2.2. UV–visible spectral evolution upon spontaneous conversion of $(ZnSe)_{34}$ to $(ZnSe)_{13}$ in an *n*-octylamine, di-*n*-octylamine cosolvent at RT. The spectra were recorded after (a) overnight, (b) 2 days, and (c) 2 weeks. Solid arrows identify $(ZnSe)_{34}$ absorptions, and dashed arrows identify $(ZnSe)_{13}$ absorptions.

We previously reported that dispersion of $(CdSe)_{34}$ in cosolvent mixtures rich in secondary

amine slowed the conversion of $(CdSe)_{34}$ to $(CdSe)_{13}$.[10] Thus, upon precipitation of the

$(ZnSe)_{34}$ derivative from the initial n-octylamine, di-n-octylamine cosolvent, the solid was

redispersed in pure di-n-octylamine and allowed to stand overnight at room temperature.

Spectroscopic monitoring confirmed that no interconversion to $(ZnSe)_{13}$ had occurred under

these conditions. After purification, the derivative $[(ZnSe)_{34}(n\text{-octylamine})_{29}(\text{di-}n\text{-}$

$\text{octylamine})_5]$ was isolated in 94% yield, and characterized as described below. A di-n-

pentylamine derivative of $(ZnSe)_{34}$ was prepared and isolated similarly.

A derivative of $(CdTe)_{34}$ was prepared in an n-octylamine, secondary-amine cosolvent at

70 °C, from $Cd(OAc)_2(H_2O)_2$ and TOPTe/and Super-Hydride as the Te^{2-} source.[16] (Super-

Hydride is lithium triethylborohydride.) In some procedures di-n-pentylamine was employed

as the secondary-amine cosolvent, and in others di-n-octylamine. Spectroscopic monitoring

in the n-octylamine, di-n-pentylamine mixture identified absorbances (at 450, 405, and 374 nm)

near those previously assigned to $(CdTe)_{34}$ after 10 min of reaction (Figure 2.3a). However,

the absorption at 374 nm, which coincides with one of the absorbances of $(CdTe)_{13}$, was

observed to increase in intensity at 15 min of reaction time (Figure 2.3b), suggesting

interconversion of $(CdTe)_{34}$ to $(CdTe)_{13}$ was initiated on that timescale. A spectrum obtained

at 20 min of reaction time confirmed this interconversion (Figure 2.3c). This $(CdTe)_{34}$ to

$(CdTe)_{13}$ interconversion was even more rapid in a n-octylamine, di-n-octylamine cosolvent

(Figure 2.4). In both cosolvent systems, complete interconversion to $(CdTe)_{13}$ occurred in

reactions mixtures allowed to stand at room temperature overnight (Figure 2.5).
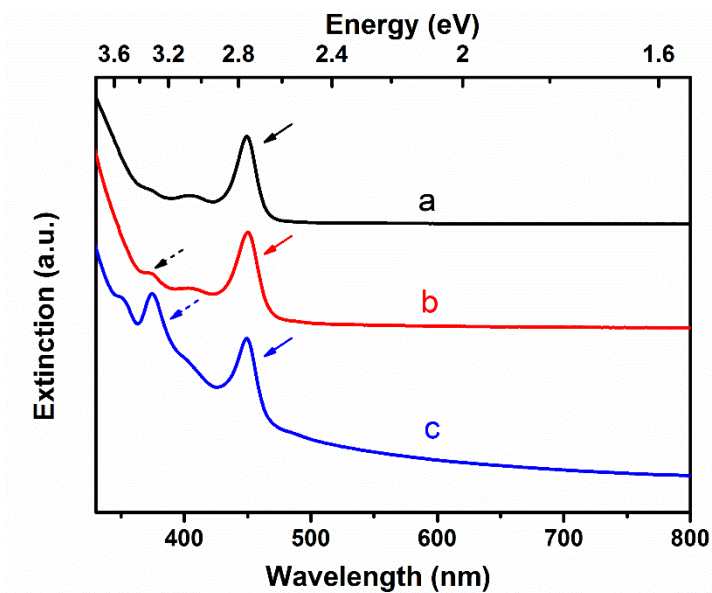
Figure 2.3. UV–visible spectral monitoring (in toluene dispersion) during the synthesis of $(CdTe)_{34}$ in an *n*-octylamine, di-*n*-pentylamine cosolvent after (a) 10 min, (b) 15 min, and (c) 25 min of reaction time. Solid arrows identify $(CdTe)_{34}$ absorptions, and dashed arrows identify $(CdTe)_{13}$ absorptions.
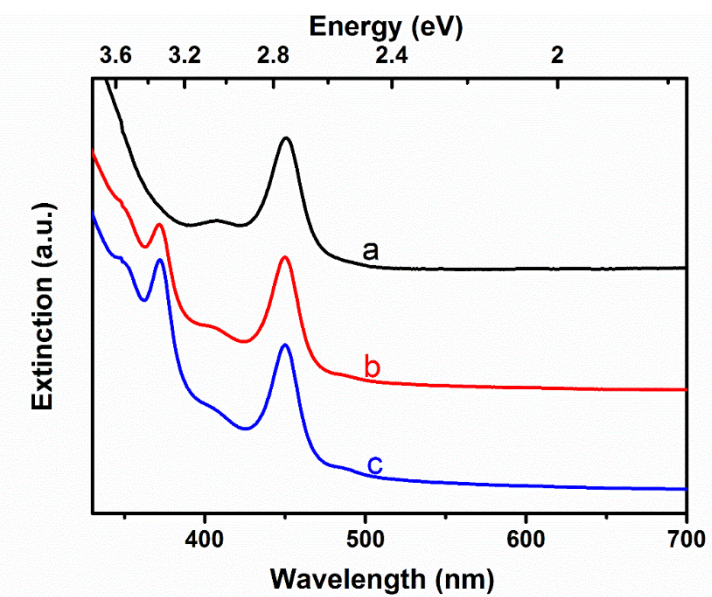
Figure 2.4. UV–visible spectral monitoring (in toluene dispersion) of $(CdTe)_{34}$ conversion in an *n*-octylamine, di-*n*-octylamine mixture at 70 °C after (a) 3 min, (b) 5 min and (c) 6 min as the reaction starts.
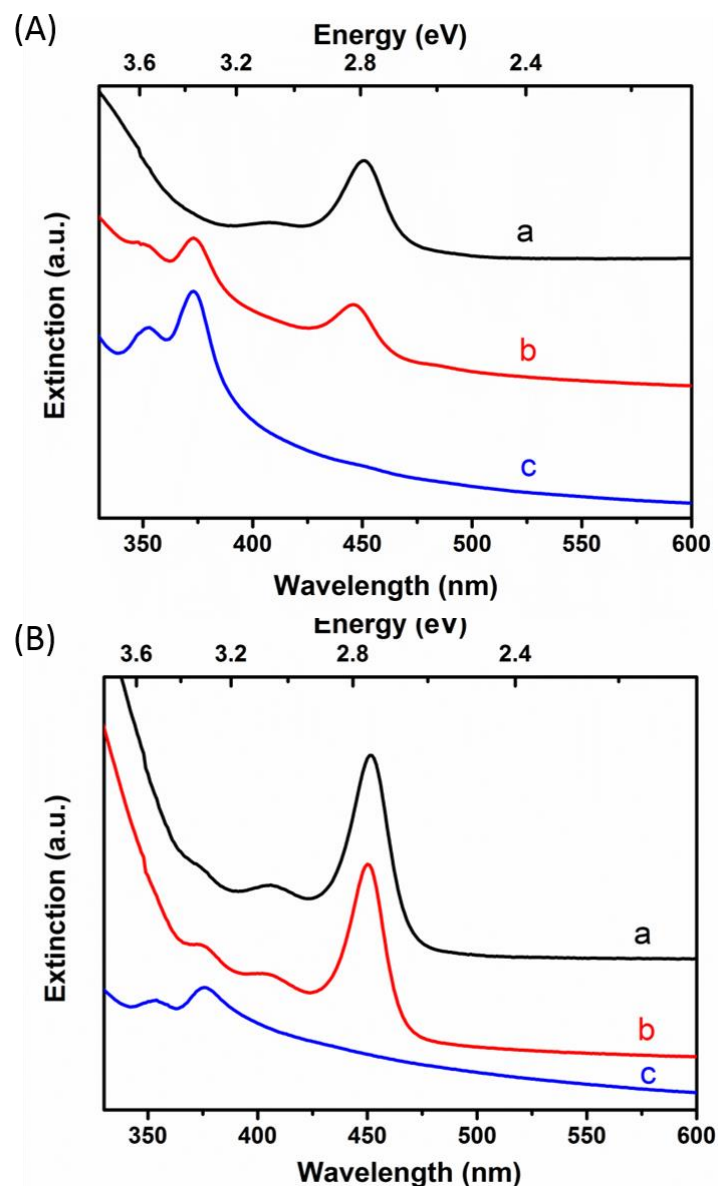
Figure 2.5. UV−visible spectral evolution upon transformation of (CdTe)$_{34}$ to (CdTe)$_{13}$ in an *n*-octylamine, secondary amine cosolvent at RT. (A) In an *n*-octylamine, di-*n*-octylamine mixture after (a) 3.5 min (at the reaction temperature of 70 °C, and then cooled to RT), (b) 3 h, and (c) 24 h. (B) In an *n*-octylamine, di-*n*-pentylamine mixture after (a) 10 min (at the reaction temperature of 70 °C, and then cooled to RT), (b) 3 h, and (c) 24 h.

A preparation of (CdTe)$_{34}$ conducted in a *n*-octylamine, di-*n*-octylamine cosolvent as described above was removed from heating after 3.5 min and washed with a mixture of toluene and methanol. (This purification step substantially slowed the interconversion of (CdTe)$_{34}$ to (CdTe)$_{13}$.) The (CdTe)$_{34}$ derivative so obtained was then redispersed in di-*n*-octylamine and

allowed to stand overnight.   No interconversion to $(CdTe)_{13}$ was spectroscopically detected after this redispersion.   After purification, the derivative $[(CdTe)_{34}(di-n\text{-}octylamine)_{73}]$ was isolated in 35% yield, and characterized as described below.   The di-n-pentylamine derivative of $(CdTe)_{34}$ was prepared and isolated similarly, in 39% yield.

2.3.2 Characterization of (II-VI)$_{34}$ Nanoclusters

Absorption spectra of isolated derivatives of $(ZnSe)_{34}$ and $(CdTe)_{34}$ are included in Figure 2.6.   We chose to include the spectra of the di-n-pentylamine derivatives, because they are better resolved than those of the corresponding di-n-octylamine derivatives (Figure 2.7).   The peak positions and intensities are also slightly dependent on the nature of the amine ligation. These spectra are consistent with those observed in the spectroscopic monitoring of the synthetic reaction mixtures (Figures 2.1 and 2.3).   Figure 2.6 compares the spectra of the $(ZnSe)_{34}$ and $(CdTe)_{34}$ to those of the other (II-VI)$_{34}$ derivatives that have been previously isolated.   These spectral comparisons are analyzed in the Discussion.
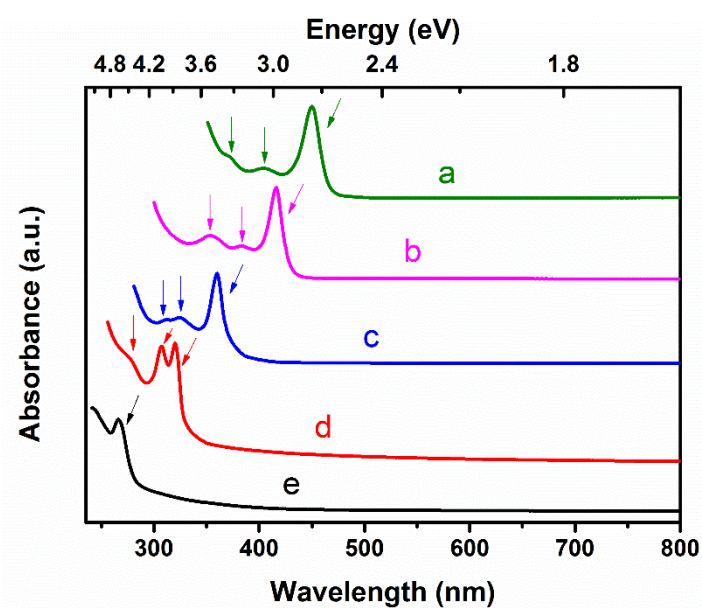
Figure 2.6.   UV–visible absorption spectra of five (II-VI)$_{34}$ derivatives: (a) $(CdTe)_{34}$, (b) $(CdSe)_{34}$, (c) $(CdS)_{34}$, (d) $(ZnSe)_{34}$, and (e) $(ZnS)_{34}$.

27
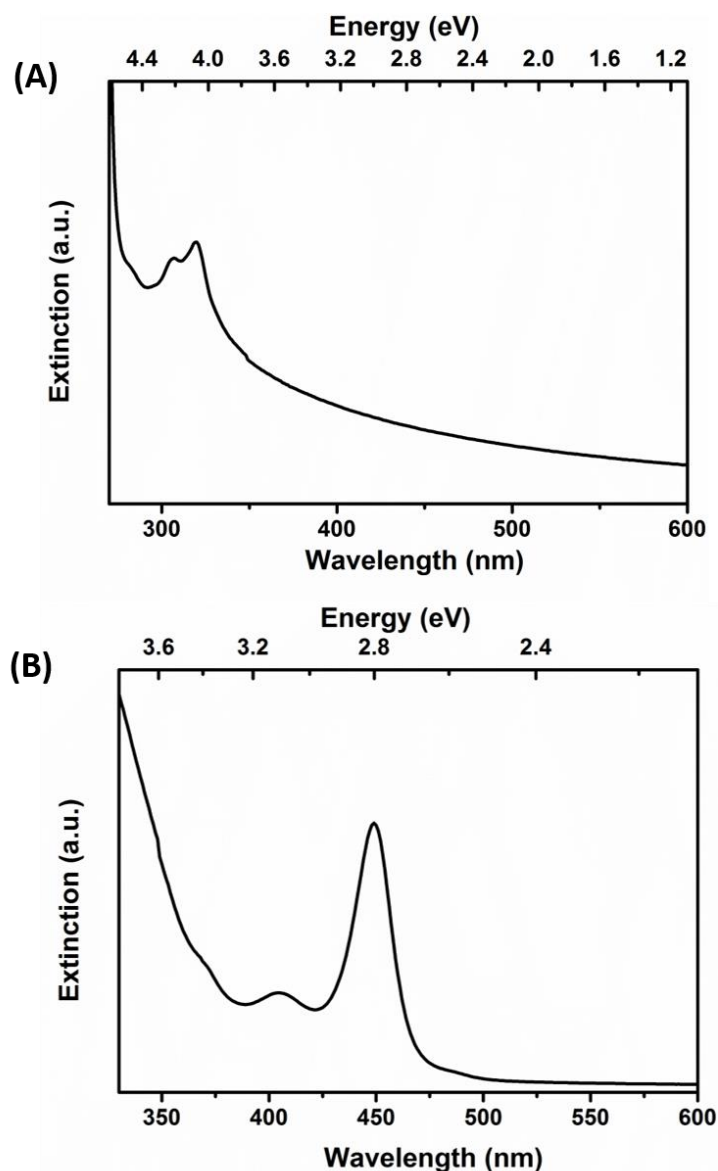
Figure 2.7. Absorption spectra of the isolated di-*n*-octylamine derivatives of (A) (ZnSe)$_{34}$ and (B) (CdTe)$_{34}$.

We next sought to characterize the isolated nanoclusters by IR spectroscopy. As all isolated derivatives were obtained from mixtures containing both primary and secondary amines, IR spectroscopy was expected to provide an initial indication of the actual ligation of the purified nanocluster products. We thus first identify the diagnostic features in the IR spectra of *n*-octylamine (Figure 2.8a) and di-*n*-octylamine (Figure 2.8b) to aid interpretation of the spectra of the isolated (ZnSe)$_{34}$ and (CdTe)$_{34}$ derivatives. The spectrum of *n*-octylamine (Figure 2.8a) contains antisymmetric and symmetric N–H stretches at 3367 and 3290 cm^{-1},

28

respectively, derived from the NH$_2$ group.   The H–N–H scissoring mode is a prominent, broad

peak at 1594 cm^{-1}.   The bending modes for CH$_2$ (methylene) and CH$_3$ (methyl) groups are

observed at 1467 and 1378 cm^{-1}, respectively.

In contrast, the IR spectrum of di-*n*-octylamine contains only a single N–H stretch (Figure

2.8b), at 3275 cm^{-1}, as secondary amines possess only one N–H bond.   This N–H stretching

feature is much weaker and broader than the corresponding antisymmetric and symmetric

features in primary amines (Figure 2.8a).   Moreover, there is no H–N–H scissoring mode in

the spectra of secondary amines, so that peak is absent in the spectrum of di-*n*-octylamine.

Consequently, the spectrum contains only the CH$_2$ (1465 cm^{-1}) and CH$_3$ (1378 cm^{-1}) bending

modes in that spectral region.   The IR spectrum of di-*n*-pentylamine is very similar to that of

di-*n*-octylamine.   Notably, in mixtures of *n*-octylamine and a secondary amine, the *n*-

octylamine is distinguished by the N–H stretching region (doublet) and H–N–H scissoring peak.

However there are no distinguishing IR features for the secondary amine in such mixtures.
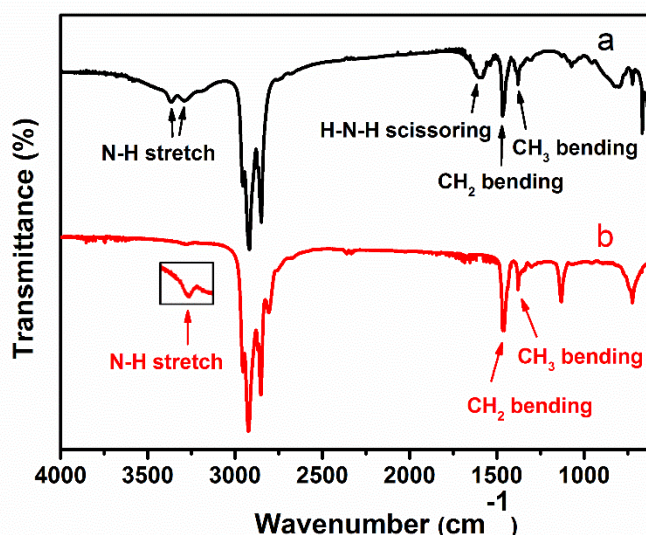
Figure 2.8. Infrared spectra (neat on KBr plates) of (a) *n*-octylamine, and (b) di-*n*-octylamine.   Features characteristic of N-H and C-H vibrations are identified by arrows.   The inset is a vertical expansion of the N-H region for di-*n*-octylamine.

We also briefly describe the key features of the IR spectra of the $Zn(OAc)_2 \cdot 2H_2O$ and $Cd(OAc)_2 \cdot 2H_2O$ starting materials employed (Figure 2.9), as IR spectroscopy is useful for characterizing the presence or absence of residual acetate groups in the nanocluster products. The characteristic absorptions of these carboxylate ligands are the antisymmetric and symmetric CO_2 stretches observed at 1556 and 1431 cm^{-1} in $Zn(OAc)_2 \cdot 2H_2O$, and at 1560 and 1419 cm^{-1} in $Cd(OAc)_2 \cdot 2H_2O$.[17] These antisymmetric and symmetric features are broad, strong, and of comparable intensities to one another in both cases (Figure 2.9).
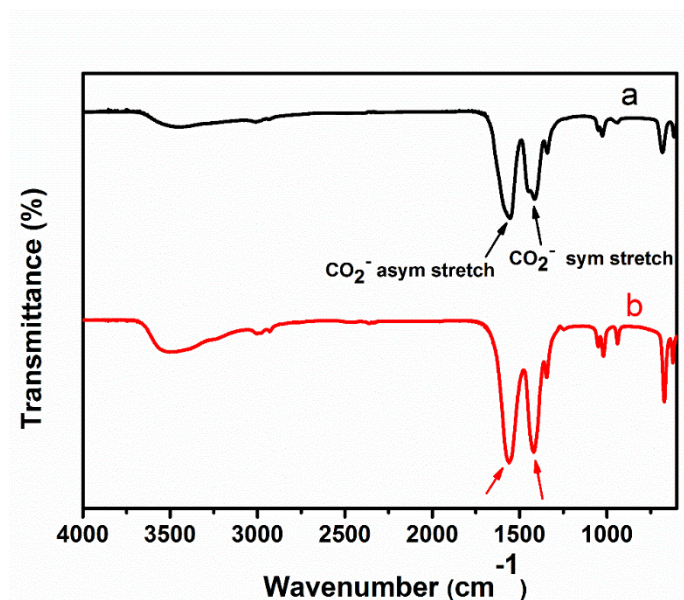
Figure 2.9. IR spectra of the $Zn(OAc)_2 \cdot 2H_2O$ (a) and $Cd(OAc)_2 \cdot 2H_2O$ (b) starting materials. Regions characteristic of the antisymmetric and symmetric CO_2 stretches are identified.

An IR spectrum of the $(ZnSe)_{34}$ prepared from an *n*-octylamine, di-*n*-octylamine cosolvent mixture, and isolated after dispersion in di-*n*-octylamine for several h, is shown in Figure 2.10a. This spectrum contained prominent features at 3203 (antisym. N–H stretch), 3120 (sym. N–H stretch), and 1577 cm^{-1} (H–N–H scissoring), assignable to primary-amine ligation by *n*-octylamine. Notably, the absorbances at 1577 and 1463 cm^{-1} assigned to H–N–H scissoring

and CH$_2$ bending, respectively, are not of similar breadth and intensity, and are thus inconsistent with residual acetate groups.
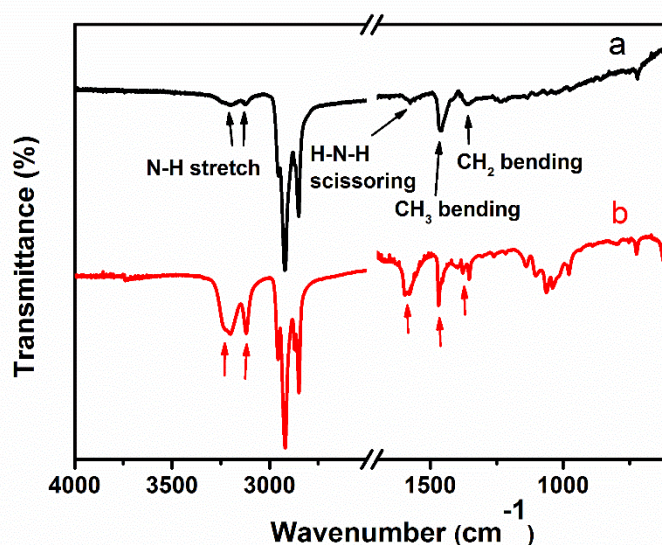
Figure 2.10. Infrared spectra (samples deposited on KBr plates) of (ZnSe)$_{34}$ prepared and isolated from (a) *n*-octylamine, di-*n*-octylamine and (b) *n*-octylamine, di-*n*-pentylamine cosolvent mixtures (see text). Features characteristic of N-H and C-H vibrations are identified by arrows. Those of *n*-octylamine were observed in both (a) and (b).

The presence of di-*n*-octylamine in the isolated (ZnSe)$_{34}$ derivative could not be determined by IR spectroscopy (see above). However, mass-spectral analysis revealed the existence of both *n*-octylamine and di-*n*-octylamine ligands (Figure 2.11a). Elemental analysis afforded the composition [(ZnSe)$_{34}$(*n*-octylamine)$_{29\pm6}$(di-*n*-octylamine)$_{5\pm4}$] for the isolated derivative. The synthetic yield of 94%, reported above, was determined from this formula. The elemental-analysis data were also inconsistent with the presence of residual acetate in this nanocluster derivative.

An IR spectrum of the (ZnSe)$_{34}$ derivative prepared in an *n*-octylamine, di-*n*-pentylamine cosolvent mixture, and isolated after dispersion in di-*n*-pentylamine for several h, is shown in Figure 2.10b. The N–H stretches and H–N–H scissoring peak corresponding to *n*-octylamine

31

were observed in the spectrum. Absorptions for residual acetate were absent. Mass spectrometry confirmed the presence of both *n*-octylamine and di-*n*-pentylamine ligands (Figure 2.11b). Elemental-analysis data gave a composition [(ZnSe)$_{34}$(*n*-octylamine)$_x$(di-*n*-pentylamine)$_{34-x}$], indicating a total of 34 amine ligands, but were insufficiently precise to determine the ratio of primary and secondary amine ligands. To calculate an approximate synthetic yield, an average formula of [(ZnSe)$_{34}$(*n*-octylamine)$_{29}$(di-*n*-pentylamine)$_5$] was assumed, to match that of the *n*-octylamine, di-*n*-octylamine derivative described above. On that basis, the synthetic yield was approximated as 42%.
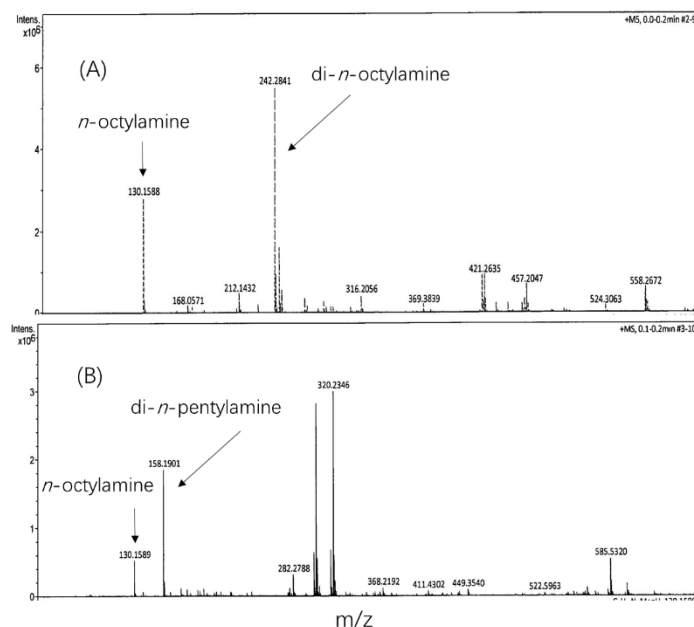
Figure 2.11. Mass spectrum of surface ligands liberated upon acid digestion of the isolated (ZnSe)$_{34}$ derivatives prepared from (A) *n*-octylamine, di-*n*-octylamine and (B) *n*-octylamine, di-*n*-pentylamine cosolvent. The peaks for both *n*-octylamine and di-*n*-octylamine (A) and *n*-octylamine and di-*n*-pentylamine (B) are labeled.

An IR spectrum of the (CdTe)$_{34}$ derivative prepared in an *n*-octylamine, di-*n*-pentylamine cosolvent mixture, and isolated after dispersion in di-*n*-pentylamine for several h, is shown in Figure 2.12a. As for the previous derivatives, the N–H stretches and H–N–H scissoring peak corresponding to *n*-octylamine were observed in the spectrum. Absorptions for residual

32

acetate were also absent.   A formula $[(CdTe)_{34}(n\text{-octylamine})_{4\pm3}(\text{di-}n\text{-pentylamine})_{13\pm3}]$ was

most consistent with the elemental-analysis data.   On that basis, a synthetic yield of 39% was

calculated.
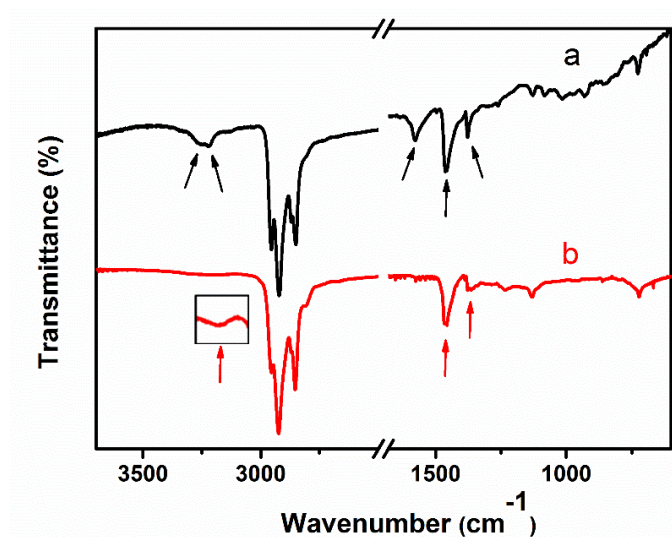
Figure 2.12.   Infrared spectra (samples deposited on KBr plates) of $(CdTe)_{34}$ prepared and isolated from (a) *n*-octylamine, di-*n*-pentylamine and (b) *n*-octylamine, di-*n*-octylamine cosolvent mixtures (see text).   Note that *n*-octylamine features were observed in (a), but absent in (b).   The inset is a vertical expansion of the N-H stretching region in (b).

Characterization of the $(CdTe)_{34}$ derivative prepared in an *n*-octylamine, di-*n*-octylamine

derivative, and isolated after dispersion in di-*n*-octylamine for several h, proved to be

challenging.   The results obtained differed significantly from those of the other derivatives

reported here, and described previously.[1,10]   An IR spectrum of this derivative is recorded in

Figure 2.12b.   Surprisingly, the features for *n*-octylamine, its two N–H stretches and H–N–H

scissoring peak, were absent from the spectrum.   The weak, broadened N–H feature observed

(inset to Figure 2.12b) was consistent with di-*n*-octylamine ligation.   Elemental analysis

suggested the formula $[(CdTe)_{34}(\text{di-}n\text{-octylamine})_{73\pm13}]$ for this isolated derivative.   On this

basis, a synthetic yield of 35% was determined.   However, we considered the very large

number of di-*n*-octylamine ligands per each $(CdTe)_{34}$ nanocluster indicated from multiple sets

33

of elemental-analysis data to be suspiciously high and possibly incorrect.

We next considered that this $(CdTe)_{34}$ derivative may have been contaminated by a di-*n*-octylamine-hydrate byproduct.   In the course of our work using di-*n*-octylamine, which is a liquid having a melting point of 13-16 °C, we observed films of di-*n*-octylamine to solidify to a white powder upon exposure to the atmosphere for 10 min.   Powder X-ray diffraction (XRD) patterns of the white solid (Figure 2.13) contained sharp reflections indicative of a crystalline phase.   Single-crystal X-ray crystallography established the solid to be a hydrate of formula di-*n*-octylamine·0.5H$_2$O (Figure 2.14).
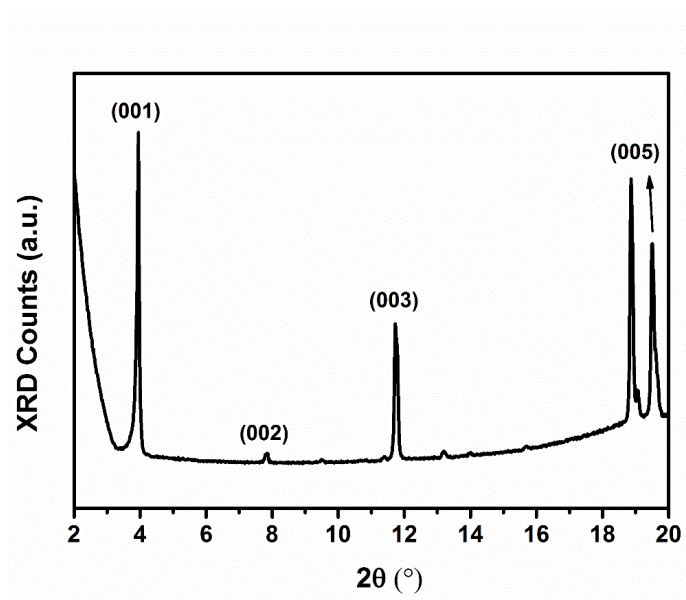
Figure 2.13.   Low-angle powder X-ray diffraction (XRD) pattern of the solid obtained upon exposure of di-*n*-octylamine to the atmosphere for 10 min.   Sharp reflections are indicative of a crystalline phase having a *d* spacing of 2.24 nm.
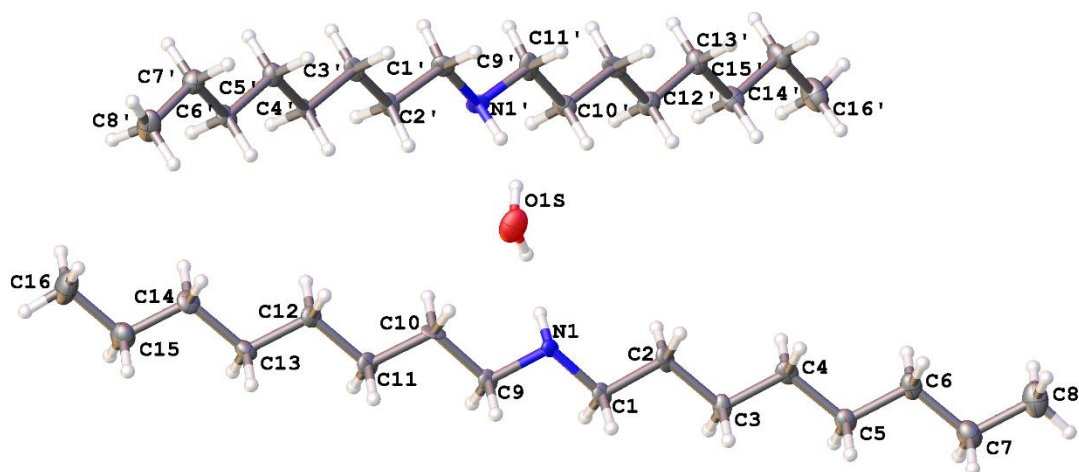
Figure 2.14. View from the x-ray crystal structure of the di-*n*-octylamine hydrate. The formula was determined to be di-*n*-octylamine·$0.5H_2O$.

Because we observed reflections corresponding to the amine-hydrate phase in XRD data collected from the di-*n*-octylamine derivative of $(CdTe)_{34}$, (Figure 2.15a, b) we considered that it might be an impurity consistently introduced into the $(CdTe)_{34}$ derivative during isolation and handling. Such an impurity could account for the comparatively large amount of di-*n*-octylamine determined in elemental analyses of the $(CdTe)_{34}$ derivative. Moreover, we observed that di-*n*-octylamine·$0.5H_2O$ exhibited low solubility in toluene, such that it may not have been removed by toluene washes in our standard purification procedure.
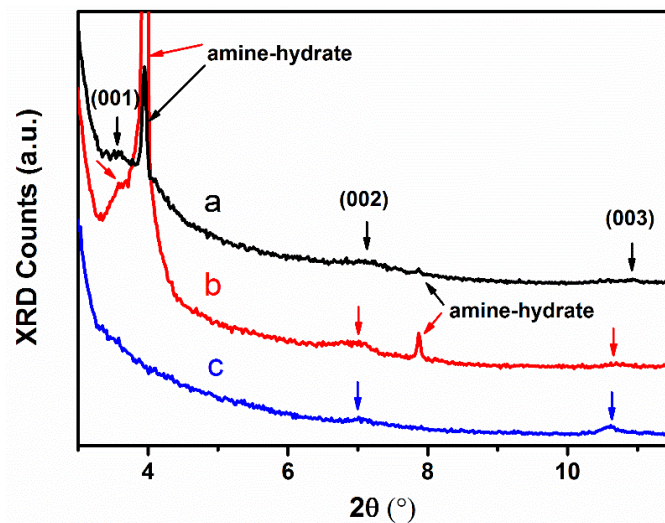
Figure 2.15. Low-angle XRD data collected from (CdTe)$_{34}$ derivatives (a) as-synthesized in an *n*-octylamine, di-*n*-octylamine cosolvent, (b) isolated after dispersion in di-*n*-octylamine for several h, and (c) isolated material after washing with THF. Reflections (see labels) corresponding to the amine-hydrate phase (see text) were observed in (a) and (b). All samples contained weak reflections corresponding to *n*-octylamine-bilayer mesophases having *d* spacings in the range of 2.43 to 2.52 nm (labeled 001, 002, and 003).

We subsequently determined that the amine-hydrate di-*n*-octylamine·0.5H$_2$O had higher solubility in THF than in toluene. Consequently, the isolated (CdTe)$_{34}$ derivative was washed with toluene/THF mixtures, and re-analyzed by XRD, which showed that the amine-hydrate phase had been removed by the new washing procedure (Figure 2.15c). Elemental analyses were obtained of the washed specimens, which indicated the formula [(CdTe)$_{34}$(di-*n*-octylamine)$_{74\pm6}$], within experimental error of the originally determined stoichiometry. We are thus unable to explain the surprisingly large amount of di-*n*-octylamine in this isolated nanocluster.

The LDI mass spectra of (ZnSe)$_{34}$ and (CdTe)$_{34}$ derivatives are given in Figure 2.16. These contained prominent peaks at m/z 4915 and 8170, close to the m/z of bare nanoclusters (CdTe)$_{34}$ and (ZnSe)$_{34}$, which are at 4908 and 8160. The discrepancies between the experimental and

36

calculated m/z values require further investigation. A sequence of fragment ions, including those corresponding to $(ZnSe)_{33}$, $(ZnSe)_{13}$, and $(CdTe)_{33}$ are also observed in the spectra.
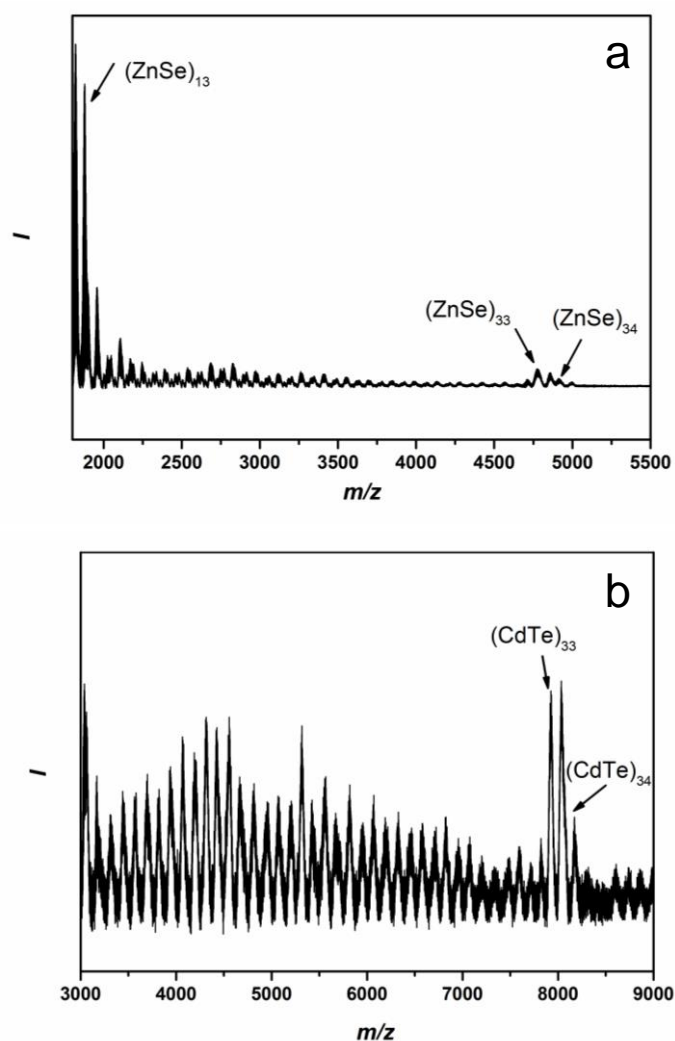
Figure 2.16. LDI mass spectra of (a) $[(ZnSe)_{34}(n\text{-octylamine})_{29\pm6}(\text{di-}n\text{-octylamine})_{5\pm4}]$ and (b) $[(CdTe)_{34}(n\text{-octylamine})_{4\pm3}(\text{di-}n\text{-pentylamine})_{13\pm3}]$. The peaks for the magic-size ZnSe and CdTe nanoclusters and labeled.

2.3.3 Formation Pathway

Previous studies established that magic-size II-VI nanoclusters prepared in primary-amine solvents grow within spontaneously formed, lamellar, amine-bilayer mesophase templates.[1,15] However, the formation pathways for magic-size II-VI nanoclusters in mixed, primary-amine,

secondary-amine cosolvent mixtures were not previously elucidated.[1,10]   Consequently, we examined the nanocluster products synthesized in this study by low-angle XRD, both before and after their redispersion in a secondary amine for nanocluster stabilization, to determine the presence or absence of spontaneous mesophase templating in their formation pathways.

As described in the Experimental Section, the synthesis of the $(ZnSe)_{34}$ derivatives proceeded by combination of a di-*n*-alkylamine solution of $Zn(OAc)_2(H_2O)_2$ with an *n*-octylamine solution of selenourea at 100 °C.   Consequently, we obtained a low-angle XRD pattern of $Zn(OAc)_2(H_2O)_2$ in di-*n*-octylamine to determine if an amine-bilayer mesophase was formed in this precursor solution.   The resulting XRD pattern (Figure 2.17a) contained no reflections assignable to such a mesophase.   (The pattern *did*, however, contain reflections for the amine-hydrate phase described above.)   We similarly obtained low-angle XRD patterns of $Cd(OAc)_2(H_2O)_2$ in both di-*n*-octylamine (Figure 2.17b) and di-*n*-pentylamine (Figure 2.17c). No evidence for the formation of amine-bilayer mesophases was found in either pattern.   We thus conclude that amine-bilayer mesophases form spontaneously when Zn or Cd salts are dissolved in *primary* amines (such as *n*-octylamine),[1,15] but not when such salts are dissolved in the corresponding *secondary* amines.
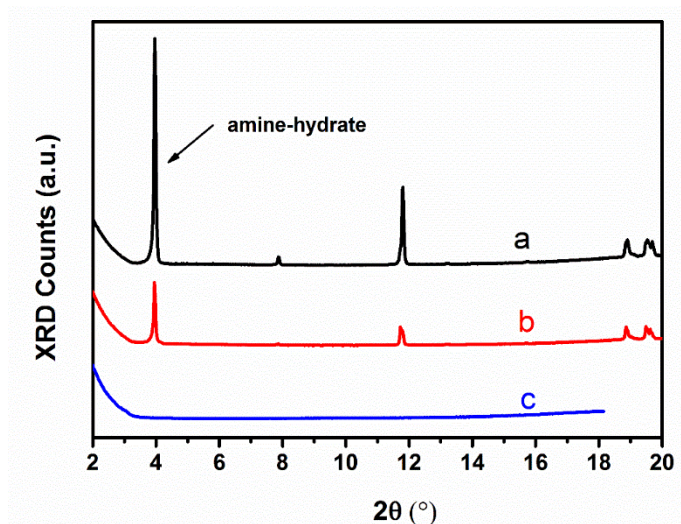
Figure 2.17. Low-angle XRD patterns of (a) $Zn(OAc)_2(H_2O)_2$ and (b) $Cd(OAc)_2(H_2O)_2$ in di-*n*-octylamine, and (c) $Cd(OAc)_2(H_2O)_2$ in di-*n*-pentylamine. The XRD pattern contained no reflections assignable to amine-bilayer mesophases. (The pattern *did*, however, contain reflections for the amine-hydrate phase shown in Figures 2.13 and 2.14.)

Although by our reaction protocol, the $Zn(OAc)_2(H_2O)_2$ precursor was initially dissolved in the secondary-amine, *non*-template-forming cosolvent, and the selenourea precursor in the primary-amine *n*-octylamine cosolvent, clear evidence was found for the intermediacy of *n*-octylamine bilayer mesophases in the synthesis of $(ZnSe)_{34}$, for both secondary-amine cosolvents employed. Low-angle XRD patterns (Figure 2.18a, b) of the $(ZnSe)_{34}$ products as-synthesized in an *n*-octylamine, di-*n*-octylamine cosolvent, and after subsequent standing in di-*n*-octylamine, contained reflections corresponding to *n*-octylamine bilayer mesophases, having *d* spacings of 2.76 and 2.81 nm, respectively. The range of *d* spacings typical of *n*-octylamine bilayer mesophases is 2.5 – 2.8 nm.[18]

39
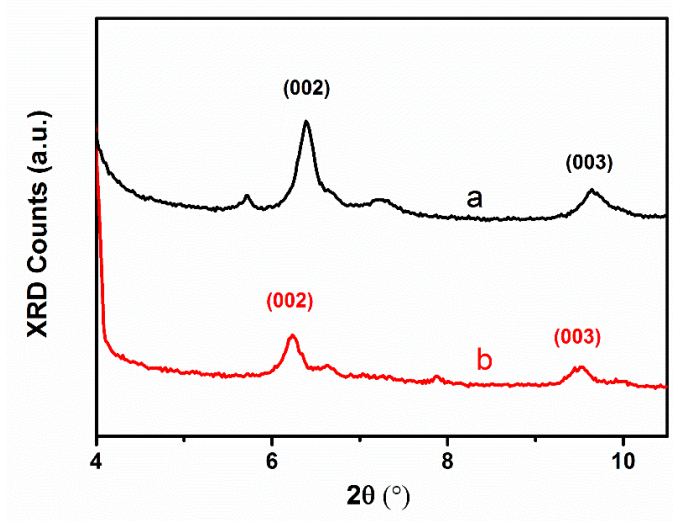
Figure 2.18. Low-angle XRD data collected from $(ZnSe)_{34}$ derivatives (a) as-synthesized in an *n*-octylamine, di-*n*-octylamine cosolvent, and (b) isolated after dispersion in di-*n*-octylamine for several h. Both samples contained reflections corresponding to *n*-octylamine-bilayer mesophases (*d* spacings (a) 2.76 and (b) 2.81 nm).

Similar results were obtained when di-*n*-pentylamine was used as the secondary-amine cosolvent (Figure 2.19); in these cases the lamellar *d* spacings obtained were 2.74 and 2.68 nm, respectively. We speculate that the amine-bilayer mesophases formed upon combination of the primary- and secondary-amine precursor solutions, under the reaction conditions employed. If correct, then the $(ZnSe)_{34}$ nanoclusters grew within the *n*-octylamine bilayer templates, as was previously demonstrated for the growth of $(CdSe)_{13}$ in various primary-amine solvents.[9,19]
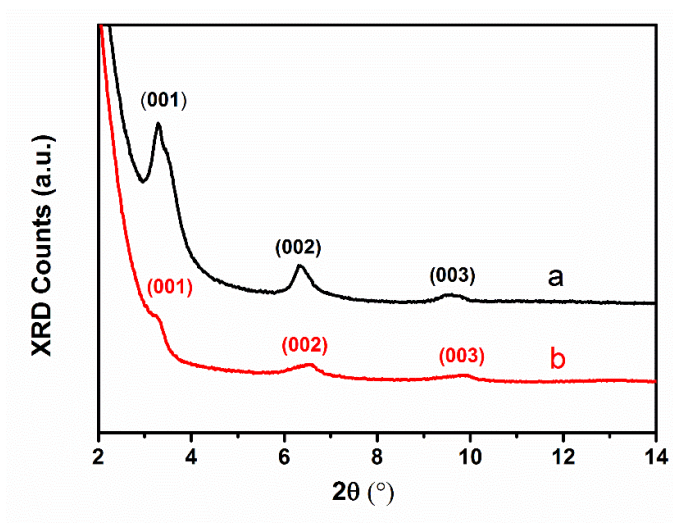
Figure 2.19. Low-angle XRD data collected from $(ZnSe)_{34}$ derivatives (a) as-synthesized in an *n*-octylamine, di-*n*-pentylamine cosolvent, and (b) isolated after dispersion in di-*n*-pentylamine for several h. Both samples contained reflections corresponding to *n*-octylamine-bilayer mesophases (*d* spacings (a) 2.74 and (b) 2.68 nm).

40

Similar low-angle XRD analyses were conducted for $(CdTe)_{34}$ derivatives prepared in *n*-octylamine, secondary-amine cosolvents. Recall that amine-bilayer mesophases were not observed upon dissolution of the precursor $Cd(OAc)_2(H_2O)_2$ in either di-*n*-octylamine (Figure 2.17b) or di-*n*-pentylamine (Figure 2.17c). As above, the $(CdTe)_{34}$ syntheses were conducted by combining $Cd(OAc)_2(H_2O)_2$ in a secondary amine with the tellurium-precursor mixture in *n*-octylamine at the reaction temperature (in these cases, at 70 °C).

The low-angle XRD data for the $(CdTe)_{34}$ derivative prepared in the *n*-octylamine, di-*n*-octylamine cosolvent were presented in Figure 2.15a-c, and discussed above in conjunction with the purification of this derivative. The as-synthesized (Figure 2.15a), di-*n*-octylamine-stabilized (Figure 2.15b), and THF-washed (Figure 2.15c) specimens all contained weak reflections corresponding to *n*-octylamine bilayer mesophases, having lamellar *d* spacings ranging from 2.43 to 2.52 nm. The low-angle XRD data for the $(CdTe)_{34}$ derivative prepared in the *n*-octylamine, di-*n*-pentylamine cosolvent (Figure 2.20) were consistent with *n*-octylamine bilayer mesophases having lamellar *d* spacings of 2.42 nm in the as-synthesized specimen, and 2.40 nm in the di-*n*-pentylamine-stabilized specimen. As for $(ZnSe)_{34}$ (see above), we surmise that the $(CdTe)_{34}$ nanoclusters grew within *n*-octylamine bilayer templates, which formed spontaneously under reaction conditions upon combination of the primary- and secondary-amine precursor solutions. The results suggest that the $(ZnSe)_{34}$ and $(CdTe)_{34}$ nanocluster syntheses all follow amine-bilayer templated pathways.[15]
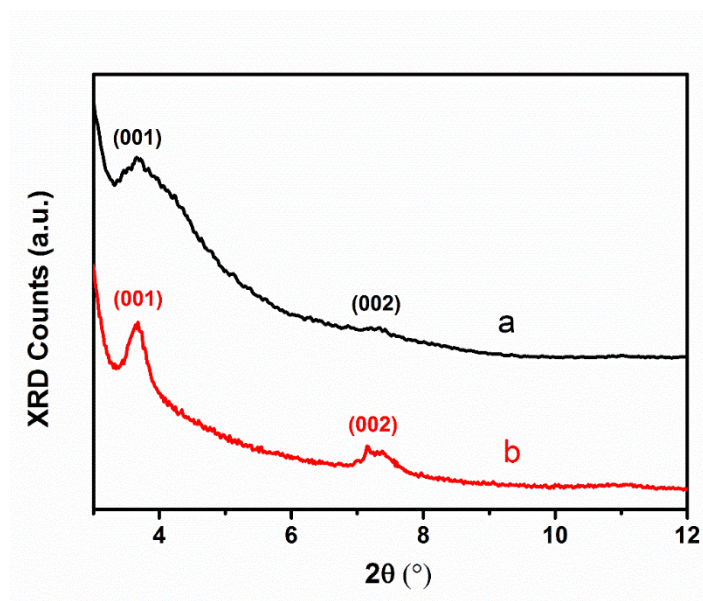
Figure 2.20. Low-angle XRD patterns collected from the $(CdTe)_{34}$ derivative prepared in the *n*-octylamine, di-*n*-pentylamine cosolvent; (a) as synthesized, (b) isolated after dispersion in di-*n*-pentylamine for several h. Both specimens contained reflections corresponding to *n*-octylamine-bilayer mesophases having *d* spacings of 2.42 (a) and 2.40 nm (b).

2.4 Discussion

2.4.1 Stoichiometries of Amine-Ligated $(II-VI)_{34}$ Nanoclusters

In prior work from our laboratory, primary-amine derivatives of $(CdSe)_{13}$,[9,19] $(CdTe)_{13}$,[1] $(ZnSe)_{13}$,[1] and $(ZnTe)_{13}$[1] were isolated and characterized. For $(CdSe)_{13}$, derivatives with four different primary amines were obtained.[19] In each of these cases, the stoichiometry determined is $(II-VI)_{13}(primary\ amine)_{13}$. We surmise that all group-II atoms are on the surface of the $(II-VI)_{13}$ nanoclusters, and each is coordinated to one primary-amine ligand. Consequently, hollow cage-like structures are suggested for all of these nanoclusters by their common stoichiometry, as has been theoretically predicted.[12, 20]

We previously determined the stoichiometries of three amine derivatives of $(II-VI)_{34}$ nanoclusters, $[(CdSe)_{34}(n\text{-octylamine})_{16}(di\text{-}n\text{-pentylamine})_2]$,[10] $(CdS)_{34}(n\text{-butylamine})_{18}$,[1] and $(ZnS)_{34}(n\text{-butylamine})_{34}$.[1] The observed $(Cd\text{-VI})_{34}L_{18}$ stoichiometries may indicate that not

all Cd atoms are on the surfaces of these nanoclusters, or that some of the surface Cd atoms remain unligated. The observed $(ZnS)_{34}L_{34}$ stoichiometry may reflect the higher Lewis acidity of Zn relative to Cd, and/or a different nanocluster structure.

The preparation of mixed-ligand nanoclusters from cosolvent mixtures, as in the present work, complicates the determination of stoichiometry from the C, H, N analyses. In general, we used the N data to determine the total number of ligands per nanocluster, and then either the C and N data or the H and N data to determine the primary-amine, secondary-amine stoichiometry. The error bars in the determined stoichiometries of the various amine derivatives reflect the scatter in the multiple C, H, N analyses determined for each. We note that these derivatives have so far not yielded to purification by crystallization or other standard methods, and thus have been purified by washing only. Thus, the lability of the ligands in these nanoclusters makes the collection of precise elemental analyses challenging, by introducing a source of scatter into the experimental data.

As reported above, the stoichiometries of the $(ZnSe)_{34}$ derivatives determined from the combination of IR spectroscopy, mass spectrometry, and C, H, N analysis are $[(ZnSe)_{34}(n\text{-octylamine})_{29\pm6}(\text{di-}n\text{-octylamine})_{5\pm4}]$ and $[(ZnSe)_{34}(n\text{-octylamine})_{x}(\text{di-}n\text{-pentylamine})_{34-x}]$. For the latter, di-$n$-pentylamine derivative, the overall ligand stoichiometry is determined from the N data, but the remaining data preclude a precise measurement of x. We note that the overall stoichiometries of $(ZnSe)_{34}L_{34-y}L'_{y}$ are consistent with that previously determined for $(ZnS)_{34}(n\text{-butylamine})_{34}$.[1]

Similarly, the stoichiometry determined for $[(CdTe)_{34}(n\text{-octylamine})_{4\pm3}(\text{di-}n\text{-pentylamine})_{13\pm3}]$ is close in overall stoichiometry to those previously determined for

[(CdSe)$_{34}$(*n*-octylamine)$_{16}$(di-*n*-pentylamine)$_2$],[10] and (CdS)$_{34}$(*n*-butylamine)$_{18}$.[1] In contrast, as discussed above, the measured [(CdTe)$_{34}$(di-*n*-octylamine)$_{74\pm6}$] stoichiometry differs substantially from those of the other (Cd-VI)$_{34}$ derivatives. Moreover, the low-angle XRD data for this derivative suggests some incorporation of *n*-octylamine (Figure 2.15c), which was not detected by IR spectroscopy or the C, H, N analyses. Thus, we are less confident of the stoichiometry measured for this derivative, and suggest that the *n*-octylamine, di-*n*-pentylamine derivative be used for preparative purposes.

2.4.2 Conversion of (II-VI)$_{34}$ derivatives to (II-VI)$_{13}$ derivatives

The results reported above establish that, as amine derivatives, the (ZnSe)$_{34}$ and (CdTe)$_{34}$ nanoclusters are thermodynamically unstable with respect to the corresponding (ZnSe)$_{13}$ and (CdTe)$_{13}$ nanocluster derivatives. These observations parallel our previous report of the spontaneous rearrangement of (CdSe)$_{34}$ derivatives to (CdSe)$_{13}$ derivatives.[10] Thus, in all three of these cases, the (II-VI)$_{34}$ derivatives are kinetic products of the syntheses, and the corresponding (II-VI)$_{13}$ derivatives are the thermodynamic products (under conditions that preclude their conversion to II-VI nano*crystals*).

The (II-VI)$_{34}$ nanoclusters in these three (CdSe, ZnSe, and CdTe) families are also shown to be kinetically stabilized in the presence of *secondary* amines, whereas their conversion to (II-VI)$_{13}$ nanoclusters is accelerated in mixtures rich in a *primary* amine.[10] The roles of the primary and secondary amines in these interconversion processes have not been determined. Prior studies with (CdSe)$_{34}$ derivatives established that stabilization by a secondary amine was not a mere dilution effect.[10] Dilution of the primary-amine component of a cosolvent mixture by an inert solvent did not afford stabilization of (CdSe)$_{34}$ with respect to (CdSe)$_{13}$. We

speculate that primary amines may function as ripening agents that stabilize small intermediate clusters that exchange $(II\text{-}VI)_n$ units between nanoclusters of differing sizes, thus facilitating the interconversion of $(II\text{-}VI)_{34}$ to $(II\text{-}VI)_{13}$. We further speculate that secondary-amine ligation may provide steric protection against exchange of $(II\text{-}VI)_m$ units in binary collisions of nanoclusters.

The facile interconversion of $(CdTe)_{34}$ to $(CdTe)_{13}$ under our synthetic conditions is responsible for the low isolated yields of the $(CdTe)_{34}$ derivatives (35-39%). The synthetic yields of the $(II\text{-}VI)_{34}$ and $(II\text{-}VI)_{13}$ derivatives reported from our laboratory are generally above 90%. However, the reaction times for the synthesis of $(CdTe)_{34}$ derivatives must be cut short to prevent interconversion to $(CdTe)_{13}$. Such interconversion might be further slowed by discovery of the appropriate secondary amine or other cosolvent to kinetically stabilize $(CdTe)_{34}$, which may increase the synthetic yields.

2.4.3 Summary of Isolated $(II\text{-}VI)_x$ Nanoclusters

Table 2.1 lists the 12 congeneric $(II\text{-}VI)_{13}$ and $(II\text{-}VI)_{34}$ nanoclusters corresponding to II = Zn, Cd and VI = S, Se, Te. As the table shows, with the results in the present report, we have now isolated 9 of the 12 cases as amine derivatives. Only three of these nanoclusters, derivatives of $(ZnS)_{13}$, $(CdS)_{13}$, and $(ZnTe)_{34}$ have so far evaded isolation.

As we have discussed extensively here, the $(II\text{-}VI)_{34}$ derivatives are generally kinetic products that convert to the thermodynamically stable $(II\text{-}VI)_{13}$ with time. Consequently, we might expect $(ZnS)_{34}$ and $(CdS)_{34}$ derivatives to eventually convert to $(ZnS)_{13}$ and $(CdS)_{13}$ derivatives, respectively, although to date we have not observed such interconversions to occur. The absorption features for $(ZnS)_{13}$ may be sufficiently high in energy (see below) to

complicate their detection.   Even so, the conditions for interconversions to $(ZnS)_{13}$ and $(CdS)_{13}$ derivatives may yield to further study.

In our prior work, primary-amine derivatives of $(ZnTe)_{13}$ were prepared in primary-amine solvents at 50 °C, which are conditions that would likely favor the interconversion of a putative kinetic product $(ZnTe)_{34}$ to $(ZnTe)_{13}$.   Alternatively, reaction conditions designed to arrest the synthesis at $(ZnTe)_{34}$, and to stabilize this nanocluster, may ultimately be accessible.

2.4.4 Trends in Stabilities and Spectroscopic Properties of $(II\text{-}VI)_x$ Nanoclusters

In a previous study we demonstrated that $(II\text{-}VI)_{34}$ derivatives of all five stoichiometries (Table 2.1) were thermally unstable with respect to growth of two-dimensional nanocrystals, either quantum platelets or belts, of the corresponding semiconductor phase.   Remarkably, these thermal conversions occurred over a wide temperature range of $0 - 100$ °C, which depended on stoichiometry (Figure Table 2.2).   The thermal stabilities of the $(II\text{-}VI)_{34}$ derivatives increased from $(Cd\text{-}VI)_{34}$ to $(Zn\text{-}VI)_{34}$, and from $(II\text{-}S)_{34}$ to $(II\text{-}Te)_{34}$, as shown in Table 2.2.   Thus, the trends in the thermal stabilities of the $(II\text{-}VI)_{34}$ derivatives appear to be periodic trends.

Table 2.1. Twelve congeneric $(II\text{-}VI)_{13}$ and $(II\text{-}VI)_{34}$ nanoclusters, where II = Zn or Cd, and VI = S, Se, or Te. Amine derivatives of nine of these nanoclusters were previously reported (as cited), or are reported here (†). Derivatives of three of these nanoclusters are presently unavailable (*).

$(ZnS)_{13}$*	$(CdS)_{13}$*
$(ZnS)_{34}$[1]	$(CdS)_{34}$[1]
$(ZnSe)_{13}$[1]	$(CdSe)_{13}$[9]
$(ZnSe)_{34}$†	$(CdSe)_{34}$[10]
$(ZnTe)_{13}$[1]	$(CdTe)_{13}$[1]
$(ZnTe)_{34}$*	$(CdTe)_{34}$†

*Unavailable derivatives (congeners)

†Described in this work

Table 2.2. Thermal-conversion temperatures for converting $(II\text{-}VI)_{34}$ derivatives to the corresponding nanocrystalline semiconductor phases. The thermal stabilities of the $(II\text{-}VI)_{34}$ derivatives increase from $(Cd\text{-}VI)_{34}$ to $(Zn\text{-}VI)_{34}$, and from $(II\text{-}S)_{34}$ to $(II\text{-}Te)_{34}$.

Increasing T

ZnS 100 ℃	CdS 0 ℃
ZnSe 100 ℃	CdSe 25 ℃
ZnTe* 120-150 ℃ *FAILED*	CdTe 70 ℃

Increasing T

*Conditions for converting $(ZnTe)_{34}$ derivatives to ZnTe were not identified.

Figure 2.6 shows the absorption spectra of the di-*n*-pentylamine-containing derivatives of

(ZnSe)$_{34}$ and (CdTe)$_{34}$, along with other amine derivatives of (II-VI)$_{34}$ nanoclusters that we

previously reported.[1,10]   Significant homology is evident in the Figure 2.6 spectral comparison.

The (Cd-IV)$_{34}$ derivatives exhibit a strong, lowest-energy peak and two smaller, higher-energy

features.   The (ZnSe)$_{34}$ derivatives also exhibit three comparable features, although the

second feature is nearly as strong as the lowest-energy peak.   The spectrum of the (ZnS)$_{34}$

derivative is shifted to sufficiently high energy that only the lowest-energy feature is resolved.

Notably, the spectra of these (II-VI)$_{34}$ derivatives are ordered energetically in the precise

sequence of the band gaps of the corresponding bulk semiconductor phases (see Table 2.3).

Moreover, the lowest-energy feature in the spectra of the (II-VI)$_{34}$ nanoclusters scales linearly

with the bulk band gap, as is shown in the plot in Figure 2.21a.   This spectroscopic behavior

is consistent with the (II-VI)$_{34}$ derivatives constituting a congeneric family of iso-

stoichiometric nanoclusters.

Table 2.3.   Band gaps of bulk II-VI semiconductor phases.[21]

Bulk Semiconductor (structure)	Band Gap (eV) (temperature, K)
CdTe (zinc blende)	1.49 (300)
CdSe (wurtzite)	1.75 (293)
CdS (wurtzite)	2.49 (293)
ZnTe (zinc blende)	2.28 (293)
ZnSe (wurtzite)	2.83 (300)
ZnS (wurtzite)	3.80 (300)
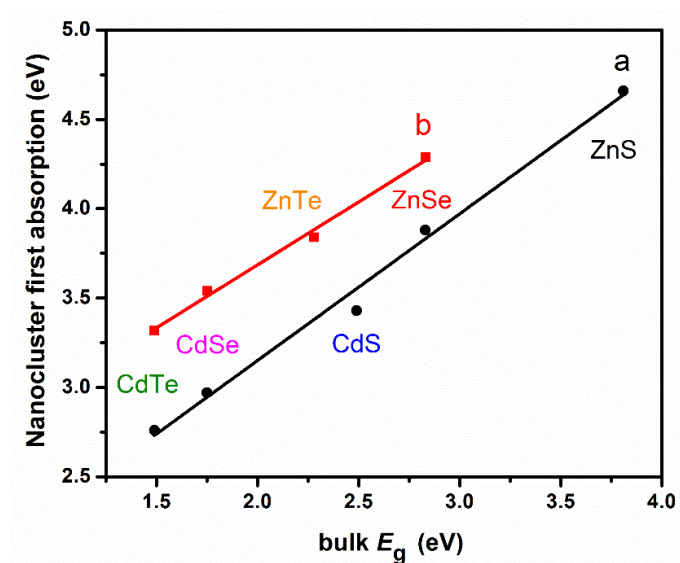
Figure 2.21. Plots of the first (lowest-energy) absorption peak in (a) (II-VI)$_{34}$ and (b) (II-VI)$_{13}$ derivatives versus the band gap of the corresponding bulk semiconductor phase. The slopes of the linear fits are (a) 0.82 ± 0.04 and (b) 0.70 ± 0.04.

For comparison, the spectra of the available (II-VI)$_{13}$ derivatives are shown in Figure 2.22. Characteristic of these spectra is a low-energy doublet feature in each. Again, the energetic ordering of these spectra accords with the bulk band gaps of the corresponding bulk semiconductor phases (Figure 2.21b). As for the (II-VI)$_{34}$ derivatives, the lowest-energy peak in these spectra scales linearly with the bulk band gap (Figure 2.21a). The spectroscopic homology and energetic ordering among the (II-VI)$_{13}$ and (II-VI)$_{34}$ families identifies each as congeneric series of iso-stoichoimetric nanoclusters.
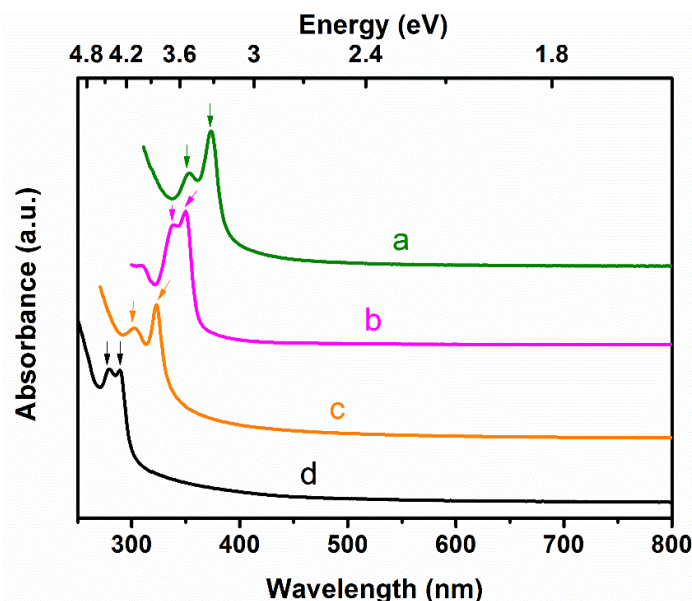
Figure 2.22. UV–visible absorption spectra of four (II-VI)$_{13}$ derivatives: (a) (CdTe)$_{13}$, (b) (CdSe)$_{13}$, (c) (ZnTe)$_{13}$, and (d) (ZnSe)$_{13}$.

2.5 Conclusions

Two new (II-VI)$_{34}$ nanoclusters were isolated as amine derivatives in this work, which had been previously observed spectroscopically as reaction intermediates. Among the derivatives obtained, [(ZnSe)$_{34}$(*n*-octylamine)$_{29\pm6}$(di-*n*-octylamine)$_{5\pm4}$] and [(CdTe)$_{34}$(*n*-octylamine)$_{4\pm3}$(di-*n*-pentylamine)$_{13\pm3}$] were fully characterized, and possessed stoichiometries similar to previously isolated amine derivatives of (II-VI)$_{34}$ nanoclusters.[1,10] Both (ZnSe)$_{34}$ and (CdTe)$_{34}$ were thermodynamically unstable with respect to (ZnSe)$_{13}$ and (CdTe)$_{13}$, as was previously demonstrated for (CdSe)$_{34}$ with respect to (CdSe)$_{13}$.[10] With the isolation of these new nanocluster derivatives, nine of the twelve nanoclusters in the (II-VI)$_{13}$ and (II-VI)$_{34}$ series (II = Zn, Cd; VI = S, Se, Te) have now been obtained.[1,9,10,19] The compelling spectroscopic homologies existing for these series establish them to be congeneric families of II-VI nanoclusters.

50

2.6 References

(1) Wang, Y. Y.; Zhou, Y.; Zhang, Y.; Buhro, W. E. *Inorg. Chem.* **2015**, *54*, 1165.

(2) Fojtik, A.; Weller, H.; Koch, U.; Henglein, A. *Ber. Bunsenges.phys. Chem.* **1984**, *88*, 969.

(3) Peng, Z. A.; Peng, X. G. *J. Am. Chem. Soc.* **2002**, *124*, 3343.

(4) Soloviev, N. V.; Eichhofer, A.; Fenske, D.; Banin, U. *J. Am. Chem. Soc.* **2001**, *123*, 2354.

(5) Cumberland, S. L.; Hanif, K. M.; Javier, A.; Khitrov, G. A.; Strouse, G. F.; Woessner, S. M.; Yun, C. S. *Chem. Mater.* **2002**, *14*, 1576.

(6) Cossairt, B. M.; Owen, J. S. **2011**, *23*, 3114.

(7) Beecher, A. N.; Yang, X. H.; Palmer, J. H.; LaGrassa, A. L.; Juhas, P.; Billinge, S. J. L.; Owen, J. S. *J. Am. Chem. Soc.* **2014**, *136*, 10645.

(8) Gary, D. C.; Flowers, S. E.; Kaminsky, W.; Petrone, A.; Li, X.; Cossairt, B. M. *J. Am. Chem. Soc.* **2016**, *138*, 1510.

(9) Wang, Y.; Liu, Y.-H.; Zhang, Y.; Wang, F.; Kowalski, P. J.; Rohrs, H. W.; Loomis, R. A.; Gross, M. L.; Buhro, W. E. *Angew. Chem. Int. Ed.* **2012**, *51*, 6154.

(10) Wang, Y. Y.; Zhang, Y.; Wang, F. D.; Giblin, D. E.; Hoy, J.; Rohrs, H. W.; Loomis, R. A.; Buhro, W. E. *Chem. Mater.* **2014**, *26*, 2233.

(11) Dolai, S.; Nimmala, P. R.; Mandal, M.; Muhoberac, B. B.; Dria, K.; Dass, A.; Sardar, R. *Chem. Mater.* **2014**, *26*, 1278.

(12) Nguyen, K. A.; Day, P. N.; Pachter, R. *J. Phys. Chem. C* **2010**, *114*, 16197.

(13) Del Ben, M.; Havenith, R. W. A.; Broer, R.; Stener, M. *J. Phys. Chem. C* **2011**, *115*, 16782.

(14) Singh, T.; Mountziaris, T. J.; Maroudas, D. *Appl. Phys. Lett.* **2012**, *100*, 053105.

(15) Liu, Y.-H.; Wang, F.; Wang, Y.; Gibbons, P. C.; Buhro, W. E. *J. Am. Chem. Soc.* **2011**, *133*, 17005.

(16) Zhang, J.; Jin, S.; Fry, H. C.; Peng, S.; Shevchenko, E.; Wiederrecht, G. P.; Rajh, T. *J. Am. Chem. Soc.* **2011**, *133*, 15324.

(17) Ishioka, T.; Shibata, Y.; Takahashi, M.; Kanesaka, I.; Kitagawa, Y.; Nakamura, K. T. *Spectrochim. Acta A* **1998**, *54*, 1827.

(18) Morrison, P. J.; Loomis, R. A.; Buhro, W. E. *Mater.* **2014**, *26*, 5012.

(19) Wang, Y. Y.; Liu, Y. H.; Zhang, Y.; Kowalski, P. J.; Rohrs, H. W.; Buhro, W. E. *Inorg. Chem.* **2013**, *52*, 2933.

(20) Nguyen, K. A.; Pachter, R.; Day, P. N. *J. .Chem. Theory and Comput.* **2013**, *9*, 3581.

(21) Madelung, O. *Semiconductors-basic data*; Springer-Verlag: Berlin, 1996.

Chapter 3

Large Exciton-Energy Shifts by Reversible Surface Exchange in 2D II-VI Nanocrystals

3.1 Introduction

In this chapter, we elucidate the contributions of lattice strain and confinement dimension to the effective band-gap changes in 2D CdSe and CdS nanocrystals upon exchange between L-type and Z-type surface passivation (Figure 3.1). We show that the reversible shifts in the absorption spectra between L-type and Z-type passivation have roughly equal contributions from changes in strain and dimensionality with $Cd(oleate)_2$ as the Z-type passivation. The smaller reversible shifts observed with $Zn(oleate)_2$ as the Z-type passivation are due entirely to changes in the strain states of the nanocrystals. The results establish that the $Cd(oleate)_2$ passivation couples to the electronic structure of the nanocrystal core, increasing the confinement dimension (box size), whereas, as expected, the $Zn(oleate)_2$ passivation does not.
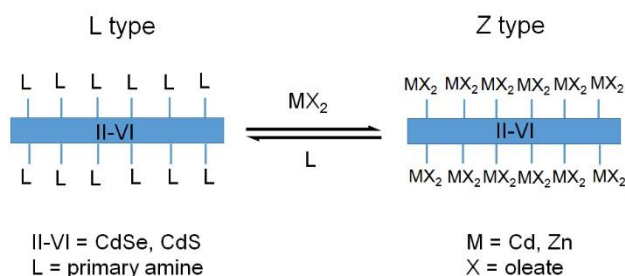
Figure 3.1. Exchange of Z and L-type surface passivation in 2D II-VI nanocrystals.

3.2 Experimental Section

3.2.1 Materials and General Procedures

Cadmium acetate dihydrate ($Cd(OAc)_2 \cdot 2H_2O$, >98%) was obtained from Sigma-Aldrich and Mallinckrodt. Zinc acetate dihydrate ($Zn(OAc)_2 \cdot 2H_2O$, 98%+) was obtained from Strem

Chemicals.   *n*-Octylamine (99%), oleylamine (70%), 1-octadecene (90%), oleic acid (90%), toluene (CHROMASOLV ® for HPLC, 99.9%), methanol (ACS Reagent, ≥ 99.8%), and dichloromethane (CHROMASOLV ® for HPLC, 99.8%) were obtained from Sigma-Aldrich. All reagents were used as received.   TEM sample grids (Cu with holey carbon film) were obtained from Ted Pella, Inc.

The {CdSe[*n*-octylamine]$_x$} quantum belts (QBs)[1] and {CdS[*n*-octylamine]$_p$} quantum platelets (QPs)[2] were prepared as previously reported.   All synthetic procedures were conducted under the ambient atmosphere unless otherwise indicated.

3.2.2 Characterization Method

UV-visible spectra were obtained from a Perkin Elmer Lambda 950 UV/Vis spectrometer or a Varian Cary 100 Bio UV-visible spectrophotometer.   Photoluminescence (PL) spectra were collected using a Varian Cary Eclipse fluorescence spectrophotometer.   XRD patterns were obtained from a Bruker d8 Advance X-ray Diffractometer.   Low-resolution TEM images were obtained from a JEOL 2000FX microscope operating at 200 kV.   IR spectra were obtained from a Perkin Elmer Spectrum BX FT-IR System.   Elemental analyses (Table 3.1; C, H, and N) were obtained from Galbraith Laboratories, Inc. (Knoxville, TN).

Table 3.1. Elemental-analysis data collected from several specimens from different synthetic batches (see Results). Each analytical specimen of {CdSe[*n*-octylamine]$_{0.53}$} or {CdSe[Cd(oleate)$_2$]$_{0.19}$} was approximately 18-22 mg, and each washing step was conducted with approximately 3 mL of solvent. The values in parentheses indicate the number of washing steps.

{CdSe[*n*-octylamine]$_{0.53}$}	%C	%H	%N	Washing Procedure
Calcd	19.59	3.90	2.86	
Found (1)	21.35	4.02	3.21	toluene (6×)
Found (2)	30.77	5.49	2.69	toluene (6×)
Found (3)	19.37	3.66	2.79	toluene/methanol (3×), toluene (3×)
Found (4)	18.20	3.41	2.60	toluene/methanol (3×), toluene (3×)
{CdSe[Cd(oleate)$_2$]$_{0.19}$}				
Calcd	25.70	3.95	0	
Found (1)	33.05	5.14	<0.5	toluene/methanol (3×)
Found (2)	26.12	3.68	<0.5	toluene (5×)
Found (3)	26.04	3.84	<0.5	toluene/methanol (1×), toluene (3×)
Found (4)	25.95	3.80	<0.5	toluene/methanol (1×), toluene (3×)

3.2.3 Preparation of an anhydrous Cd(oleate)$_2$ solution and Zn(oleate)$_2$ dispersion

Cd(oleate)$_2$ solution: In a typical procedure Cd(OAc)$_2$·2H$_2$O, (69 mg, 0.26 mmol) and oleic acid (147 mg, 0.52 mmol) were dissolved in 1-octadecene (1.5 g) in a septum-capped test tube, and transferred to a 120 °C oil bath for 20 min to achieve a colorless, viscous solution. The tube was then shaken vigorously a few times, and heated under vacuum (200 mTorr) at 120 °C for 20 min to remove water and acetic acid. The concentration of the resulting Cd(oleate)$_2$ solution was determined to be 0.11 M by integration against an internal standard using ^{1}H NMR.

Zn(oleate)$_2$ dispersion: In a typical procedure, Zn(OAc)$_2$·2H$_2$O, (57 mg, 0.26 mmol) and oleic acid (147 mg, 0.52 mmol) were dissolved in 1-octadecene (1.5 g) in a septum-capped test tube, and transferred to a 120 °C oil bath for 30 min. The solution became colorless and viscous, with a small amount of white solid remaining on the bottom of the tube. The tube was then heated under vacuum (200 mTorr) at 120 °C for 20 min to remove water and acetic acid. The clear and colorless supernatant was transferred to another test tube and the remaining solid was discarded. The Zn(oleate)$_2$ solution remained colorless while hot, but a white precipitate formed, giving a cloudy suspension, upon cooling. The mixture was shaken before use to provide a uniform dispersion. An effective concentration of 0.13 M was assumed by the reagent quantities employed.

3.2.4 Preparation of a Stock Mixture of {CdSe[*n*-octylamine]$_x$} QBs and {CdS[*n*-octylamine]$_p$} QPs

{CdSe[*n*-octylamine]$_x$} QBs: The synthesis of {CdSe[*n*-octylamine]$_x$} QBs was conducted

on the same scale as that previously reported[1] (corresponding to 0.27 mmol of $Cd(OAc)_2 \cdot 2H_2O$ and 0.47 mmol of selenourea. The yellow dispersion obtained after TOP addition was stored under N_2 at room temperature for use as a stock mixture.

{CdS[n-octylamine]$_p$} QPs: The synthesis of {CdS[n-octylamine]$_p$} QPs was conducted on the same scale as that previously reported[2] (corresponding to 0.20 mmol of $Cd(OAc)_2 \cdot 2H_2O$ and 0.40 mmol of thioacetamide). After the reaction mixture was stored at 0 °C overnight, the bundled {CdS[n-octylamine]$_p$} QPs precipitated as a yellowish white solid under a colorless supernatant. The QPs were redispersible by vigorous shaking. This dispersion was stored under N_2 at room temperature for use as a stock mixture.

3.2.5 Surface Exchange of {II-VI[amine]$_g$} QBs/QPs with M(oleate)$_2$

Surface Exchange of {CdSe[n-octylamine]$_x$} QBs with Cd(oleate)$_2$: An aliquot (0.2 mL) of the CdSe QB stock mixture was transferred to a septum-capped test tube and toluene (1 mL) was added. The resulting pale-yellow precipitate was separated by a benchtop centrifuge (1500 RPM, 5 min), and the supernatant was discarded. The dispersion-centrifugation cycle was repeated 2 additional times. The purpose of this purification process was to remove excess n-octylamine.

Anhydrous Cd(oleate)$_2$ solution (1 mL) was added to the purified {CdSe[n-octylamine]$_x$} QBs resulting in a clear, bright-yellow solution of {CdSe[Cd(oleate)$_2$]$_y$} instantaneously upon mixing. Two drops of {CdSe[Cd(oleate)$_2$]$_y$} were taken to obtain a PL spectrum.

Subsequent analyses were conducted using purified {CdSe[Cd(oleate)$_2$]$_y$}. Toluene (1.5 mL) and methanol (0.5 mL) were added to the CdSe[Cd(oleate)$_2$]$_y$} solution, resulting in a bright-yellow precipitate, which was collected after centrifugation (4500 rpm, 5 min). This

precipitate was used for UV-vis and XRD analyses.   For FT-IR analysis, the toluene-methanol dispersion and centrifugation cycle was conducted two additional times to ensure removal of free ligands.

Surface Exchange of {CdS[n-octylamine]$_p$} QPs with Cd(oleate)$_2$.: The same procedure as described above for the CdSe QBs was employed.   The yellowish-white CdS QP dispersion became more transparent upon addition of the anhydrous Cd(oleate)$_2$ solution.   The exchanged {CdS[Cd(oleate)$_2$]$_q$} QPs were collected as a white precipitate after the purification step.

Surface Exchange of {CdSe[n-octylamine]$_x$} QBs and {CdS[n-octylamine]$_p$} QPs with Zn(oleate): Aliquots from the CdSe QB and CdS QP stock mixtures were purified as above. The purified CdSe QB or CdS QP solids were dispersed in toluene (1 mL) to form cloudy suspensions.   Separately, the Zn(oleate)$_2$ stock suspension was well mixed by stirring to form a viscous white mixture.   The Zn(oleate)$_2$ suspension was added to the CdSe QB or CdS QP dispersions drop by drop in a total amount of 16 drops.   The cloudy pale yellow CdSe dispersion gradually turned clearer and brighter upon addition of Zn(oleate)$_2$, and became completely clear in 0.5-1 min.   The cloudy CdS dispersion became almost clear in 1 min upon addition of Zn(oleate)$_2$.

The resulting {CdSe[Zn(oleate)$_2$]$_m$} dispersion was purified once as described above for {CdSe[Cd(oleate)$_2$]$_y$}   The {CdS[Zn(oleate)$_2$]$_n$} dispersion was purified in the same manner.

3.2.6 Back Exchange of {II-VI[M(oleate)$_2$]$_f$} QBs/QPs to {II-VI[amine]$_g$} QBs/QPs

Back exchange was conducted using both the initial $\{CdSe[Cd(oleate)_2]_y\}$ solution, or the purified $\{CdSe[Cd(oleate)_2]_y\}$ solid. Addition of *n*-octylamine (or oleylamine, 1.5 mL) converted the bright-yellow solid or solution to a pale-yellow color. Two drops of the resulting $\{CdSe[n\text{-octylamine}]_{x'}\}$ or ($\{CdSe[oleylamine]_{z'}\}$) solution were taken to obtain PL spectra. Subsequent analyses were conducted after purification as described above for the M(oleate)$_2$-passivated QBs/QPs (M = Cd, Zn). Back exchange of the other $\{II\text{-}VI[M(oleate)_2]_f\}$ QBs/QPs was conducted similarly.

3.3 Results

3.3.1 Reversible spectroscopic changes accompanying exchange of L- and Z-type passivation in CdSe QBs

The synthesis of amine-passivated CdSe QBs was previously reported.[1] A UV-visible extinction spectrum of as-synthesized CdSe QBs passivated by *n*-octylamine, $\{CdSe[n\text{-octylamine}]_x\}$, is given in Figure 3.2a. These QBs were previously shown to possess the wurtzite structure and to have thicknesses of 1.8 nm (corresponding to 5 monolayers of CdSe),[3] establishing the confinement dimension. The spectrum of the QBs (Fig. 3.2a) contained three absorption features, previously assigned to quantum-well transitions.[3] The lowest-energy feature appeared at 449 nm (2.76 ± 0.01 eV).
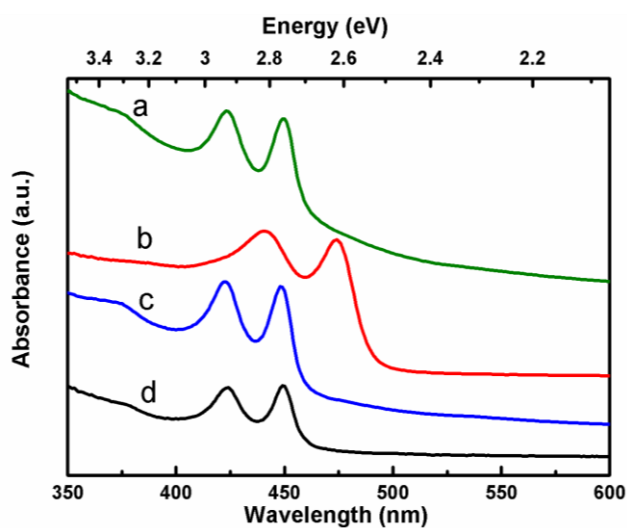
Figure 3.2. UV-visible extinction spectra (in toluene dispersion, at RT) of (a) starting {CdSe[*n*-octylamine]$_x$},
(b) {CdSe[Cd(oleate)$_2$]$_y$}, (c) back-exchanged {CdSe[*n*-octylamine]$_{x'}$}, and (d) back-exchanged
{CdSe[oleylamine]$_{z'}$}.

Washed {CdSe[*n*-octylamine]$_x$} QBs were combined with anhydrous Cd(oleate)$_2$ in ODE

solvent.   The color of the dispersion changed from pale yellow to bright yellow

instantaneously upon mixing at room temperature.   An extinction spectrum of the resulting

{CdSe[Cd(oleate)$_2$]$_y$} QBs is given in Figure 3.2b.   The QB absorption features were shifted

to lower energy.   The lowest-energy feature was shifted by 24 nm (140 ± 20 meV) to 473 nm

(2.62 ± 0.01 ev), and the second feature also by a significant amount.   The third, weakest

feature was broadened and obscured after the change in surface passivation.

Addition of primary amine to {CdSe[Cd(oleate)$_2$]$_y$} QB dispersions was found to reverse

these spectroscopic shifts.   A {CdSe[Cd(oleate)$_2$]$_y$} dispersion and *n*-octylamine reacted

instantaneously to restore a cloudy, pale-yellow {CdSe[*n*-octylamine]$_{x'}$} dispersion giving the

extinction spectrum in Figure 3.2c.   The lowest-energy QB feature appeared at 449 nm, and

the third, weakest feature reappeared at its original position.   Similarly, a $\{CdSe[Cd(oleate)_2]_y\}$

dispersion and oleylamine reacted instantaneously to generate a clear, pale-yellow solution

(dispersion) giving the extinction spectrum in Figure 3.2d.   The QB absorption features were

restored to similar, higher-energy positions (449 nm, 423 nm, and 375 nm).   The lowest-

energy λ_{max} values , spectral shifts, and energy shifts associated with the variously passivated

CdSe QBs are summarized in Table 3.2.

Table 3.2.   Lowest-energy λ_{max} values, spectral shifts, and energy shifts associated
with the variously passivated CdSe QBs.

QB/QP	λ_{max} (nm)[a]	$\Delta\lambda_{max}$ (nm)[b]	ΔE (meV)
$\{CdSe[n\text{-octylamine}]_{0.53}\}$	449 ± 1	0	0
$\{CdSe[Cd(oleate)_2]_{0.19}\}$	473 ± 1	24 ± 2	140 ± 20
$\{CdSe[Zn(oleate)_2]_m\}$	454 ± 1	5 ± 2	30 ± 20
$\{CdS[n\text{-octylamine}]_p\}$	373 ± 1	0	0
$\{CdS[Cd(oleate)_2]_q\}$	384 ± 1	11 ± 2	90 ± 20
$\{CdS[Zn(oleate)_2]_n\}$	379 ± 1	6 ± 2	50 ± 20

[a]For the lowest-energy absorption feature.
[b]Relative to the n-octylamine-passivated QB or QP.

The reversible shifting observed in the extinction spectra was paralleled by corresponding

changes in the photoluminescence (PL) spectra.   As discussed previously,[3] amine-passivated

2D II-VI nanocrystals exhibit strong, sharp emission features, which are minimally Stokes-

shifted from the lowest-energy absorptions.   Thus, the as-synthesized $\{CdSe[n\text{-octylamine}]_x\}$

QBs gave the PL spectrum in Figure 3.3, having a λ_{max} at 452 nm.   The PL intensity was

largely quenched by the washing step to remove excess n-octylamine, which preceded surface

exchange (Figure 3.3).   The PL spectrum remained very weak in the exchanged

{CdSe[Cd(oleate)$_2$]$_y$} product, but gave a discernible feature at $\lambda_{max} = 479$ nm. Replacement of the Cd(oleate)$_2$ surface passivation by oleylamine passivation restored the PL intensity and shifted λ_{max} back to 452 nm. The emission feature in the back-exchanged oleylamine-passivated QBs exhibited a prominent low-energy shoulder presumably indicative of surface traps introduced during the ligand-exchange process.
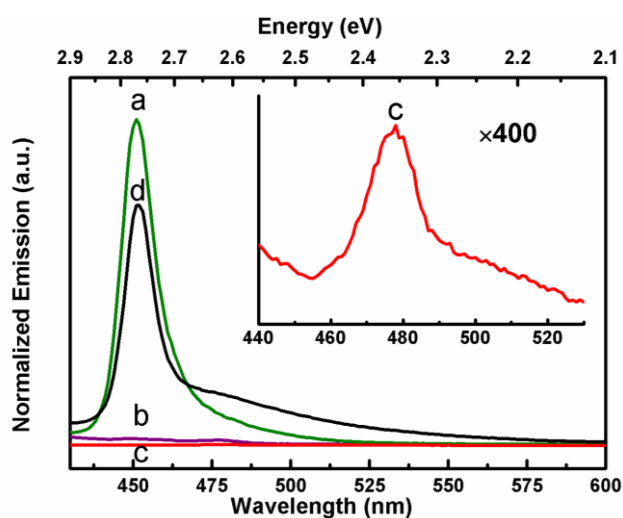
Figure 3.3. PL spectra (in toluene dispersion, at RT) of (a) as-synthesized {CdSe[n-octylamine]$_x$} (green), (b) {CdSe[n-octylamine]$_x$} after removal of excess n-octylamine (purple), (c) {CdSe[Cd(oleate)$_2$]$_y$} (red), and (d) back-exchanged {CdSe[oleylamine]$_z$} (black). The inset is a vertical expansion of (c).

If exchanges in CdSe QB surface passivation were indeed responsible for the reversible spectral shifting described above, then the overall morphologies of the QBs should not be greatly affected by the exchange process. Figure 3.4a is a TEM image of the starting {CdSe[n-octylamine]$_x$} QBs, after unbundling with oleylamine (see ref. [1]). The mean width and length of the QBs were 6 ± 1 and 335 ± 70 nm, respectively. Figure 3.4b is a corresponding image of the {CdSe[Cd(oleate)$_2$]$_y$} QBs resulting from surface exchange with

Cd(oleate)$_2$, in which the mean length has decreased to 271 ± 79 nm.   Figure 3.4c is an image

of the {CdSe[oleylamine]$_{z'}$} QBs back-exchanged to amine passivation, in which the mean

length has further decreased to 236 ± 52 nm.
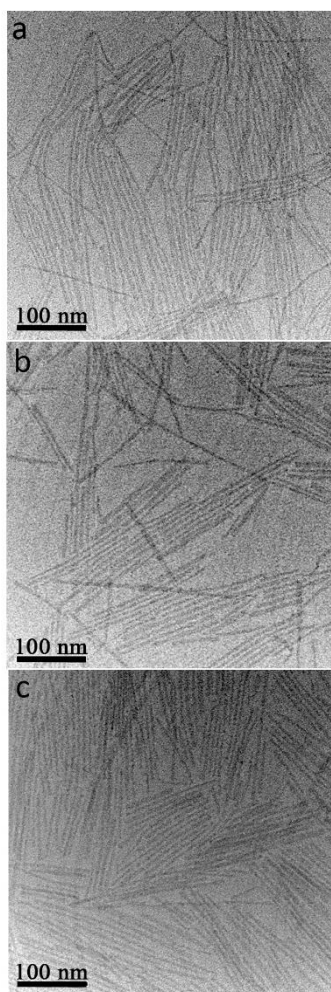
Figure 3.4.   TEM images of (a) starting {CdSe[n-octylamine]$_x$} after unbundling with oleylamine, (b) {CdSe[Cd(oleate)$_2$]$_y$}, and (c) back-exchanged {CdSe[oleylamine]$_{z'}$}.

3.3.2. Characterization of L- and Z-passivated CdSe QBs

Apart from the progressive decrease in mean length, the QBs underwent no distinct morphological changes as a result of the exchange process. The decrease in length may have been due to cleavage resulting from changes in the strain states of the QBs (see below), or merely to mechanical intercontact during the physical manipulations. Note that the changes in length did not influence the spectroscopic properties of the QBs, as length is not a confinement dimension. The results were consistent with a QB surface-exchange process.

The identities of the surface-bound ligands were examined by IR spectroscopy. The IR spectrum of the starting {CdSe[n-octylamine]$_x$} QBs contained three distinct N–H stretches in the range of 3330-3132 cm^{-1} diagnostic of the primary-amine passivation (Figure 3.5a). Upon surface exchange to {CdSe[Cd(oleate)$_2$]$_y$} the N–H stretches disappeared, and asymmetric and symmetric CO_2 stretches appeared at 1536 and 1412 cm^{-1}, respectively (Figure 3.5b). The resulting Δ value, 1536 cm^{-1} – 1412 cm^{-1} = 124 cm^{-1}, in comparison to Δ = 128 cm^{-1} for sodium oleate, was indicative of bridging carboxylate ligands.[4] Asymmetric and symmetric CO_2 stretches were also observed at 1528 and 1400 cm^{-1} (Δ = 128 cm^{-1}), in the IR spectrum of zinc-carboxylate-passivated {CdSe[Zn(oleate)$_2$]$_m$} QBs (discussed below; Figure 3.5c). The latter Δ value was also indicative of bridging oleate ligands. Back exchange to oleylamine-passivated {CdSe[oleylamine]$_{z'}$} QBs restored the N–H stretches to the IR spectrum, and removed the CO_2 features (Figure 3.5d). Thus, the IR analysis supported the surface-exchange processes claimed above.
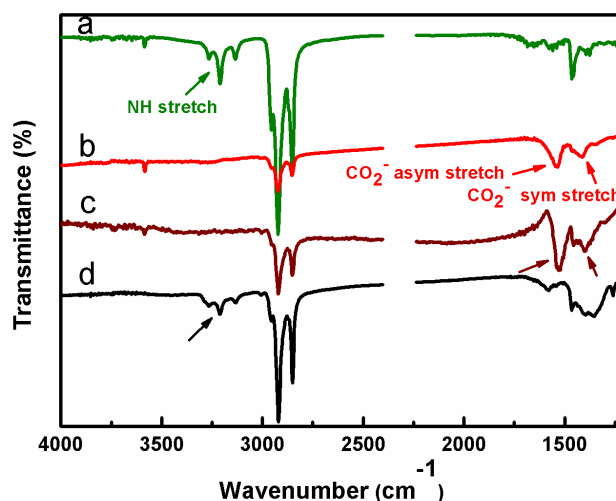
Figure 3.5. IR spectra (from KBr pellets) of (a) starting {CdSe[n-octylamine]$_x$}, (b) {CdSe[Cd(oleate)$_2$]$_y$}, (c) {CdSe[Zn(oleate)$_2$]$_m$}, and (d) back-exchanged {CdSe[oleylamine]$_z$'} from (b). N–H stretches are identified by arrows in (a) and (d); asymmetric and symmetric CO_2 stretches are identified in (b) and (c).

Low-angle XRD provided a second means of characterizing the QB surface exchange. The QBs exhibit a strong tendency to bundle into pseudo-parallel alignment, having their broad top and bottom surfaces stacked together, and so precipitated QB solids give low-angle 00ℓ reflections corresponding to the lamellar spacings in these bundles. These interlayer spacings correspond to the sum of thicknesses of the QBs and the ligand bilayers separating them. XRD patterns obtained from the initial {CdSe[n-octylamine]$_x$} QBs, the exchanged {CdSe[Cd(oleate)$_2$]$_y$} QBs, and the back-exchanged {CdSe[n-octylamine]$_x$'} and {CdSe[oleylamine]$_z$'} QBs are recorded in Figure 3.6. The interlayer (d) spacings calculated from these patterns are given in Table 3.3.
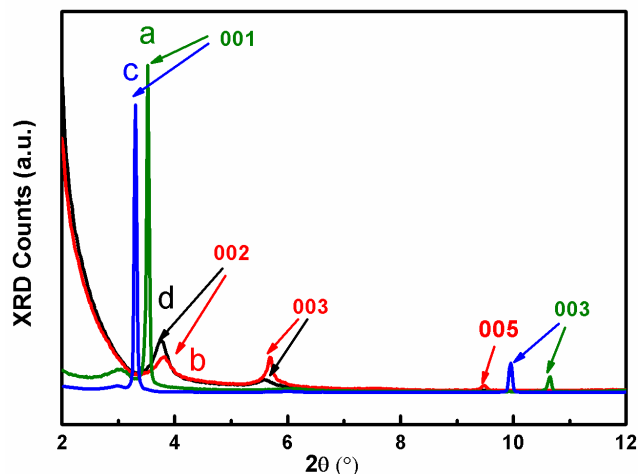
Figure 3.6. Low-angle XRD patterns of (a) starting {CdSe[n-octylamine]$_x$} (green), (b) {CdSe[Cd(oleate)$_2$]$_y$} (red), (c) back-exchanged {CdSe[n-octylamine]$_{x'}$} (blue), and (d) back-exchanged {CdSe[oleylamine]$_{z'}$} (black). The lamellar 00ℓ reflections are indexed.

Table 3.3. Interlamellar d spacings in variously passivated CdSe QBs.

Variously passivated CdSe QBs	d spacing (nm)
{CdSe[n-octylamine]$_x$}	2.51
{CdSe[Cd(oleate)$_2$]$_y$}	4.66
{CdSe[n-octylamine]$_{x'}$}	2.68
{CdSe[oleylamine]$_{z'}$}	4.65

We considered that differences in the d spacings of the variously passivated QBs should be largely determined by the lengths of the alkyl chains on the surface-bound species.   Thus the

67

d spacings for the *n*-octylamine-passivated QBs (Table 3.3) were 2.51 and 2.68 nm, respectively, before and after a surface-exchange cycle.   The small difference in these values likely reflects various degrees of disordering in the bundled QB assemblies.   Both of these *d* spacings were consistent with other, related *n*-octylamine-bilayer mesophases (*d* = 2.5 – 2.8 nm).[1,5]   Exchange to oleylamine or $Cd(oleate)_2$ passivation expanded the observed *d* spacings to 4.65 and 4.66 nm, respectively, reflecting the increased length of the 18-carbon chains vs. the 8-carbon alkyl chain of *n*-octylamine.   Thus, the QB spacings within their aggregated bundles determined by low-angle XRD were consistent with the proposed surface-exchange processes.

The variously passivated CdSe QBs were also characterized by elemental analysis.   Four samples of $\{CdSe[n\text{-octylamine}]_x\}$ were analyzed, producing the results recorded in Table 3.1. These samples were obtained from different synthetic batches, and were washed by slightly different methods to remove excess *n*-octylamine.   One of the analyses differed markedly from the other three (see Table 3.1).   The formula $\{CdSe[n\text{-octylamine}]_{0.53}\}$ (or $x = 0.53 \pm 0.06$) was obtained by averaging the results of the three consistent analyses.

Similarly, four samples of $\{CdSe[Cd(oleate)_2]_y\}$ were analyzed, giving the results in Table 3.1.   These samples were obtained by surface exchange of the four batches of $\{CdSe[n\text{-octylamine}]_{0.53}\}$ used for the analyses above, and were washed by slightly different methods. Again, one analysis was an outlier, and not used in calculating the average composition of $\{CdSe[Cd(oleate)_2]_{0.19}\}$ ($y = 0.19 \pm 0.02$).   Significantly, nitrogen was below the detection limit in all four specimens, establishing the complete removal of *n*-octylamine by the exchange process.   Therefore, CdSe QB characterization by IR spectroscopy, low-angle XRD, and

elemental analyses confirmed the surface-exchange processes proposed above.   The empirical

formulas determined by elemental analysis are used later to determine surface coverages.

3.3.3 Additional examples of reversible exchange of L- and Z-type passivation

A related surface exchange between {CdSe[n-octylamine]$_{0.53}$} QBs and anhydrous

Zn(oleate)$_2$ was undertaken, which required about 30 s at room temperature, and afforded

{CdSe[Zn(oleate)$_2$]$_m$} QBs.   The UV-visible extinction spectrum of this exchange product in

Figure 3.7b is compared to those of {CdSe[n-octylamine]$_{0.53}$} and {CdSe[Cd(oleate)$_2$]$_{0.19}$} QBs

(Figure 3.7a and c, respectively).   The absorption features of the {CdSe[Zn(oleate)$_2$]$_m$} QBs

were shifted to lower energy than those of the amine-passivated {CdSe[n-octylamine]$_{0.53}$}, the

lowest-energy feature by 5 nm (30 ± 20 meV).   Thus, the shifts were smaller in magnitude

than those reported above for {CdSe[Cd(oleate)$_2$]$_{0.19}$}, but in the same direction.   Back

exchange of the CdSe[Zn(oleate)$_2$]$_m$} QBs to {CdSe[n-octylamine]$_{x'}$} by exposure to excess n-

octylamine gave the spectrum in Figure 3.7d, which matched that of the starting {CdSe[n-

octylamine]$_{0.53}$} QBs, establishing that the surface-exchange process was again reversible.
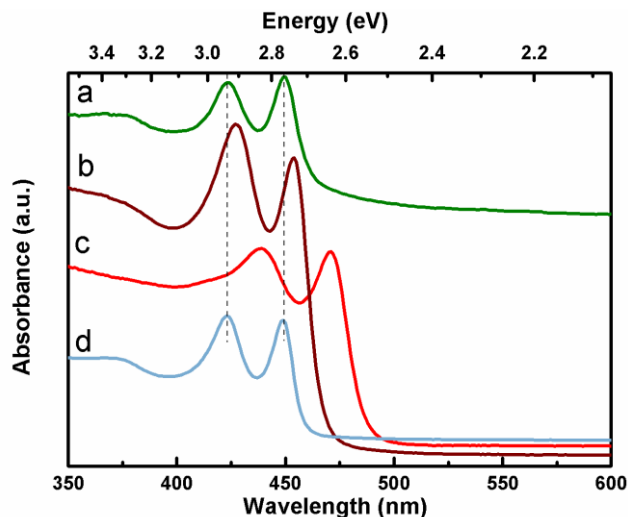
Figure 3.7. UV-visible extinction spectra (in toluene dispersion at RT) of (a) starting {CdSe[*n*-octylamine]$_{0.53}$}, (b) {CdSe[Zn(oleate)$_2$]$_m$}, (c) {CdSe[Cd(oleate)$_2$]$_{0.19}$}, and (d) back-exchanged {CdSe[*n*-octylamine]$_{x'}$} from (b).

Additional experiments conducted with amine-passivated CdS quantum platelets (QPs), {CdS[*n*-octylamine]$_p$}, prepared by a method we previously reported,[2] giving TEM images in Figure 3.8. These QPs had discrete thicknesses of 1.5 nm, widths of ≈ 5 nm, and lengths in the range of 30-40 nm.[2] The UV-visible extinction spectrum of the QPs (Figure 3.9a) contained two features, a strong absorption at 373 nm, and a weaker absorption at 337 nm. Two features were observed, rather than the three features exhibited by the CdSe QBs (Figure 3.2), because the light- and heavy-hole transitions are not resolved in CdS QPs of such small

thickness.[2]   The spectrum also contained a weak shoulder near 400 nm, which has not been assigned.
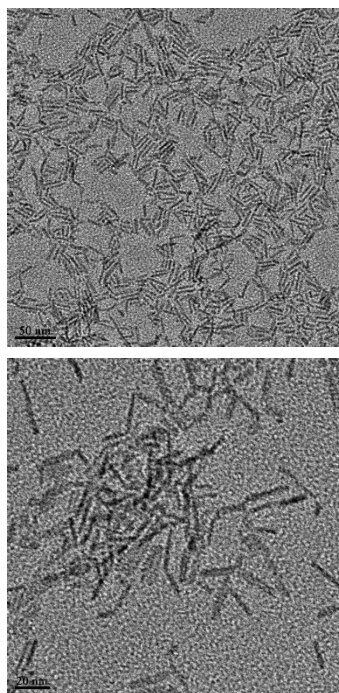
Figure 3.8.   TEM images of {CdS[n-octylamine]$_p$} quantum platelets, prepared by a literature method.[6]

Addition of anhydrous Cd(oleate)$_2$ to the {CdS[n-octylamine]$_p$} QPs at room temperature resulted in an instantaneous shift of the prominent lower-energy absorption from 373 to 384 nm, a shift of 90 ± 20 meV (Figure 3.9b), upon surface exchange to {CdS[Cd(oleate)$_2$]$_q$}. Similarly, surface exchange between {CdS[n-octylamine]$_p$} and Zn(oleate)$_2$ resulted in shift of this feature to 379 nm (by 50 ± 20 meV, Figure 3.9c), upon formation of {CdS[Zn(oleate)$_2$]$_n$}. The spectra for both of the carboxylate-passivated QP derivatives were returned to that of the initial {CdS[n-octylamine]$_{p'}$} QPs upon back exchange by addition of n-octylamine (Figure 3.9d, e).   The results established that CdS QPs were also capable of reversible surface

exchange. The lowest-energy λ_{max} values , spectral shifts, and energy shifts associated with the variously passivated CdS QPs are summarized in Table 3.2.
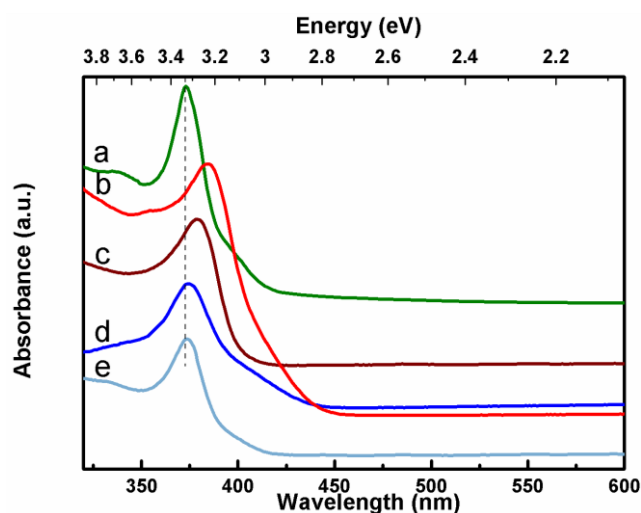
Figure 3.9. UV-visible extinction spectra (in toluene dispersion at RT) of (a) starting {CdS[n-octylamine]$_p$}, (b) {CdS[Cd(oleate)$_2$]$_q$}, (c) {CdS[Zn(oleate)$_2$]$_n$}, (d) back-exchanged {CdS[n-octylamine]$_{p'}$} from (b), and (e) back-exchanged {CdS[n-octylamine]$_{p'}$} from (c).

The IR spectra of the CdS QPs are given in Figure 3.10. The spectrum of {CdS[n-octylamine]$_p$} (Figure 3.10a) contains N-H stretching vibrations in the expected range (3300 – 3130 cm^{-1}). These N-H stretches are absent in the IR spectra of {CdS[Cd(oleate)$_2$]$_q$} and {CdS[Zn(oleate)$_2$]$_n$} (Figure 3.10b, c), and are replaced by asymmetric CO_2 stretches at 1532 and 1538 cm^{-1}, and symmetric CO_2 stretches at 1406 and 1404 cm^{-1}, respectively, close to the positions of the corresponding vibrations in {CdSe[Cd(oleate)$_2$]$_{0.19}$} and {CdSe[Zn(oleate)$_2$]$_m$} QBs reported above (Figure 3.5). The resulting Δ values again established bridging coordination modes for the oleate ligands in both cases.[4] Back exchange of {CdS[Cd(oleate)$_2$]$_q$} to the L-type {CdS[oleylamine]$_{r'}$} restored the N-H stretches and

removed the CO_2 stretches (Figure 3.10d). Thus, the IR data confirmed the surface exchanges in these additional examples.
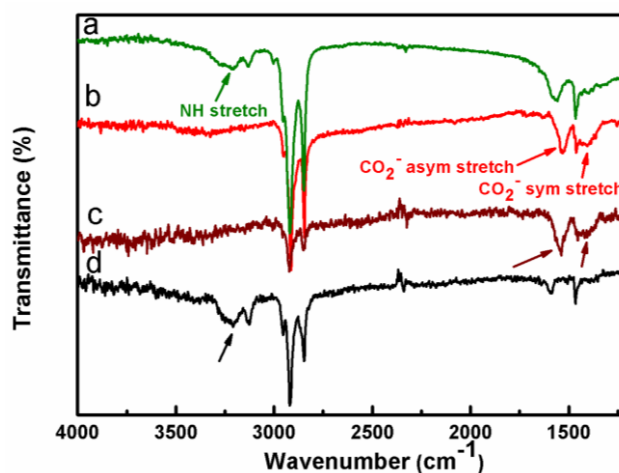
Figure 3.10. IR spectrum of (a) starting {CdS[*n*-octylamine]$_p$}, (b) {CdS[Cd(oleate)$_2$]$_q$}, (c) {CdS[Zn(oleate)$_2$]$_n$}, and (d) back-exchanged {CdS[oleylamine]$_r$·} from (b). N–H stretches are identified by arrows in (a) and (d); asymmetric and symmetric CO_2 stretches are identified in (b) and (c).

3.3.4 Analysis of lattice strain in the 2D II-VI nanocrystals

As noted in the Introduction, lattice strain influences the effective band gaps of semiconductor nanocrystals. This lattice strain results from surface reconstruction and passivation, and may be either compressive or tensile in character, producing lattice contractions or dilations, respectively.[3,7-9] We[10,11] and others[12-14] previously reported lattice contractions of up to 6.5% in amine-passivated 2D II-VI nanocrystals having wurtzite structures. Contractions were observed in both *a* and *c* lattice parameters, but were larger in the thickness dimension of the 2D nanocrystals. Because *a* has a component in the thickness dimension, whereas *c* does not (lying parallel to the long dimension of the QB or QP),[3] the %

contractions, determined from XRD data, were greater in *a*. Consequently, we considered

that changes in the strain states of the QBs and QPs accompanying the changes in surface

passivation from L to Z type may have been responsible for the reversible spectral shifting

detailed above.

High-angle XRD data obtained from the variously passivated CdSe QBs, in the range of the

first three (100, 002, and 101) reflections, are plotted in Figure 3.11. These reflections were

shifted relative to one another and from the bulk values by lattice contractions. For example,

the 100 reflection in unstrained, bulk CdSe appears at 23.8° 2θ, whereas that in the

{CdSe[oleylamine]$_z$} QBs appeared at 24.7° 2θ (Figure 3.11b).
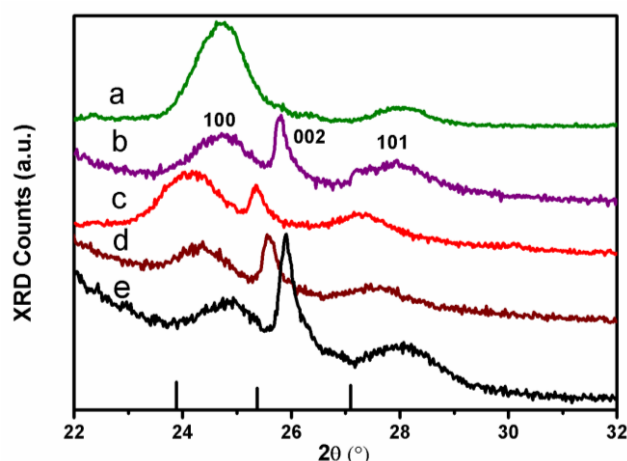
Figure 3.11. High-angle XRD data from (a) starting {CdSe[n-octylamine]0.53}, (b) {CdSe[oleylamine]z}, (c) {CdSe[Cd(oleate)2]0.19}, (d) {CdSe[Zn(oleate)2]m}, and (e) back-exchanged {CdSe[oleylamine]z'} from (c), in the range of the first three (100, 002, and 101) reflections. The black lines on the x axis are the positions of these reflections in bulk CdSe.

We note that the 002 reflection is missing from the XRD pattern of the {CdSe[*n*-

octylamine]$_{0.53}$} QBs (Figure 3.11a). This absence is due to the tightly bundled nature of the

74

n-octylamine derivative, which preferentially oriented the long axis of the QBs in the substrate plane, removing the (002) planes from the diffraction condition.   However, the 100 and 101 reflections of the {CdSe[*n*-octylamine]$_{0.53}$} and {CdSe[oleylamine]$_z$} QBs appeared at nearly the same angle 2θ, indicating that the primary-amine (L-type) passivation induced similar lattice contractions in both specimens.

   The values of the lattice contractions were determined from the positions of the 100 and 002 reflections for the variously passivated CdSe QBs (Table 3.4).   The results indicated higher strain (larger contractions) in the L-type amine-passivated QBs than in the Z-type metal-carboxylate-passivated QBs.

   Two patterns are provided for {CdSe[oleylamine]$_{z,z'}$} QBs.   The specimen used for Figure 3.11b was obtained by surface exchange from {CdSe[*n*-octylamine]$_{0.53}$}, and the specimen used for Figure 3.11e was obtained by back exchange from {CdSe[Cd(oleate)$_2$]$_{0.19}$}.   The lattice contractions determined for the two specimens were similar, but not identical (Table 3.4). Their similarity established that changes in the strain states resulting from surface exchange were largely reversible.

Table 3.4.   Values of the lattice parameters and strain states of variously passivated 2D II-VI nanocrystals.

QB/QP specimens	a (Å)	contraction in a (%)	c (Å)	contraction in c (%)
{CdSe[*n*-octylamine]$_{0.53}$}	4.15	3.4 ± 0.1	6.90	1.6
{CdSe[oleylamine]$_z$}	4.15	3.4 ± 0.1	6.90	1.6
{CdSe[Cd(oleate)$_2$]$_{0.19}$}	4.26	0.9 ± 0.3	7.02	0
{CdSe[Zn(oleate)$_2$]$_m$}	4.22	1.9 ± 0.1	6.97	0.7

Cont.

{CdSe[oleylamine]$_z$·}	4.13	4.0 ± 0.1	6.88	2.0
{CdS[*n*-octylamine]$_p$}	3.99	3.3 ± 0.2	6.61	2.1
{CdS[Cd(oleate)$_2$]$_q$}	4.08	1.2 ± 0.2	6.70	0.7
{CdS[Zn(oleate)$_2$]$_n$}	4.08	1.2 ± 0.1	6.68	1.0

High-angle XRD data for the variously passivated CdS QPs are given in Figure 3.12, and the corresponding lattice contractions are recorded in Table 3.4. Because the 100 reflections are not well resolved in these patterns, the lattice parameters were calculated using the positions of the 002 and 101 reflections. The magnitudes of the lattice contractions in the CdS QPs were quite similar to the correspondingly passivated CdSe QBs. As for the CdSe QBs, the lattice contractions were larger, and the compressive strains higher, in the L-type amine-passivated CdS QPs than in the Z-type metal-carboxylate-passivated CdS QPs. The contribution of changes in the strain states to the reversible spectral shifts is analyzed in the Discussion.
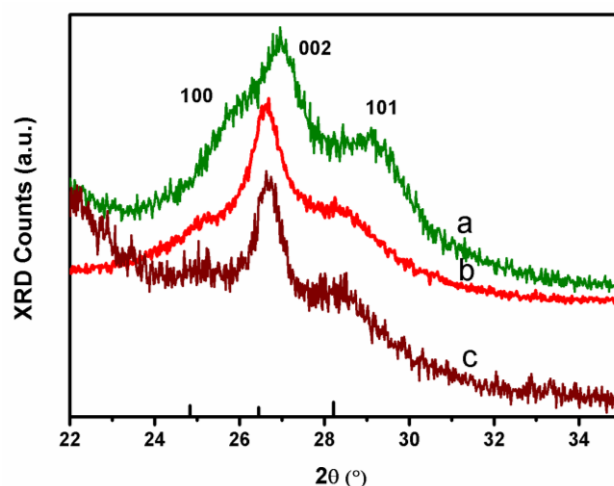
Figure 3.12. High-angle XRD data from (a) starting {CdS[*n*-octylamine]$_p$}, (b) {CdS[Cd(oleate)$_2$]$_q$}, and (c) {CdS[Zn(oleate)$_2$]$_n$}, in the range of the first three (100, 002, and 101) reflections.

3.3.5 Surface coverage in CdSe QBs

The elemental-analysis data and mean QB dimensions allowed calculations of the average surface coverages of the CdSe QBs. Figure 3.13 represents a view perpendicular to the small end facet of a QB. From this perspective, the structure is bounded by the broad top and bottom facets at the top and bottom of the lattice, and by the thin, long edge facets on the left and right edges.[3] The thickness dimension is oriented vertically. We defined one crystallographic monolayer in the quantum-confined thickness dimension as the thinnest layer constituting a contiguously bonded net,[3] and the top and bottom monolayers are so identified in Figure 3.13. The monolayers are nominally corrugated (if unreconstructed), consisting of parallel, alternating ridges and valleys (like corduroy) on the top and bottom facets, running perpendicular to the plane of the Figure.

77
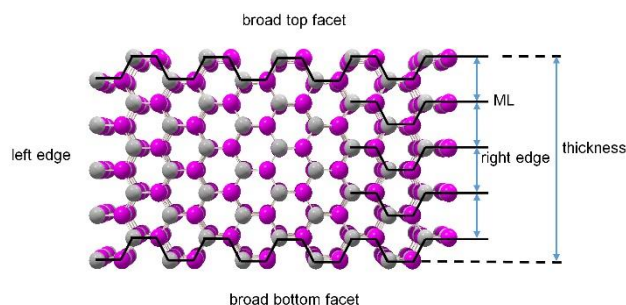
Figure 3.13. A view perpendicular to the small end facet of a QB. Cd and Se atoms are grey and magenta, respectively.

The CdSe QBs used in this study had a discrete thickness of 1.8 nm, or 5 CdSe monolayers. Thus, the 2 monolayers forming the top and bottom facets account for 40% of the CdSe in the QBs; or, 40% of the Cd and Se atoms in the QBs are on the broad top and bottom surfaces. Notably, the Cd and Se atoms in the surface, valley positions are nominally 4 coordinate, whereas those in the surface, ridge positions are nominally 3-coordinate, prior to surface-ligand coordination.

The overall composition of the amine-passivated QBs was determined to be {CdSe[*n*-octylamine]$_{0.53\pm0.06}$} (see above). If an *n*-octylamine ligand were bonded to each Cd atom on the top and bottom QB facets, in both the ridge *and* valley positions, the composition would be {CdSe[*n*-octylamine]$_{0.40}$}. Alternatively, if an *n*-octylamine ligand were bonded to each Cd and each *Se* atom in the *ridge* positions of the top and bottom facets, the composition would be {CdSe[*n*-octylamine]$_{0.40}$}. These alternatives are analyzed in the Discussion.

The thin, edge facets of the CdSe QBs are also nonpolar surfaces with structures related to the top and bottom facets. We considered that *n*-octylamine may be bound to those facets as

78

well. Because the ratio of the mean thickness to mean width of the QBs was 1.8:6.0, an additional 12% of the Cd and Se atoms were on the edge facets. By the arguments above, n-octylamine coordination to these surfaces, in addition to the top and bottom surfaces, would result in the composition $\{CdSe[n\text{-octylamine}]_{0.40+0.12}\}$ or $\{CdSe[n\text{-octylamine}]_{0.52}\}$, well within the error of the elemental-analysis results. This analysis ignored the small relative areas of the two end facets of the QBs.

The overall composition of the $Cd(oleate)_2$-passivated QBs was determined to be $\{CdSe[Cd(oleate)_2]_{0.19\pm0.02}\}$ (see above). According to the analysis above, if one $Cd(oleate)_2$ were bonded for every Se atom in a ridge position of the top and bottom QB facets, the composition would be $\{CdSe[Cd(oleate)_2]_{0.20}\}$. Alternatively, if one $Cd(oleate)_2$ were bonded for every Se atom in a ridge position on the top, bottom, and two edge QB facets, the composition would be $\{CdSe[Cd(oleate)_2]_{0.26}\}$. These two surface-bonding models provide compositions close to and not likely distinguishable by the elemental-analysis results. Again, the small relative areas of the two end facets of the QBs were ignored.

The analyses presented in this section demonstrated that plausible surface-coverage models rationalized the overall compositions determined experimentally.

3.4 Discussion

3.4.1 Proposed Surface Structures for Passivated CdSe QBs

The coverage models elucidated above indicate a *stoichiometry* of one bound n-octylamine ligand for each surface Cd atom in the $\{CdSe[n\text{-octylamine}]_{0.53}\}$ QBs, on the top, bottom, and

the two edge facets.   However, the unreconstructed top and bottom facets contain two types

of Cd atoms, those in 3-coordinate ridge positions, and those in 4-coordinate valley positions.

Figure 3.14a provides a view of a top facet, in which the valley positions are shaded to

distinguish them from the ridge positions.   Both the valleys and ridges consist of parallel, zig-

zag chains of alternating Cd and Se atoms.   Coordination of *n*-octylamine ligands to the 3-

coordinate ridge Cd atoms is readily imagined, whereas coordination to the valley Cd atoms

seems less likely because those atoms are ostensibly tetrahedrally coordinated by lattice atoms,

are thus coordinatively saturated, and are much less sterically accessible.   Therefore, a

structural model for amine passivation in which one *n*-octylamine ligand is bound to *every*

surface Cd atom is questionable.
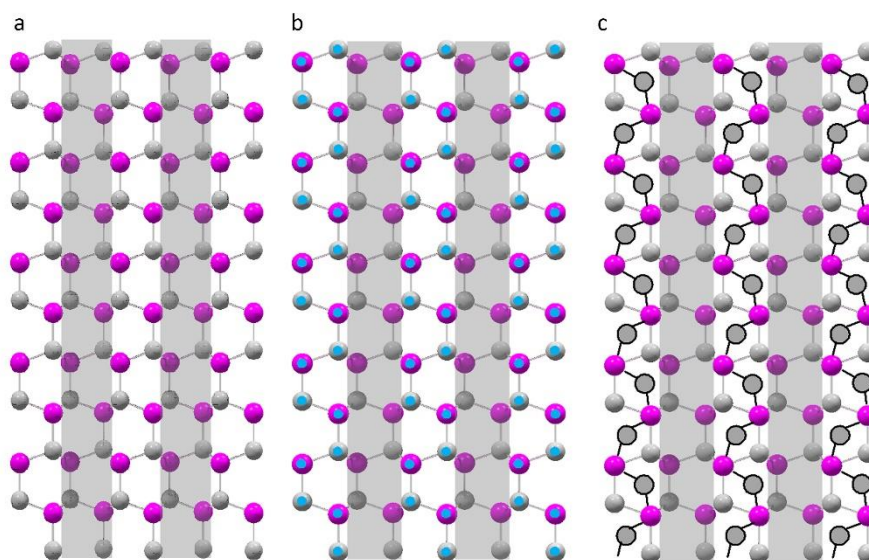
Figure 3.14.   (a) A view of a top CdSe QB facet, with the valley positions shaded. (b) Blue dots represent *n*-octylamine ligands bonded to both Cd and Se atoms in only the *ridge* positions on a top QB facet.   (c) Grey circles (with black borders) represent the proposed coordination of the Cd atoms in the Cd(oleate)$_2$ units to ridge Se atoms, in a bridging, μ_2 mode, on a top QB facet

A different surface structure is suggested by a recent study of Zhang and coworkers.[15]

They analyzed the surface bonding of primary amines to CdSe, ZnSe, and ZnS quantum dots

by IR spectroscopy, finding evidence of strong inter-amine hydrogen bonding among the surface-coordinated ligands. Moreover, the results established the existence of two types of surface-bound primary amines, one of which was selectively removed by methanol substitution. Zhang and coworkers proposed that the two types were amines coordinated to surface Cd atoms, and amines coordinated to surface Se atoms, the latter in a hydrogen-bonding-like interaction. In support of that argument, they demonstrated that amine ligands bound only to surface Cd atoms were too widely separated to engage in inter-amine hydrogen bonding, whereas amines bound to both surface Cd and Se atoms were optimally positioned for hydrogen bonding with one another.

By analogy, we consider *n*-octylamine bonding to both Cd and Se atoms in only the *ridge* positions on the top and bottom QB surfaces (Figure 3.14b), which allows contiguous strips of inter-amine hydrogen bonding. The edge facets do not have precisely the same ridge-and-valley structure. They lack the Cd-Se zig-zag chains, but are non-polar surfaces having equal numbers of Cd-Se dimers in ridge, 3-coordinate environments, and valley, 4-coordinate environments. Consequently, *n*-octylamine ligands could be bound to both Cd and Se atoms in ridge positions on the edge facets as well. The attractive features of this model are that coordination to the sterically hindered, coordinatively saturated surface sites is not required, and that the model is consistent with the experimental surface coverage determined by elemental analysis, {CdSe[*n*-octylamine]$_{0.53\pm0.06}$} (see Results).

The surface structure proposed here for the amine-passivated CdSe QBs resembles that calculated for CdSe nanosheets by Hyeon, Hoffmann, and coworkers.[13] Their surface structure features primary-amine ligands bound to Cd atoms in the ridge positions on the top

and bottom facets, but not to Cd atoms in the valley positions. Amine ligands bound to surface Se atoms are not present. That model, however, is inconsistent with our elemental-analysis data, having too few amine ligands by half.

As reported in the Results, the overall composition of the Cd(oleate)$_2$-passivated QBs was determined to be $\{CdSe[Cd(oleate)_2]_{0.19\pm0.02}\}$. Surface models in which one Cd(oleate)$_2$ unit is bound for each surface Se atom in a ridge position are consistent with this composition. We imagine coordination of the Cd atom in the Cd(oleate)$_2$ units to ridge Se atoms in a bridging, μ_2 fashion as shown in Figure 3.14c. The IR data confirm that the oleate ligands adopt bridging modes, of which several variations are possible. We note that the ridge Cd atoms are nominally three coordinate, such that oleate bridging to those Cd atoms could relieve their steric unsaturation. Thus, Cd(oleate)$_2$ surface bonding in the proposed μ_2 mode allows the Z-type Cd, the ridge Cd, and the ridge Se atoms to become coordinatively saturated, avoids interactions with the saturated valley atoms, is consistent with the IR data, and corresponds to the measured composition of $\{CdSe[Cd(oleate)_2]_{0.19}\}$.

We suggest that the surface configurations for *n*-octylamine and Cd(oleate)$_2$ binding proposed here clarify the L- and Z-type surface interactions depicted only schematically in Figure 3.1.

3.4.2 Contributions of Strain and Dimensional Changes to the Reversible Exciton Energy Shifts

As noted in the Introduction, changes in the pressure exerted by the surfaces of nanocrystals upon the cores, and changes in the dimensions (in this case effective thicknesses)

of the nanocrystals may both contribute to changes in exciton energies. Here we separate and analyze those contributions.

Table 3.4 records the strain states of the variously passivated 2D II-VI nanocrystals, determined by XRD. The nanocrystals are under varying degrees of compressive strain, with the strain highest in the L-type, amine-passivated cases. The differences in strain ($\Delta\varepsilon$) and Young's modulus (Y) of the semiconductors determines the difference in surface pressure (or difference in stress, $\Delta\sigma$) exerted by the L- and Z-type surfaces. The expected spectral energy shifts (ΔE_{strain}) due to changes in the strain states are then determined from the band-gap pressure coefficient (α) of the semiconductors. Overall, ΔE_{strain} is calculated by eq 3.1, which is derived below.

Derivation of eq 3.1 and calculation of Young's modulus:

From Hooke's Law, Young's modulus, Y, is stress divided by strain:

$$Y = \sigma \text{ (Gpa, stress)}/\varepsilon \text{ (unitless, strain)} \qquad \text{(a)}$$

Thus a change in surface pressure (or change in stress, $\Delta\sigma$) is determined from the change in strain ($\Delta\varepsilon$) and Young's modulus:

$$\Delta\sigma = \Delta\varepsilon Y \qquad \text{(b)}$$

The band-gap pressure coefficient (α) relates changes in the semiconductor effective band gap (ΔE_{strain} (ev)) to $\Delta\sigma$.[16] The α values for bulk CdSe (43.1 meV/GPa)[17] and bulk CdS (42 meV/GPa)[18] were taken from the literature.

$$\alpha = \Delta E_{strain} \text{ (ev)}/\Delta\sigma \text{ (Gpa)} \qquad \text{(c)}$$

By rearranging eq c,

$$\Delta E_{strain} = \Delta\sigma\alpha \qquad \text{(d)}$$

Equation 3.1   was obtained by substituting the derived values of $\Delta\sigma$ in b into eq d,

$$\Delta E_{strain} = \alpha(\Delta\varepsilon)Y \qquad (3.1)$$

Because experimental values of Young's modulus are not known precisely for CdSe or CdS,

we calculated Y from the better-known bulk modulus B ($B_{cdse} = 53.5$ GPa,[19] and $B_{cds} = 62$ GPa[20]),

and Poisson's ratio μ ($\mu_{cdse} = 0.345$[21] and $\mu_{cds} = 0.344$[21]) for these semiconductors, according

to eq e.[22]

$$Y = 3B(1 - 2\mu) \qquad (e)$$

For CdSe,

$Y_{cdse} = 3B_{cdse}(1 - 2\mu_{cdse}) = 3(53.5$ GPa$)(1 - 2(0.345)) = 49.8$ GPa

For $\{CdSe[Cd(oleate)_2]_{0.19}\}$,

ΔE_{strain} (eV) $= \alpha(\Delta\varepsilon)Y_{cdse} = 43.1(meV/GPa)(0.034 - 0.009)(49.8$ GPa$) = 53.7$ meV

For $\{CdSe[Zn(oleate)_2]_m\}$,

ΔE_{strain} (eV) $= 43.1$(meV/Gpa)$(0.034 - 0.019)(49.8$ Gpa$) = 32.3$ meV

For CdS,

$Y_{cds} = 3B_{cds}(1 - 2\mu_{cds}) = 3(62$ GPa$)(1 - 2(0.344)) = 58.0$ GPa

For $\{CdS[Cd(oleate)_2]_q\}$,

ΔE_{strain} (eV) $= \alpha(\Delta\varepsilon)Y_{cds} = 42(meV/GPa)(0.033 - 0.012)(58.0$ GPa$) = 51.2$ meV

For $\{CdS[Zn(oleate)_2]_n\}$,

ΔE_{strain} (eV) $= 42$(meV/GPa)$(0.033 - 0.012)(58.0$ GPa$) = 51.2$ meV

Because the changes in strain are greater in the lattice parameter *a* than in *c* (Table 3.4),

and more importantly because only *a* has a component in the quantum-confined thickness

dimension largely responsible for the reversible energy shifts, $\Delta\varepsilon$ was determined only from the varying strain in a.   Additionally, because Young's modulus is not known precisely for CdSe or CdS, we calculated Y from the bulk modulus B and Poisson's ratio μ for these semiconductors.   In these calculations we employ bulk values for α, B, μ, and Y.   The details are given in eq 3.1.   The energy shifts ΔE_{strain} so obtained are recorded in Table 3.5.

Table 3.5. Observed spectroscopic energy shifts separated into strain (ΔE_{strain}) and confinement-dimension ($\Delta E_{thickness}$) components.

QB/QP specimen	contraction in a (%)[a]	spectroscopic energy shift (meV)[b]	ΔE_{strain} (meV)[c]	$\Delta E_{thickness}$ (meV)[d]
{CdSe[n-octylamine]$_{0.53}$}	3.4 ± 0.1	0	0	0
{CdSe[oleylamine]$_z$}	3.4 ± 0.1	0	0	0
{CdSe[Cd(oleate)$_2$]$_{0.19}$}	0.9 ± 0.3	140 ± 20	53 ± 8	87 ± 28
{CdSe[Zn(oleate)$_2$]$_n$}	1.9 ± 0.1	30 ± 20	32 ± 4	0
{CdS[n-octylamine]$_p$}	3.3 ± 0.2	0	0	0
{CdS[Cd(oleate)$_2$]$_q$}	1.2 ± 0.2	90 ± 20	51 ± 7	39 ± 27
{CdS[Zn(oleate)$_2$]$_n$}	1.2 ± 0.1	50 ± 20	51 ± 5	0

[a]From Table 3.4.
[b]From Table 3.2, relative to the lowest-energy feature in the n-octylamine-passivated QB or QP.
[c]Calculated from eq 3.1.
[d]The difference in the spectroscopic energy shift and ΔE_{strain}.

Table 3.5 compares the energy shifts observed spectroscopically for the Z-type surface passivation, relative to the L-type, *n*-octylamine-passivated nanocrystals, to the energy shifts (ΔE_{strain}) predicted by the observed changes in the strain states of the nanocrystals. Interestingly, the spectral shifts obtained by Zn(oleate)$_2$ passivation agree quantitatively with the values calculated from the changes in strain. That is, the spectral shifts observed for Zn(oleate)$_2$ passivation may be attributed entirely to strain differences ($\Delta\varepsilon$).

In contrast, $\Delta\varepsilon$ can account for only a portion of the spectral shifts observed for Cd(oleate)$_2$ passivation of the CdSe and CdS nanocrystals (ΔE_{strain}, Table 3.5). The components unaccounted for by changes in strain states ($\Delta E_{\text{thickness}}$, Table 3.5) are of comparable magnitude to those predicted by $\Delta\varepsilon$; indicating that they are due to comparably large effects. We propose that these additional components in the spectral shifts for the Cd(oleate)$_2$ cases are due to extension of the CdSe and CdS lattices by the Cd atoms in the coordinated Cd(oleate)$_2$ units, providing an effective thickness increase.

Useful comparisons may be drawn by comparing to the spectral shifts that occur from Cd(oleate)$_2$ passivation to those occurring upon addition of complete II-VI monolayers to the 2D II-VI nanocrystals. As noted above, the CdSe QBs employed here contain 5 monolayers in the thickness dimension. Addition of a complete 6th CdSe monolayer to the QBs results in a shift of the lowest-energy absorption from 2.76 to 2.40 eV, or by 360 meV.[3] This corresponds to the addition of one Cd and one Se atom for each Cd and Se atom in, for example, the top monolayer of the 5-monolayer QB.

Upon passivation of the CdSe QBs by Cd(oleate)$_2$, the equivalent of one Cd atom (in/from the Cd(oleate)$_2$) has been added for (not *to*) every *ridge* Cd atom on the top and bottom QB

facets, corresponding to *half* of the Cd atoms from the CdSe lattice on these surfaces.   No Se atoms have been added.   Thus, we may imagine the surface coordination of Cd(oleate)$_2$ as adding a quarter of a monolayer to the top facet, and a quarter of a monolayer to the bottom facet, for a total of a half of a monolayer.   A true half monolayer of CdSe should have caused a shift to lower energy of approximately 360/2 meV, or 180 meV.   A half monolayer consisting entirely of Cd atoms is not electronically equivalent to a true half CdSe monolayer, and has apparently induced a (non-strain) shift component of 87 meV (Table 3.5), on the same order as that predicted for a true half monolayer.   We consider that the addition of Cd(oleate)$_2$ to the QB surfaces allows the exciton wave functions to delocalize to the Cd atoms within this passivation layer, and therefore to have effectively increased the confinement dimension, or the thickness of the box.

A similar analysis may be applied to the CdS QPs.   The amine-passivated {CdS[*n*-octylamine]$_p$} QPs used here have a thickness of 4 CdS monolayers.[3]   Addition of a complete 5th CdS monolayer results in a shift of the lowest-energy absorption from 3.28 to 2.98 eV, or by 300 meV.[3,14]   Addition of a half monolayer of CdS should have caused a shift to lower energy of approximately 300/2 meV, or 150 meV.   Addition of a half monolayer of Cd atoms by passivation with Cd(oleate)$_2$ has induced a shift component of 39 meV (Table 3.5), on the order of that expected of a true half CdS monolayer.   Thus, the effective thickness dimension of the CdS QPs has been increased by exchanging L-type amine passivation for Z-type Cd(oleate)$_2$ passivation.

Significantly, Z-type passivation with Zn(oleate)$_2$ does not increase the effective thickness dimension of the CdSe or CdS nanocrystals; in those cases the spectral shifts observed are due

entirely to changes in the strain states (see Table 3.5, and the discussion above). Thus, addition of Zn atoms to the top and bottom surfaces does not induce exciton delocalization into the Zn(oleate)$_2$ passivation layers. Rather the excitons remain confined within the CdSe and CdS lattices. Recall that the Zn atoms in Zn(oleate)$_2$ are coordinating to surface Se and S atoms, respectively, forming nascent ZnSe and ZnS layers. The band offsets of ZnSe and ZnS relative to those of CdSe and CdS, respectively, indicate that these should be Type-I interfaces[23,24], thus confining the electrons and holes within the CdSe and CdS core lattices.

3.5 Conclusion

The large, reversible spectral shifts observed in 2D CdSe and CdS nanocrystals when L-type amine passivation is exchanged for Z-type Cd(oleate)$_2$ passivation have both strain and confinement-dimensionality components of comparable magnitude. Excitons delocalize into the Cd(oleate)$_2$ passivation layers. In contrast, the smaller, reversible spectral shifts that occur upon exchanging amine and Zn(oleate)$_2$ passivation are due only to strain, as the surface-bound Zn atoms do not extend the CdSe and CdS lattices. We propose that the fairly large changes in the strain states upon surface exchange are due to the very large surface areas of the 2D II-VI nanocrystals, and the large spectral-shift components due to changes in confinement dimensionality are due to the small thicknesses of the nanocrystals.

3.6 References

(1) Liu, Y. H.; Wang, F. D.; Wang, Y. Y.; Gibbons, P. C.; Buhro, W. E. *J. Am. Chem. Soc.* **2011**, *133*, 17005.

(2) Wang, Y. Y.; Zhou, Y.; Zhang, Y.; Buhro, W. E. *Inorg. Chem.* **2015**, *54*, 1165.

(3) Wang, F.; Wang, Y.; Liu, Y.-H.; Morrison, P. J.; Loomis, R. A.; Buhro, W. E. *Acc. Chem. Res.* **2015**, *48*, 13.

(4) Zelenak, V.; Vargova, Z.; Gyoryova, K. *Spectrochim. Acta A* **2007**, *66*, 262.

(5) Morrison, P. J.; Loomis, R. A.; Buhro, W. E. *Chem. Mater.* **2014**, *26*, 5012.

(6) Wang, Y.; Zhou, Y.; Zhang, Y.; Buhro, W. E. *Inorg. Chem.* **2015**, *54*, 1165.

(7) Li, Z.; Peng, X. G. *J. Am. Chem. Soc.* **2011**, *133*, 6578.

(8) Ithurria, S.; Tessier, M. D.; Mahler, B.; Lobo, R. P. S. M.; Dubertret, B.; Efros, A. *Nat. Mater.* **2011**, *10*, 936.

(9) Meulenberg, R. W.; Jennings, T.; Strouse, G. F. *Phys. Rev. B* **2004**, *70*.

(10) Wang, Y. Y.; Zhang, Y.; Wang, F. D.; Giblin, D. E.; Hoy, J.; Rohrs, H. W.; Loomis, R. A.; Buhro, W. E. *Chem. Mater.* **2014**, *26*, 6318.

(11) Liu, Y. H.; Wayman, V. L.; Gibbons, P. C.; Loomis, R. A.; Buhro, W. E. *Nano Lett.* **2010**, *10*, 352.

(12) Joo, J.; Son, J. S.; Kwon, S. G.; Yu, J. H.; Hyeon, T. *J. Am. Chem. Soc.* **2006**, *128*, 5632.

(13) Son, J. S.; Wen, X. D.; Joo, J.; Chae, J.; Baek, S. I.; Park, K.; Kim, J. H.; An, K.; Yu, J. H.; Kwon, S. G.; Choi, S. H.; Wang, Z. W.; Kim, Y. W.; Kuk, Y.; Hoffmann, R.; Hyeon, T. *Angew. Chem.; Int. Ed.* **2009**, *48*, 6861.

(14) Son, J. S.; Park, K.; Kwon, S. G.; Yang, J.; Choi, M. K.; Kim, J.; Yu, J. H.; Joo, J.; Hyeon, T. *Small* **2012**, *8*, 2394.

(15) Cooper, J. K.; Franco, A. M.; Gul, S.; Corrado, C.; Zhang, J. Z. *Langmuir* **2011**, *27*, 8486.

(16) Li, J. B.; Wang, L. W. *Appl. Phys. Lett.* **2004**, *85*, 2929.

(17) Shan, W.; Walukiewicz, W.; Ager, J. W.; Yu, K. M.; Wu, J.; Haller, E. E. *Appl. Phys. Lett.* **2004**, *84*, 67.

(18) Béliveau, A.; Carlone, C. *Phys. Rev. B* **1990**, *41*, 9860.

(19) Yang, J. W.; Hou, H. J. *High Pressure Res.* **2012**, *32*, 376.

(20) Wei, S.-H.; Zunger, A. *Phys. Rev. B* **1999**, *60*, 5404.

(21) Deligoz, E.; Colakoglu, K.; Ciftci, Y. *Physica. B: Condensed Matter.* **2006**, *373*, 124.

(22) Jastrzebski, Z. D. *The Nature and Properties of Engineering Materials,* 2nd ed.; John Wiley & Sons: New York, 1977; pp 202.

(23) Wei, S. H.; Zunger, A. *Appl. Phys. Lett.* **1998**, *72*, 2011.

(24) Reiss, P.; Protière, M.; Li, L. *Small* **2009**, *5*, 154.

Chapter 4

Reversible Exchange of L-type and Bound-Ion-Pair X-type Ligation on Cadmium Selenide Quantum Belts

4.1 Introduction

We now demonstrate facile interchange of neutral-donor amine (L-type) and anionic (X-type) ligation[1] of CdSe quantum belts[2] (QBs, Figure 4.1a). Exposure of *n*-octylamine-passivated QBs to protic acids HX (X = halide, nitrate, or carboxylate) results in the surface displacement of the amine ligands by X^- anions and protonation of the liberated amines, forming surface-bound ion pairs,[3,4] with the newly formed *n*-octylammonium ions or protonated phosphines balancing the surface charge. The bound-ion-pair X-type ligation is in turn displaced by excess *n*-octylamine, restoring the original L-type ligation. These ligand exchanges are readily monitored spectro-scopically.
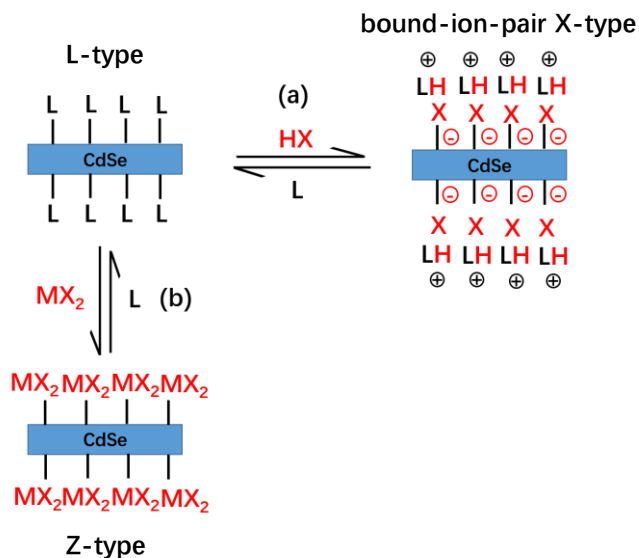
Figure 4.1. Surface-exchange pathways in CdSe QBs. (a) L-type to bound-ion-pair X-type exchange. (b) L-type to Z-type (MX_2) exchange.

The nature of the surface ligation on semiconductor nanocrystals greatly influences their lumi-nescence,[5-8,] charge-transport properties,[9,10] and band-edge energies,[11,12] but was not well charac-terized until fairly recently.[13,14] Nanocrystal surface ligation was recently systematized by Owen

and coworkers,[1,8] who classified ligands as anionic X-type, neutral-donor L-type, and neutral-acceptor Z-type (Figure 4.2), using Green's covalent-bond classification.[15] Their analysis accounted for the coexistence of X, L, and/or Z-type ligation commonly observed on nanocrystal surfaces. Moreover, they demonstrated reversible exchange between L and Z-type passivation. This work explained the varying surface ligation and lattice stoichiometries (cation-anion ratios) produced by nominally similar nanocrystal syntheses. We subsequently reported reversible L-type, Z-type exchange in CdSe QBs (Scheme 4.1b).[16]

L-type   **Z-type**
Lewis base   **Lewis acid**

L MX_2

X $\text{X}^{\ominus}$

X-type $\text{LH}^{\oplus}$
charge balancing   **X-type**
                   bound ion pair
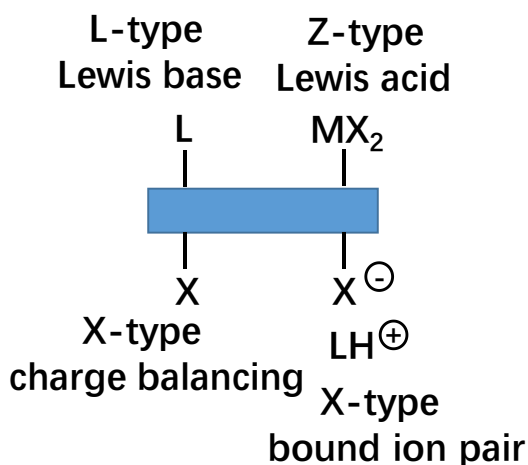
Figure 4.2. Types[1] of nanocrystal ligation according to Green's covalent-bond classification.[15]

Owen and coworkers have identified a specific X-type ligation and configuration, the bound ion pair (Figure 4.2), that is employed in this work.[3,4] X-type ligation occurs in at least two forms: anionic ligands that balance lattice charge resulting from lattice non-stoichiometry, and anionic ligands that add surface charge, which is balanced by a counter ion, forming a bound ion pair. Owen and coworkers also demonstrated that L-type passivation can be converted to bound-

ion-pair X-type passivation on colloidal CdSe nanocrystals.[4] We show here that L-type and bound-ion-pair X-type ligation can be extensively and reversibly interchanged on CdSe QBs.

4.2 Experimental Section

4.2.1 Materials and General Procedures

Cadmium acetate dihydrate ($Cd(OAc)_2 \cdot 2H_2O$, >98%) was obtained from Sigma-Aldrich and Mallinckrodt. Selenourea (98%), *n*-octylamine (99%), tri-*n*-octylphosphine (97%), toluene (CHROMASOLV ® for HPLC, 99.9%), acetonitrile (CHROMASOLV ® for HPLC, 99.9%), hydrochloric acid (ACS reagent, 37%), hydrobromic acid (ACS reagent, 48%), acetic acid (ACS reagent, ≥99.7%), and benzoic acid (ACS reagent, ≥99.5%) were obtained from Sigma-Aldrich. Nitric Acid (A.C.S. reagent, 69.0-70%) was obtained from J. T. Baker. All reagents were used as received. TEM sample grids (Cu with holey carbon film) were obtained from Ted Pella, Inc.

The {CdSe[*n*-octylamine]$_{0.53}$} quantum belts (QBs)[18] were prepared as previously reported. All other synthetic procedures were conducted under the ambient atmosphere unless otherwise indicated.

4.2.2 Analyses

UV-visible spectra were obtained from a Varian Cary 100 Bio UV-visible spectrophotometer. XRD patterns were obtained from a Bruker d8 Advance X-ray Diffractometer. Low-resolution TEM images were obtained from a JEOL 2000FX microscope operating at 200 kV. IR spectra were obtained from a Perkin Elmer Spectrum BX FT-IR System. Elemental analyses (Table S2; C, H, N, Br, and P) were obtained from Galbraith Laboratories, Inc. (Knoxville, TN).

Table 4.1. Elemental-analysis data collected from several specimens from different synthetic batches and the empirical formulas of {CdSe[X]$_a$[n-octylammonium]$_b$[TOP]$_c$} determined from them.

{CdSe[Br]$_{0.44 \pm 0.03}$[**n-octylammonium**]$_{0.41 \pm 0.05}$[**TOPH**]$_{0.003}$}	%C	%H	%N	%P	Br%
Calcd	14.02	2.94	2.04	0.030	12.52
Found (Avg.)	14.53	2.57	1.75	0.030	12.64
Found (1)	15.80	2.89	2.13	0.030	13.02
Found (2)	14.87	2.76	1.4	N/A	12.26
Found (3)	12.91	2.07	1.73	N/A	N/A

{CdSe[OBz]$_{0.08 \pm 0.06}$[**n-octylammonium**]$_{0.02 \pm 0.01}$[**TOPH**]$_{0.06 \pm 0.01}$}					
Calcd	11.48	1.75	0.1	0.822	
Found (Avg.)	13.06	1.59	<0.5	0.814	
Found (1)	13.24	1.82	<0.5	0.814	
Found (2)	12.88	1.36	<0.5	N/A	

{CdSe[OAc]$_{0.16 \pm 0.2}$[**n-octylammonium**]$_{0.02 \pm 0.01}$[**TOPH**]$_{0.14 \pm 0.02}$}					
Calcd	18.05	3.22	0.1	1.70	
Found (Avg.)	18.99	2.83	<0.5	1.71	
Found (1)	19.0	2.98	<0.5	1.59	
Found (3)	19.45	2.92	<0.5	1.83	
Found (2)	18.51	2.60	<0.5	N/A	

{CdSe[NO$_3$]$_{0.10 \pm 0.01}$[**TOPH**]$_{0.12 \pm 0.02}$}	%C	%H	%N	%P	%Br
Calcd	14.28	2.60	0.58		
Found (Avg.)	15.16	2.23	0.56		
Found (1)	17.09	2.59	0.62		
Found (2)	13.22	1.86	<0.5		

4.2.3 Preparation of HX solutions

Benzoic acid solution: benzoic acid (1.2 g) was dissolved in acetonitrile (6 mL) and toluene (3 mL) in a test tube and sonicated for 10 min to obtain a clear solution.

Nitric acid solution: 60-70% nitric acid (5 drops) was dissolved in acetonitrile (1.5 mL).

Hydrochloric acid solution: 37% hydrochloric acid (10 drops) was dissolved in acetonitrile (1.8 mL).

Hydrobromic acid solution: 48% hydrobromic acid (10 drops) was dissolved in acetonitrile (1.8 mL).

The Acetic acid solution was used as received.

4.2.4 Preparation of a Stock Dispersion of {CdSe[*n*-octylamine]$_{0.53}$} QBs

The synthesis of {CdSe[*n*-octylamine]$_{0.53}$} QBs was conducted on the same scale as that previously reported[18] (corresponding to 0.27 mmol of Cd(OAc)$_2 \cdot$2H$_2$O and 0.47 mmol of selenourea. The yellow dispersion obtained after TOP addition was stored under N$_2$ at room temperature for use as a stock dispersion.

4.2.5 Surface Exchange of {CdSe[*n*-octylamine]$_{0.53}$} QBs with HX

An aliquot (0.5 g) of the CdSe QB stock dispersion was transferred to a test tube and toluene (1 mL) was added. The resulting pale-yellow precipitate was separated by a benchtop centrifuge (1500 RPM, 5 min), and the supernatant was discarded. The dispersion-centrifugation cycle was repeated one additional time. The purpose of this purification process was to remove excess *n*-octylamine. In a typical surface exchange with HOAc, toluene (1 mL) and TOP (0.4 mL) were added to the precipitated {CdSe[*n*-octylamine]$_{0.53}$} QBs, resulting in a cloudy, pale-yellow mixture, followed by the addition of acetic acid solution (1.5 mL). The pale yellow solution turned

brighter instantaneously upon mixing. Two drops of this solution were taken to obtain an absorption spectrum. The reactions with other acids were conducted similarly, except that various amounts of TOP (0.8 mL for HCl and HBr, 0.4 mL for HOBz and HNO_3) and acid (5 drops of HNO_3 solution, 10 drops of HCl and HBr solutions, and 9 mL of HOBz solution) were used.

Subsequent analyses were conducted using purified X-ligated CdSe QBs. Toluene (1.5 mL) and acetonitrile (0.5 mL) were added to the X-ligated QB dispersions, resulting in a bright-yellow precipitate, which was collected after centrifugation (4500 rpm, 5 min). This precipitate was used for XRD analyses. For IR and elemental analysis, the toluene-acetonitrile dispersion and centrifugation cycle was conducted 2-4 additional times to ensure removal of free ligands.

4.2.6 Back Exchange of X-ligated CdSe QBs to {CdSe[*n*-octylamine]$_x$} QBs

Back exchange reactions were conducted using the X-ligated CdSe QB dispersions prior to purification. Addition of *n*-octylamine (3 mL) converted the bright-yellow dispersions to a pale-yellow color. Two drops of the resulting {CdSe[*n*-octylamine]$_x$} dispersion were taken to obtain absorption spectra. Subsequent analyses such as IR spectroscopy were conducted after purification as described above for the X-ligated QBs.

4.3 Results and Discussion

Pseudo-2D CdSe QBs provide an excellent system for studies of surface exchanges because their absorption (extinction) spectra are highly sensitive to changes in surface ligation. For example, we previously reported that the lowest-energy feature in the spectrum of CdSe QBs (1.8-nm thickness) shifts by 140 meV when L-type *n*-octylamine passivation is exchanged to Z-type Cd(oleate)$_2$ passivation.[16] Back exchange to L-type amine ligation restores the original spectral

positions. That spectral sensitivity is used here as a useful barometer for monitoring the surface exchanges in the present study.

L-ligated CdSe QBs of composition {CdSe[n-octylamine]$_{0.53}$}, were dispersed in toluene solutions containing (n-octyl)$_3$P (TOP), and were titrated with the acids HX (X = OBz, OAc, NO$_3$, Cl, or Br) to achieve the maximum shifts in their absorption spectra. Figure 4.3 compares the initial spectra of the amine-ligated QBs with and without added TOP (which are effectively identical) to the spectra obtained with the maximum shift for each HX. The shifts in the lowest-energy feature ranged from 49 meV for addition of benzoic acid (HOBz) to 112 meV for addition of HCl or HBr (Table 4.2). In all cases, the spectral shifts induced by HX addition occurred within seconds at 25 °C.
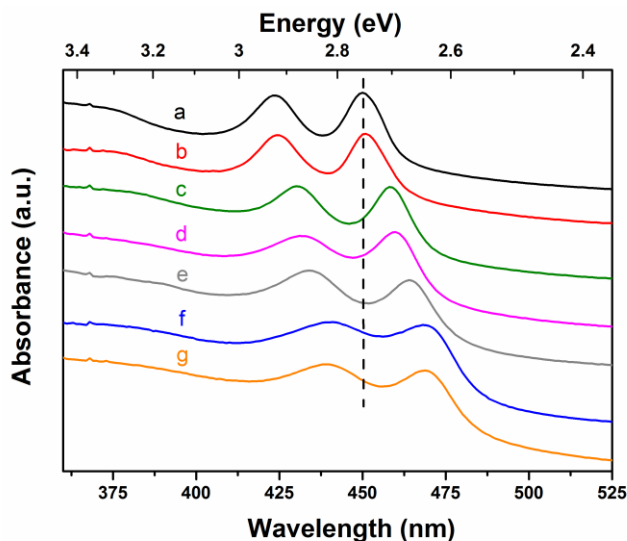

Figure 4.3. Absorption (extinction) spectra of CdSe QBs before and after addition of HX. (a) starting n-octylamine-ligated QBs; (b) starting QBs after addition of TOP; (c) X = OBz; (d) X = OAc; (e) X = NO$_3$; (f) X = Cl; (g) X = Br.

Table 4.2. Lowest-energy λ_{max} values and energy shifts associated with the variously passivated CdSe QBs.

QBs	λ_{max} (first absorption, nm)	spectroscopic energy shift (meV)
{CdSe[n-octylamine]$_{0.53}$}	450	0
{CdSe[n-octylamine]$_x$[TOP]$_y$}	451	6
{CdSe[OBz]$_{0.08}$[n-octylammonium]$_{0.02}$[TOPH]$_{0.06}$}	458	49
{CdSe[Ac]$_{0.16}$[n-octylammonium]$_{0.02}$[TOPH]$_{0.14}$}	460	60
{CdSe[NO$_3$]$_{0.10}$[TOPH]$_{0.12}$}	464	84
{CdSe[Cl]$_n$[n-octylammonium]$_p$[TOP]$_q$}	469	112
{CdSe[Br]$_{0.44}$[n-octylammonium]$_{0.41}$}	469	112

Upon addition of n-octylamine to the QBs treated with benzoic, nitric, or acetic acid, the spectral features were observed to shift back to their original positions in the L-passivated starting QBs (Figure 4.4). In contrast, addition of n-octylamine to the QBs treated with HCl or HBr resulted in partial spectral shifts of approximately halfway toward the original positions (Figure 4.5). We surmised that the surface exchanges induced by addition of benzoic, nitric, or acetic acid were fully reversed upon addition of n-octylamine, whereas those induced by HCl or HBr were only partially reversed. As judged by the spectral shifts, all of these exchanges also occurred within seconds at 25 °C.
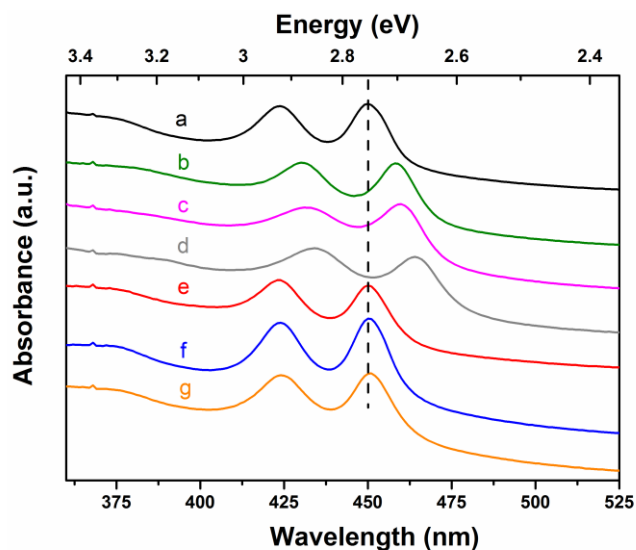
Figure 4.4. Absorption spectra of CdSe QBs. (a) starting *n*-octylamine-ligated QBs; (b-d) after treatment with HX (X = OBz (b), OAc (c), NO$_3$ (d)); and (e-g) after re-exposure to *n*-octylamine ((e) from b, (f) from c, (g) from d).
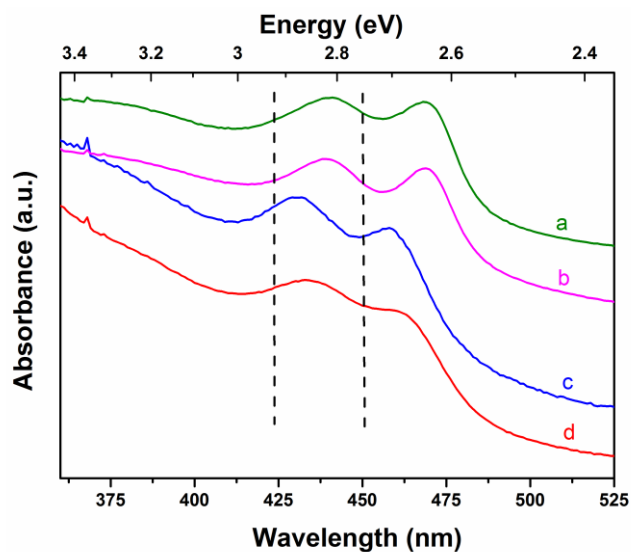
Figure 4.5. Absorption spectra of CdSe QBs after treatment with HCl (a), HBr (b), and after re-exposure to *n*-octylamine ((c) from a, (d) from purified b). The dashed lines indicate the peak positions for the fully amine-ligated {CdSe[*n*-octylamine]$_{0.53}$} QBs.

IR spectra of the CdSe QBs after reaction with the protic acids HX are recorded in Figure 4.6. The spectra after reaction with acetic and benzoic acids (Figure 4.6a, b) contained features assigned to the asymmetric and symmetric stretches of the carboxylate ligands. The spectrum obtained

100

upon reaction of QBs and nitric acid contained a feature assignable to the nitrate ligand (Figure 4.6c).[17] All of the spectra contained vibrational frequencies associated with *n*-octylamine, indicating that (at least some of) the original L-type ligation had been retained in some form. For comparison, the IR spectrum of sodium benzoate is provided in Figure 4.7.

Figure 4.6. IR spectra of CdSe QBs after reaction with HX; X = (a) OAc, (b) OBz, (c) NO_3, (d) Br, and (e) Cl. Various vibrational modes are assigned by arrows and text.

Figure 4.7. IR spectrum of pure sodium benzoate. The asymmetric and symmetric CO_2 stretches are identified.
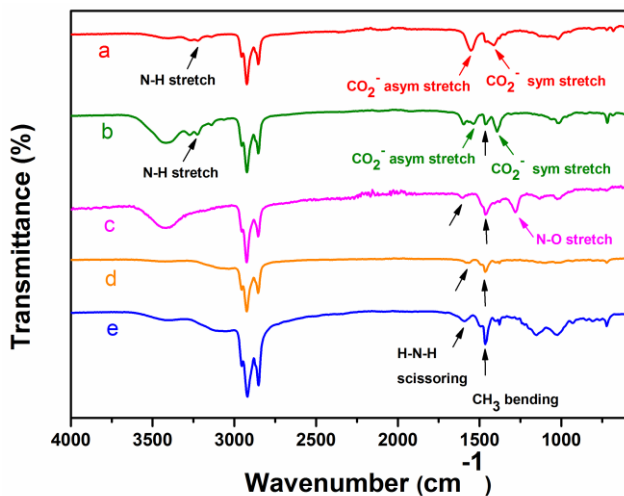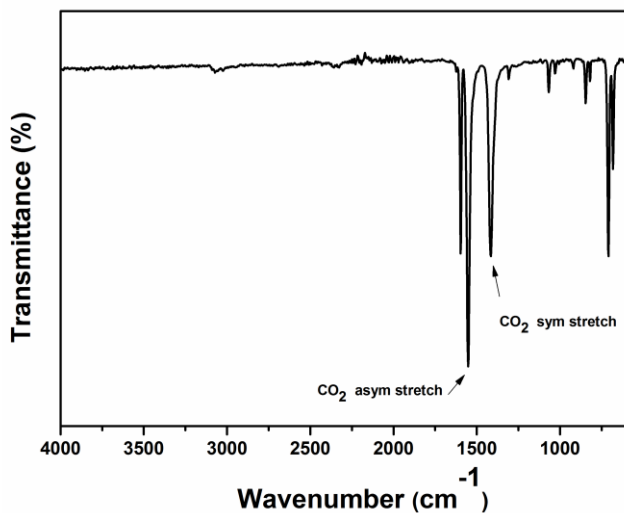
Figure 4.8 provides the IR spectra of the QBs, initially treated with HX (X = OAc, OBz, and NO$_3$), after back exchange with *n*-octylamine. The features characteristic of the X ligation were no longer present, and the spectra were consistent with that of the starting, *n*-octylamine-ligated QBs (Figure 4.8d). The results were also consistent with the UV-visible spectral evolution for these cases, which suggested complete reversal of the surface exchanges induced by initial addition of acetic, benzoic, and nitric acid.
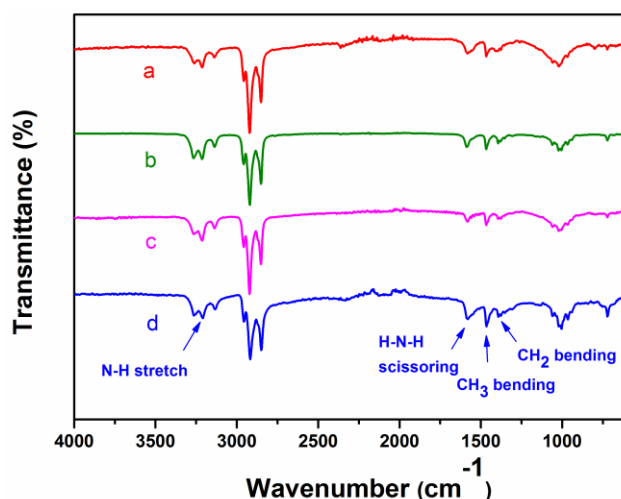
Figure 4.8. IR spectra of CdSe QBs, initially treated with HX (X = OAc, OBz, and NO$_3$), after back exchange with *n*-octylamine; X = (a) OAc, (b) OBz, (c) NO3. Spectrum (d) is of starting *n*-octylamine-ligated CdSe QBs, for comparison.

Information about the passivation of the CdSe QBs after reaction with HX was also obtained by low-angle XRD. The QBs tend to align in stacked bundles in the solid state, such that the low-angle XRD 00ℓ reflections provide a measure of the inter-QB *d* spacing in such bundles. The *d* spacings extracted from the data (Figure 4.9) were in the range of 2.37 − 2.61 nm, which is consistent with the retention of the *n*-octylamine groups (in some form) in the passivation layers surrounding the QBs. For comparison, the inter-QB *d* spacing in the starting, *n*-octylamine-ligated QBs was 2.51 nm.[16]
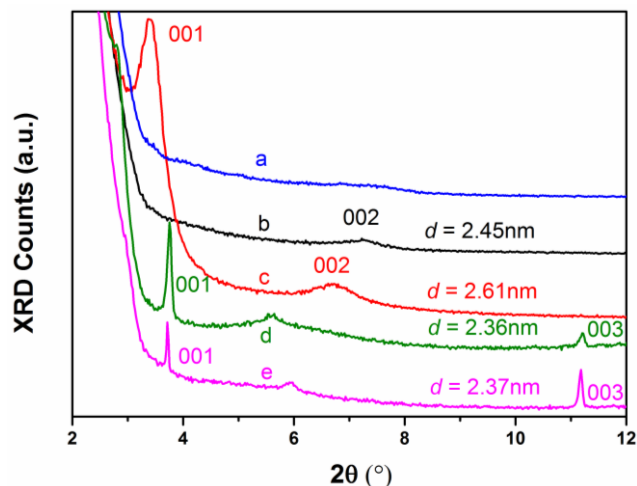
Figure 4.9. Low-angle XRD patterns of CdSe QBs after treatment with HX (X = OBz (a), OAc (b), NO_3 (c), Cl (d), and Br(e)) The lamellar 00ℓ reflections are indexed. The lamellar d spacing are also provided as insets.

The L- to bound-ion-pair X-type exchange process proposed above was slightly modified by the elemental-analysis data for the HX-treated QBs. The best exchange results were obtained in the presence of added TOP, which we surmise served to buffer the acidity of the strong acids. Consequently, two L-type ligands were present in the reaction mixtures, *n*-octylamine and TOP, and two possible charge-balancing countercations, *n*-octylammonium and $TOPH^+$.

The elemental-analysis data (Table 4.1) for the HBr-treated QBs were consistent with the formula $\{CdSe[Br]_{0.44}[n\text{-octylammonium}]_{0.41}\}$, indicating retention and incorporation of the original L-type ligands. However, the analyses of the HNO3-treated QBs gave the formula $\{CdSe[NO_3]_{0.10}[TOPH]_{0.12}\}$, showing the original ligands to have been replaced by TOPH as the counter-cations. The HOBz- and HOAc-treated QBs gave mixed ligation: $\{CdSe[OBz]_{0.08}[n\text{-octylammonium}]_{0.02}[TOPH]_{0.06}\}$ and $\{CdSe[OAc]_{0.16}[n\text{-octylammonium}]_{0.02}[TOPH]_{0.14}\}$. We suspect that even the HNO3-treated QBs contained traces of *n*-octylammonium ions given the N-H stretch evident in the IR spectrum (Figure 4.6c). (The HCl-treated QBs were insufficiently stable to send for elemental analysis.)

103

We previously proposed surface-structure models for the L-type ligation in {CdSe[*n*-octyla-mine]$_{0.53}$} and Z-type ligation in {CdSe[Cd(oleate)$_2$]$_{0.19}$}.[16] The large-area top and bottom fac-ets, and the smaller edge facets of the CdSe QBs, if un-reconstructed, possess corrugated, ridge-and-valley structures with half of the surface Cd and Se atoms in nominally three-coordinated ridge positions. In contrast the half of the Cd and Se atoms in valley positions are nominally four coordinated and sterically hindered. We proposed that the L-type ligation in {CdSe[*n*-octyl-amine]$_{0.53}$} consisted of one L coordinated to each surface Cd and Se in a ridge position. The ideal stoichiometry calculated for that arrangement was {CdSe[L]$_{0.52}$}. We proposed that the Z-type ligation in {CdSe[Cd(oleate)$_2$]$_{0.19}$} consisted of one Z-type unit per surface Se in a ridge po-sition. The ideal stoichiometry for that arrangement ranged from {CdSe[Z]$_{0.20-0.26}$}, depending on the degree of passivation of the thin edge facets. The stoichiometries of the X-type ligation determined here ranged from CdSe[OBz]$_{0.08}$ to CdSe[Br]$_{0.44}$. While surface-structure models have not yet been developed, we note that the stoichiometries for the X-type ligation are close to the values previously determined for L-type and Z-type ligation.[16]

If, as we have proposed, the processes responsible for the observed spectral changes are merely surface exchanges, then the QB morphologies should not be grossly altered by these processes. A TEM image of the initial amine-ligated {CdSe[*n*-octylamine]$_{0.53}$} QBs is shown in Figure 4.10a. The QBs are synthesized in bundled stacks with their thin edges evident. We demon-strated elsewhere that the mean lengths of such QBs are >350 nm.[16,18] Figure 4.10b-d show the QBs after reaction with HX (X = OBz, NO$_3$, and Br). The nanocrystal morphologies remained intact, except that the QBs were largely unbundled from the as-synthesized stacks, and were shortened (to 100 – 150 nm). We previously observed such QB shortening to result from L-type to Z-type exchange, and attributed the shortening to the additional physical manipulations of the

QBs involved in the exchange processes. Because the QBs are quantum confined in only the thickness dimension, which is unchanged, their extinction (absorption) spectra are not affected by shortening. Images of Cl-ligated QBs are provided in Figure 4.11.
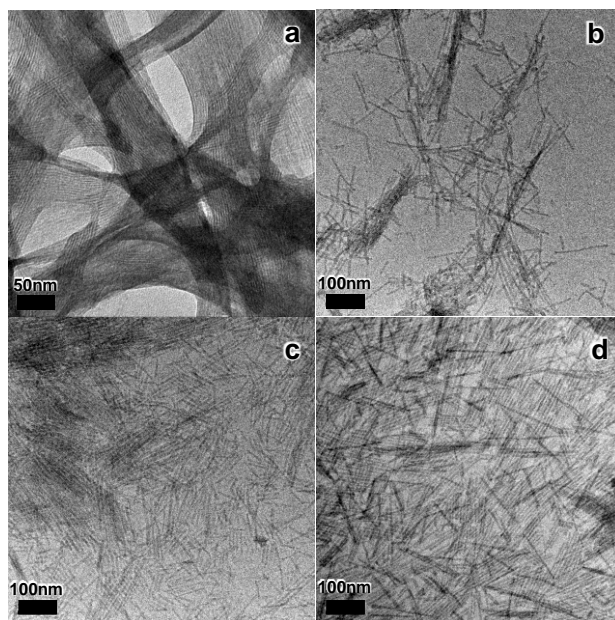

Figure 4.10. TEM images of variously ligated CdSe QBs. (a) starting, bundled *n*-octylamine-ligated QBs, (b) OBz⁻-ligated QBs, (c) NO3⁻-ligated QBs, and (d) Br⁻-ligated QBs.
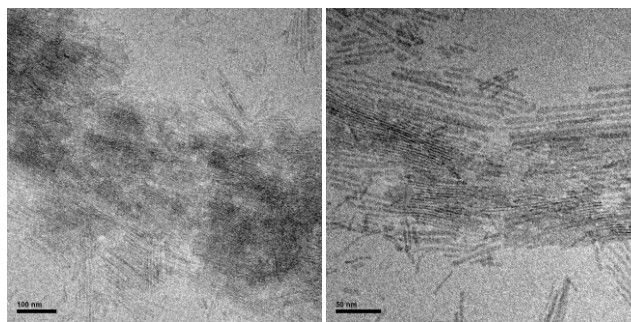

Figure 4.11. TEM images of Cl-ligated CdSe QBs.

The surface exchanges studied here resulted in spectral shifts of 49 -112 meV (Figure 4.3). Our previous study of L-type, Z-type exchange in CdSe QBs established that a significant component of such shifts resulted from changes in the strain state of the QBs upon surface exchange.[16] The amine-passivated QBs are significantly compressively strained (3.4% in lattice parameter *a*), which is largely relaxed upon exchange for Z-type ligation. The strain states of the exchanged QBs here were extracted from the high-angle XRD patterns (Figure 4.12). Interestingly, exchange of L-type for X-type ligation did not markedly change the strain states of the CdSe QBs, which remained significantly compressively strained (2.4 – 3.4% in *a*). Consequently, the observed spectral shifting (Figure 4.3) must have a different origin (discussed below).
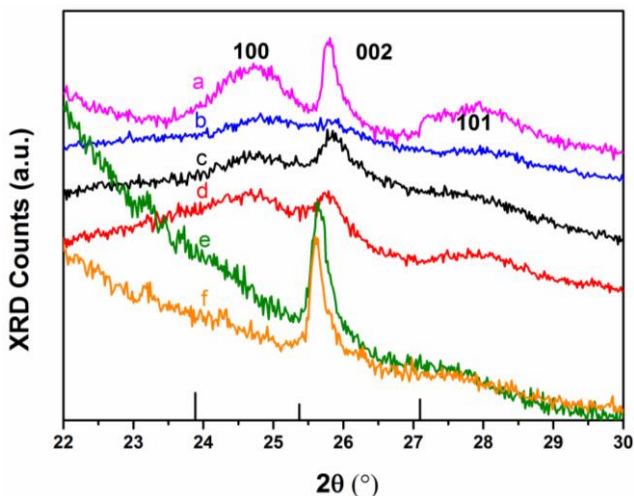
Figure 4.12. High-angle XRD patterns of *n*-octylamine-ligated CdSe QBs after unbundling with oleylamine (a) and treatment with HX (X = OBz (b), OAc (c), NO_3 (d), Cl (e), and Br(f)), in the range of the first three (100, 002, and 101) reflections. The black lines on the *x* axis are the positions of these reflections in bulk CdSe.

The results above support the exchange process proposed in Figure 4.1a. The spectral shift obtained upon L- to X-type exchange varies by the X^- ligand (except for Cl^- and Br^-, which give equal 112 meV shifts), consistent with the surface binding of a different X-type group in each case. The expected IR features are observed for the X-type ligands, and the spectra support the

retention of the original L-type ligands as protonated n-octylammonium groups. Retention of the n-octylammonium ions, and/or the incorporation of TOPH$^+$ counter-cations, which also contain n-octyl chains, was also supported by the inter-QB spacings measured by low-angle XRD in aggregates of the exchanged X-type QBs. TEM images confirmed overall retention of the QB morphologies, and the elemental-analysis data were also consistent with the proposed exchanges. Finally, the L- for X-type exchanges were fully reversible in three of the cases (X = OBz, OAc, and NO$_3$). Taken together, these results provide compelling support for Figure 4.1a.

The modest spectral shifts observed upon L- to X-type exchange (49 – 112 meV) apparently resulted from the surface charges introduced by the exchanges. Two contributions to spectral shifting were previously identified in L- to Z-type ligand exchange, which were changes in the lattice strain of the QB cores and extension (thickening) of the crystal lattice by the Cd atoms in the Z-type ligands, decreasing the quantum confinement.[16] Neither of these contributions is active here, as the lattice strain is largely unchanged by L- to X-type exchange, and none of the X groups involve Cd or Se atoms. Gamelin and coworkers have previously proposed that surface dipoles induced by charged surface ligation were responsible for large shifts in CdSe-nanocrystal band-edge potentials.[11] In the present cases, negative surface charges and associated dipoles should slightly increase the energy of the valence-band edge, and decrease the energy of the conduction-band edge, inducing the modest observed X-ligand-dependent spectral shifts to lower energies.

4.4 Conclusions

In summary exchange of L-type to bound-ion-pair X-type ligation in CdSe QBs is facile, and in some cases fully reversible. Such exchange processes may become useful tools for purposeful functionalization of nanocrystal surfaces.

4.5 References

(1) Anderson, N. C.; Hendricks, M. P.; Choi, J. J.; Owen, J. S. *J. Am. Chem. Soc.* **2013**, *135*, 18536.

(2) Liu, Y. H.; Wang, F. D.; Wang, Y. Y.; Gibbons, P. C.; Buhro, W. E. *J. Am. Chem. Soc.* **2011**, *133*, 17005.

(3) Anderson, N. C.; Owen, J. S. *Chem. Mater.* **2013**, *25*, 69.

(4) Chen, P. E.; Anderson, N. C.; Norman, Z. M.; Owen, J. S. *J. Am. Chem. Soc.* **2017**, *139*, 3227.

(5) Houtepen, A. J.; Hens, Z.; Owen, J. S.; Infante, I. *Chem. Mater.* **2017**, *29*, 752.

(6) Peterson, M. D.; Cass, L. C.; Harris, R. D.; Edme, K.; Sung, K.; Weiss, E. A. *Annu. Rev. Phys. Chem.* **2014**, *65*, 317.

(7) Swenson, N. K.; Ratner, M. A.; Weiss, E. A. *J. Phys. Chem. C* **2016**, *120*, 6859.

(8) Owen, J. *Science* **2015**, *347*, 615.

(9) Carey, G. H.; Abdelhady, A. L.; Ning, Z.; Thon, S. M.; Bakr, O. M.; Sargent, E. H. *Chem. Rev.* **2015**, *115*, 12732.

(10) Milliron, D. J. *Nat. Mater.* **2014**, *13*, 772.

(11) Carroll, G. M.; Tsui, E. Y.; Brozek, C. K.; Gamelin, D. R. *Chem. Mater.* **2016**, *28*, 7912.

(12) Soreni-Harari, M.; Yaacobi-Gross, N.; Steiner, D.; Aharoni, A.; Banin, U.; Millo, O.; Tessler, N. *Nano Lett.* **2008**, *8*, 678.

(13) Hens, Z.; Martins, J. C. A *Chem. Mater.* **2013**, *25*, 1211.

(14) Morris-Cohen, A. J.; Malicki, M.; Peterson, M. D.; Slavin, J. W. J.; Weiss, E. A. *Chem. Mater.* **2013**, *25*, 1155.

(15) Green, M. L. H. *J. Organomet. Chem.* **1995**, *500*, 127.

(16) Zhou, Y.; Wang, F.; Buhro, W. E. *J. Am. Chem. Soc.* **2015**, *137*, 15198.

(17) Addison, C. C.; Logan, N.; Wallwork, S. C.; Garner, C. D. *Q. Rev. Chem. Soc.* **1971**, *25*, 289.

(18) Liu, Y. H.; Wayman, V. L.; Gibbons, P. C.; Loomis, R. A.; Buhro, W. E. *Nano Lett.* **2010**, *10*, 352

Chapter 5

Conclusions and Future Work

5.1 Conclusions

In this dissertation, synthesis of II-VI magic-size clusters as well as the ligand exchange on the corresponding 2D QBs/QPs were reported. Specifically, L- to Z- type and L- to bound-ion-pair X- type ligand exchange were discussed in detail.

In Chapter 2, $(ZnSe)_{34}$ and $(CdTe)_{34}$ were characterized by UV-Visible spectroscopy, IR spectroscopy, mass spectrometry and elemental analysis. The stoichiometries of $[(ZnSe)_{34}(n\text{-octylamine})_{29}(\text{di-}n\text{-octylamine})_5]$ and $[(CdTe)_5(\text{di-}n\text{-pentylamine})_{12}]$ were consistent with other amine-ligated $(II\text{-}VI)_{34}$ we previously obtained[1,2]. Now conversion of three $(II\text{-}VI)_{34}$ derivatives: $(CdSe)_{34}$ $(ZnSe)_{34}$ and $(CdTe)_{34}$ to the corresponding $(II\text{-}VI)_{13}$ derivatives were observed because those three $(II\text{-}VI)_{34}$ were not as thermally stable as the corresponding $(II\text{-}VI)_{13}$ clusters. The thermal stabilities of the $(II\text{-}VI)_{34}$ derivatives increased from $(Cd\text{-}VI)_{34}$ to $(Zn\text{-}VI)_{34}$, and from $(II\text{-}S)_{34}$ to $(II\text{-}Te)_{34}$, obeying periodic trends. Both $(II\text{-}VI)_{34}$ and $(II\text{-}VI)_{13}$ clusters showed spectral homology and the lowest-energy feature of $(II\text{-}VI)_{34}$ scales linearly with the bulk band gap.

In Chapter 3, L- and Z-type surface exchange were conducted on 2D II-VI nanocrystals. Large, reversible spectral shifts were observed when the L-type amine passivation was exchanged to Z-type $Cd(oleate)_2$ passivation on CdSe QBs and CdS QPs. We reported here that both strain and confinement dimensionality contributed to the large spectral shifts comparably. The larger, reversible spectral shifts observed during the L-type to Z-type $Cd(oleate)_2$ exchange possessed both contributions while the smaller, reversible spectral shifts observed during the L-type to Z-type $Zn(oleate)_2$

exchange were due only to strain as the surface-bound Zn atoms did not increase CdSe or CdS thinkness as Cd(oleate)$_2$ unit did.

In Chapter 4, CdSe quantum belts of composition {CdSe[n-octylamine]$_{0.53}$} and protic acids HX (X = Cl, Br, NO$_3$, acetate (OAc), and benzoate (OBz)) reacted to exchange the L-type amine ligation to bound-ion-pair X-type ligation.   The latter ligation had X$^-$ anions bound to the nanocrystal surfaces and closely associated LH$^+$ counter-cations (protonated n-octylamine or tri-n-octylphosphine (TOP)) to balance the surface charges.   The compositions of the exchanged QBs were {CdSe[Br]$_{0.44}$[n-octylammonium]$_{0.41}$}, {CdSe[NO$_3$]$_{0.10}$[TOPH]$_{0.12}$}, {CdSe[OBz]$_{0.08}$[n-octylammonium]$_{0.02}$[TOPH]$_{0.06}$} and {CdSe[OAc]$_{0.16}$[n-octylammonium]$_{0.02}$[TOPH]$_{0.14}$}.   (The HCl-exchanged QBs were insufficiently stable for elemental analysis.)   The bound-ion-pair X-type ligation was fully reversed to L-type n-octylamine ligation in the cases of X = NO$_3$, acetate, and benzoate.   The ligand exchanges were monitored by absorption spectroscopy, and the exchanged, bound-ion-pair X-type ligated nanocrystals were characterized by a range of methods. These surface exchange processes provide a powerful tool for purposeful surface functionalization.

5.2 Future Work

First of all, since we have 9 of the 12 congeneric (II-VI)$_{13}$ and (II-VI)$_{34}$ nanoclusters corresponding to II = Zn, Cd and VI = S, Se, Te, we may explore the possibility to isolate the remaining three derivatives, (ZnS)$_{13}$, (CdS)$_{13}$, and (ZnTe)$_{34}$. In our previous

research, we studied the reactivity of the $(CdSe)_{34}$ clusters and realized the conversion of $(CdSe)_{34}$ to $(CdSe)_{13}$ or CdSe QPs was a competing process. In detail, the conversion of $(CdSe)_{34}$ to $(CdSe)_{13}$ after reacting $Cd(OAc)_2 \cdot 2H_2O$ and selenourea in an *n*-alkylamine/di-*n*-alkylamine solvent occurred at 0 °C while conversion of $(CdSe)_{34}$ to CdSe QBs required a relatively higher temperature of 25 °C.[1] Similarly, $(ZnSe)_{34}$ was reacting as a synthon in ZnSe QPs synthesis in alkylamine/di-*n*-alkylamine cosolvent at 100°C, for 18h,[2] but was readily converted to $(ZnSe)_{13}$ when removing from heat (100 °C) upon the formation of $(ZnSe)_{34}$ (4-10 min) and stood at RT for 2-7 days. We established that the conversion of $(II-VI)_{34}$ to corresponding QBs/QPs might require a higher energy than the conversion to $(II-VI)_{13}$ derivatives, which were thermodynamically more stable products under certain conditions. Notably, the thermal stabilities of the $(II-VI)_{34}$ derivatives increased from $(II-S)_{34}$ to $(II-Se)_{34}$. In the case of $(CdS)_{34}$, conversion of $(CdS)_{34}$ to QPs in an *n*-octylamine-di-*n*-pentylamine cosolvent mixture only required a temperature as low as 0 °C.[2] Thus, the conversion of $(CdS)_{34}$ to $(CdS)_{13}$ might occur at even lower temperature below 0 °C, making it difficult to observe under normal experimental conditions. As for $(ZnS)_{13}$ clusters, reaction of $Cd(OAc)_2 \cdot 2H_2O$ and selenourea in butylamine solvent at RT resulted in $(ZnS)_{34}$ cluster instead of $(ZnS)_{13}$, though the other $(II-VI)_{34}$ clusters were normally observed in *n*-alkylamine/di-*n*-alkylamine solvent, and the high-energy absorptions of $(ZnS)_{13}$ made it difficult to observe spectroscopically even if it was formed under certain conditions. For $(ZnTe)_{34}$ clusters, attempts to prepare $(ZnTe)_{34}$ from RT to 100 °C all gave poorly characterizable reaction product, which implied the synthesis of $(ZnTe)_{34}$ may require

a high temperature above 100 °C. Thus, $(ZnS)_{13}$, $(CdS)_{13}$, and $(ZnTe)_{34}$ could be possibly accessed by varying different amine combinations or applying different temperature.

Moreover, this dissertation focused on the synthesis and isolation of the binary II-VI magic-size clusters and corresponding flat nanocrystals, but doping in these clusters to form ternary magic-size clusters is also worth investigating. Hyeon and coworkers demonstrated giant Zeeman splitting in doped $CdSe:M^{2+}$ quantum nanoribbons[3] and the formation of the M^{2+}-Doped $(CdSe)_{13}$ clusters.[4] Fainblat and coworkers illustrated the correlations of the magneto-optical response and $(CdSe)_{13}$ clusters on the discrete number of Mn^{2+} ion dopants.[5] Cation exchange has proven to be a powerful tool for nanomaterials synthesis.[6,7] As a result, the formation of ternary magic-size clusters or nanocrystals may be realized by cation exchange process during or post the binary II-VI magic-size clusters and 2D semiconductors synthesis.

Last, in chapter 3 and 4 we investigated the reversible surface exchange of amine passivated L-type Cd-VI nanocrystals to metal oleate Z-type ligand and bound-ion-pair X-type (X = halide, nitrate, or carboxylate) ligand. This ligand exchange process may be applied to other amine passivated nanocrystals such as Zn-VI QBs or QPs[2], and also (II-VI) clusters[2,8]. Sardar and coworkers reported the reversible L- to Z-type ligand exchange by reaction of oleylamine-passivated $(CdSe)_{34}$ nanocrystals and $Cd(O_2CPh)_2$ complex at RT.[8] Reverse surface exchange of X-type to L-type is also possible upon addition of L-type ligand to those originally X-type or Z-type ligated QBs or QPs[9]. Purposely surface modification on semiconductor surface can be realized by surface

exchange.

5.3 References

(1) Wang, Y. Y.; Zhang, Y.; Wang, F. D.; Giblin, D. E.; Hoy, J.; Rohrs, H. W.; Loomis, R. A.; Buhro, W. E. *Chem. Mater.* **2014**, *26*, 6318.

(2) Wang, Y. Y.; Zhou, Y.; Zhang, Y.; Buhro, W. E. *Inorg. Chem.* **2015**, *54*, 1165.

(3) Yu, J. H.; Liu, X.; Kweon, K. E.; Joo, J.; Park, J.; Ko, K.-T.; Lee, D. W.; Shen, S.; Tivakornsasithorn, K.; Son, J. S.; Park, J.-H.; Kim, Y.-W.; Hwang, G. S.; Dobrowolska, M.; Furdyna, J. K.; Hyeon, T. *Nat. Mater.* **2010**, *9*, 47.

(4) Yang, J.; Fainblat, R.; Kwon, S. G.; Muckel, F.; Yu, J. H.; Terlinden, H.; Kim, B. H.; Iavarone, D.; Choi, M. K.; Kim, I. Y.; Park, I.; Hong, H.-K.; Lee, J.; Son, J. S.; Lee, Z.; Kang, K.; Hwang, S.-J.; Bacher, G.; Hyeon, T. *J. Am. Chem. Soc.* **2015**, *137*, 12776.

(5) Muckel, F.; Yang, J.; Lorenz, S.; Baek, W.; Chang, H.; Hyeon, T.; Bacher, G.; Fainblat, R. *ACS Nano* **2016**, *10*, 7135.

(6) Beberwyck, B. J.; Surendranath, Y.; Alivisatos, A. P. *J. Phys. Chem. C.* **2013**, *117*, 19759.

(7) De Trizio, L.; Manna, L. *Chem. Rev.* **2016**, *116*, 10852.

(8) Lawrence, K. N.; Dutta, P.; Nagaraju, M.; Teunis, M. B.; Muhoberac, B. B.; Sardar, R. *J. Am. Chem. Soc.* **2016**, *138*, 12813.

(9) Ithurria, S.; Tessier, M. D.; Mahler, B.; Lobo, R. P. S. M.; Dubertret, B.; Efros, A. L. *Nat. Mater.* **2011**, *10*, 936.